ISSN 0038-531X

Russian Original Vol. 49, No. 1, July, 1980

January, 1981

[redacted]

PEEL HERE

SATEAZ 49(1) 423-504 (1980)

SOVIET ATOMIC ENERGY

АТОМНАЯ ЭНЕРГИЯ
(ATOMNAYA ÉNERGIYA)

TRANSLATED FROM RUSSIAN

c/b CONSULTANTS BUREAU, NEW YORK

SOVIET ATOMIC ENERGY

Soviet Atomic Energy is a translation of *Atomnaya Énergiya*, a publication of the Academy of Sciences of the USSR.

An agreement with the Copyright Agency of the USSR (VAAP) makes available both advance copies of the Russian journal and original glossy photographs and artwork. This serves to decrease the necessary time lag between publication of the original and publication of the translation and helps to improve the quality of the latter. The translation began with the first issue of the Russian journal.

Consultants Bureau journals appear about six months after the publication of the original Russian issue. For bibliographic accuracy, the English issue published by Consultants Bureau carries the same number and date as the original Russian from which it was translated. For example, a Russian issue published in December will appear in a Consultants Bureau English translation about the following June, but the translation issue will carry the December date. When ordering any volume or particular issue of a Consultants Bureau journal, please specify the date and, where applicable, the volume and issue numbers of the original Russian. The material you will receive will be a translation of that Russian volume or issue.

Subscription (2 volumes per year)

Vols. 46 & 47: $147.50 per volume (6 Issues)
Vols. 48 & 49: $167.50 per volume (6 Issues)

Single Issue: $50
Single Article: $7.50

Prices somewhat higher outside the United States.

Soviet Atomic Energy is abstracted or indexed in *Chemical Abstracts, Chemical Titles, Pollution Abstracts, Science Research Abstracts, Parts A and B, Safety Science Abstracts Journal, Current Contents, Energy Research Abstracts,* and *Engineering Index.*

CONSULTANTS BUREAU, NEW YORK AND LONDON

227 West 17th Street
New York, New York 10011

Published monthly. Second-class postage paid at Jamaica, New York 11431.

SOVIET ATOMIC ENERGY

A translation of *Atomnaya Énergiya*

January, 1981

Volume 49, Number 1 July, 1980

CONTENTS

CONTENTS

(continued)

The Russian press date (podpisano k pechati) of this issue was 6/24/1980. Publication therefore did not occur prior to this date, but must be assumed to have taken place reasonably soon thereafter.

ARTICLES

CRITERIA FOR THE ECONOMIC EFFECTIVENESS OF THE USE OF RESEARCH REACTORS FOR MATERIALS TESTING

V. A. Tsykanov, B. A. Zaletnykh,
E. V. Kirillov, and V. A. Kuprienko

UDC 621.039.553

In designing a new research reactor or reconstructing and operating an existing reactor, one invariably encounters problems of making a comparative assessment of the possible technical solutions. Such assessments require the use of some comparison criteria or other. The choice of criteria can prove to have a significant or even decisive effect on the final solution.

In [1, 2] one of the present authors considered possible physical criteria which could be used to compare research reactors or various operating conditions of one and the same reactor as well as to optimize some of its characteristics. Since these criteria incorporate only the physical and operational parameters of the reactors, they permit quantitative comparisons to be made in physical units, e.g., according to output defined as the total number of useful utilized neutrons per unit time:

$$\Pi = \sum_{i=1}^{n} \Phi_i \Sigma_i V_i, \tag{1}$$

where Φ_i, V_i, and Σ_i, respectively, are the neutron flux density (neutrons/cm^2 · sec), the effective experimental volume (cm^3), and the macroscopic neutron cross-section of the specimens for the i-th experimental port (cm^{-1}), and n is the number of experimental ports in the reactor.

These criteria do not make it possible, however, to carry out quantitative economic assessments, to more fully characterize the suitability of one variant or other in the construction of a new research reactor, or to determine the efficiency of the operating or reconstruction conditions for existing reactors. In the present paper we propose to use the economic effect as a criterion for the quantitative economic evaluation of the effectiveness of possible technical solutions.

In the general form, in accordance with the technique of determining the economic effectiveness of a new technology [3], the more rational variant seems to be the one which ensures the lowest normalized expenditures in comparison with other possible (existing) variants:

$$E = c + E_n C, \tag{2}$$

where E are the expenditures per unit production (operation) (rubles/unit); c, cost of unit production (operation (rubles/unit); E_n, normative coefficient of effectiveness of one-time expenditures (1/yr); and C, one-time expenditures (capital expenditures, expenditures on development, etc.), relative to the annual volume of production (operation) (rubles/unit).

The annual economic effect from the application of a new technique is found from

$$E = (E_1 - E_2) A_2, \tag{3}$$

where E_1 and E_2 are the normalized expenditures per unit production (operation) according to the base and new techniques, respectively, and A_2 is the annual volume of production (operation) with the new technique (units/yr).

It must be borne in mind that besides (or instead of) an economic effect a new technical solution may yield a scientific and technical effect, a social effect, etc., which should be taken into account in the choice of

Translated from Atomnaya Énergiya, Vol. 49, No. 1, pp. 3-6, July, 1980. Original article submitted May 7, 1979.

0038-531X/80/4901-0423$07.50

termining only the economic effect. In this case the effectiveness of the use of the reactor is assessed not from the position of the effectiveness of the results of NIOKR performed on it (which would make it necessary to consider the value and appropriateness of the research, its importance to the national economy, etc.) but from the position of its as a research instrument.

Index of Normalized Expenditures for Research Reactors

Let us consider the principal concepts in Eqs. (2) and (3) as applied to research reactors.

One-time Expenditures. Depending on the problem under consideration, one-time expenditures on the design of a new reactor and the pertinent NIOKR forming the basis of the design, the capital expenditures in the construction of a new reactor, expenditures for elaborating a project for the reconstruction of an existing reactor and the corresponding NIOKR underlying the project, the capital expenditures in the reconstruction of an existing reactor, or finally, expenditures on the realization of one variant or other of the operation of an existing reactor. On the methodological plane, determining the one-time expenditures for research reactors poses no difficulties.

Annual Volume of Output and Cost of Unit Product (Operation). As applied to the new technology employed in the national economy for turning out a concrete production, defining these concepts most often also poses no difficulty. As a rule, the production carried out is measured with certain natural indicators and its cost, by relating the expenses to the volume of output. Research reactors are used not to turn out any kind of production but to perform a wide range of scientific-research. Therefore, the problems concerning the determination of the volume of work done on a research reactor and the concrete units for measuring this volume of work are not simple ones.

It must be pointed out that the problem of measuring the volume of work done on experimental and test facilities (research reactors fall in this category) has been elucidated inadequately, in our opinion, in the literature. The most widely held viewpoint is that the maximum volume of work which can be performed on an experimental or test facility (its throughput) is determined by the useful fund of operating time during the concrete calendar segment of time [4]. The throughput of testing operations is defined in much the same way in [5].

This approach probably appears to be highly arbitrary and, in the best case, to be valid only for facilities operating according to one possible technological cycle while ensuring a strictly defined result of its operation. If the facility can ensure a single result but can do so by means of several technological cycles, then the efficiency of its operation can differ for one and the same time. This approach is all the more invalid if the facility is used for several purposes or if it carries out diverse production; the relation between the volumes of production may depend on the operating conditions of the test (experimental) facility.

In determining the productivity or results of the operation of such test and experimental facilities, one must include natural indicators along with the indicator of their use in time. Research reactors are in the category of such test facilities. As a rule, they are used to simultaneously perform various experimental work whose value usually cannot be evaluated with one indicator. Unlike conditions are produced in various experimental devices of the reactor for carrying out this work and, moreover, these conditions (and thus the quantity and the time in which the intended result is reached) depends essentially on the operating conditions. Moreover, the differences in the designation of research reactors also affect the choice of the characteristic natural indicators for evaluating their operating efficiency. Accordingly, they will be different for universal reactors (e.g., the SM-2) than for loop reactors intended for testing trial fuel assemblies (e.g., the MIR) [6]. The characteristic features of research reactors are discussed in detail in [7].

Criteria of Economic Effectiveness

The ideas discussed above concerning the choice of indicators of the volume of work and the cost of unit production (operation) of research reactors are taken into account in determining the criteria for the evaluation of their economic effectiveness.

Universal Research Reactors. The experimental ports of universal research reactors are used to irradiate specimens of various materials and fuel compositions, to study their properties during irradiation, and also to perform other experiments requiring the interaction of neutrons with specimens of the material being irradiated. It is usually necessary to maintain maximum neutron flux density in the reactor ports since under such conditions the minimum time is required for each experiment. For this purpose the power of a universal research reactor should always be kept at maximum. If according to the conditions of some experiment is is not necessary to have maximum neutron flux density or it is necessary to have a temperature which can be

provided only at reduced reactor power, then such an experiment is, as a rule, performed in experimental devices which enable the necessary parameters to be maintained without reducing the reactor power, i.e., without detriment to all other experiments [6]. Thus, in the case of the universal research reactor the natural indicator on the basis of which the necessary criteria can be obtained is the total number of neutrons utilized usefully per unit time; this number is given by Eq. (1). Since this indicator depends on the properties of the irradiated specimens (through Σ_i), it is more convenient to consider for each port the product $\Phi_i V_i$ which characterizes only the reactor capabilities which do not depend on the properties of the irradiated specimens. When the foregoing is taken into account the indicator of the annual volume of work of a universal research reactor (neutrons · cm/yr) can be written as

$$A = 31{,}54 \cdot 10^6 K_r K_p \sum_{i=1}^{n} \Phi_i V_i K_{ex_i}, \tag{4}$$

where $31.54 \cdot 10^6$ is the number of seconds in a calendar year (sec/yr); K_r, coefficient of reactor utilization in time, defined as the ratio of the time of power operation by the reactor to the calendar time (rel. units); K_p, coefficient of utilization of the rated power of the reactor defined as the ratio of the power production of the reactor to the power production it would have if it operated at rated power all the time (rel. units); and K_{ex_i}, coefficient of utilization of the i-th experiment port, defined as the ratio of the time of useful operation of the i-th port to the reactor operating time (rel. units).

If the coefficient K_{ex_i} is taken equal to unity and if K_r and K_p are taken to be the theoretically maximum values possible for the given reactor, Eq. (4) will show the maximum annual volume of work which can be performed on the reactor (or its annual throughput). If these coefficients are assumed to be equal to the planned or actual values, Eq. (4) will give the planned and actual volumes of the reactor, respectively.

The annual expenditures for the reactor operation (for simplicity we consider the case without regeneration of the spent fuel) in accordance with [8] are given by

$$C = C_{op} = \frac{8760 K_r K_p N g c_f}{\alpha}, \tag{5}$$

where C_{op} are the annual expenditures on the reactor operation (without inclusion of the expenditures for nuclear fuel) (rubles/yr); 8760, number of hours in a year (h/yr); N, rated power of the reactor (MW); g, nuclear fuel consumption for the production of unit thermal energy (kg ^{235}U/MW · h); c_f, cost of the nuclear fuel in the fuel elements, including the expenditures on their fabrication (rubles/kg ^{235}U); and α, average nuclear fuel burnup defined as the ratio of burntout ^{235}U to the initial quantity of it (rel. units).

Dividing Eq. (5) by Eq. (4), we determine the cose of unit work done on the research reactor and, adding $E_n C$ to it, we get an expression for the normalized expenditures:

$$E = c + E_n C = \frac{C}{A} + E_n C = \frac{1}{3600 \sum_{i=1}^{n} \Phi_i V_i K_{ex_i}} \left(\frac{C_{op}}{8760 K_r K_p} + \frac{N g c_f}{\alpha} \right) + E_n C, \text{ rubles/neutrons} \cdot \text{cm}. \tag{6}$$

Loop Reactors. Loop research reactors are intended for testing trial fuel assemblies. Testing is conducted in experimental ports connected to special cooling circuits which are called loops.

In order to test trial fuel elements in loops it is necessary to imitate the operating conditions of regular fuel assemblies in the future reactors. The operating conditions of the loop reactor, therefore, should provide the desired conditions for testing fuel assemblies in all the loop channels operating at the same time. The initial matching of the necessary testing conditions in each channel is achieved with special regulating devices which make it possible to establish various conditions at a certain (by far not always maximum) reactor power. During the testing the conditions change and become mismatched. In order to keep these conditions within the prescribed limits, use is made of operational control elements and in a number of cases the reactor power is adjusted (usually increased). The process of establishing and maintaining the operating conditions of a loop reactor is assumed to be all the more ideal if the prescribed testing conditions in the loop ports are attained at lower reactor power and deviate slightly during the reactor operation. Thus, the operating conditions of a loop reactor and the characteristics of the experimental ports are variable quantities and depend on the character of the tests. Accordingly, for a loop reactor, unlike a universal reactor, the number of neutrons usefully utilized per unit time cannot be chosen for the natural indicator of output as a general case.

Therefore, [7] proposed that the output of a loop reactor be measured as

$$\Pi = \sum_{i=1}^{n} (K_{ex}K_{con})_i = n\bar{K}_{ex}\bar{K}_{con}, \tag{7}$$

where K_{con_i} is the coefficient of fulfillment of the prescribed test conditions for the i-th port and K_{con} is the average over the number of channels when the output of the reactor is determined for some interval of time. The existence of this coefficient is due to the fact that the time taken to test fuel assemblies in any loop port with deviation from the prescribed conditions cannot be taken into account in the total testing time. This coefficient is defined as the ratio of the port operating time under the prescribed conditions to the total time for which the port is occupied with the given experiment.

Thus, for a loop reactor the output is measured by the number of experiments conducted under prescribed conditions during the interval of time under consideration. In this case the annual volume of work done in a loop reactor is written as

$$A = 8760K_r \sum_{i=1}^{n} (K_{ex}K_{con})_i = 8760K_r\bar{K}_{ex}\bar{K} \quad n, \text{ h/yr}. \tag{8}$$

When account is taken of the specific nature of the use of a loop reactor (variable power depending on the testing conditions) it is appropriate to write the annual expenditures for its operation in the form

$$C = C_{op} + Wgc_f/\alpha, \text{ rubles/yr}, \tag{9}$$

where W is the power production of the reactor (MW·h/yr). Dividing Eq. (9) by Eq. (8), we find the cost of unit work in the loop reactor. Setting it equal to E_nK, we get a criterion for the economic effectiveness of a loop reactor in the form of normalized expenditures:

$$E = c + E_nC = \frac{C}{A} + E_nC = \frac{(Wgc_f/\alpha) + C_{op}}{8760K_r \sum_{i=1}^{n} (K_{ex}K_{con})_i} + E_nC, \text{ rubles/yr}. \tag{10}$$

When the value calculated from Eq. (8) is used as an indicator of the volume of work, it is not possible to determine the maximum volume of work which can be done in the loop reactor; this is required, e.g., in comparing designed or existing reactors with the same purpose but of different design. For this case, the maximum annual volume of work which can be performed in a loop reactor can, it is proposed, be determined as follows:

$$A = 8760K_r \sum_{i=1}^{n} (q_{max}VK_{ex}K_{con})_i, \text{ kW·h/yr}, \tag{11}$$

where q_{max_i} is the specific power production in the i-th channel attained when the reactor operates at maximum power (kW/cm^3).

In Eq. (11) the natural indicator of output chosen for the loop reactor is the total maximum power of all experimental ports unlike the case of the universal reactor where the output is measured by the total number of neutrons usefully utilized per unit time. Thus, the volume of work in Eq. (11) is measured by the usefully utilized total power produced by the loop ports (kW·h). This is in keeping with the purpose to which loop reactors are devoted, i.e., testing of fuel assemblies, one of whose principal indicators (burnup fraction) for power reactors is most often determined by the specific power production of the fuel assemblies (e.g., MW·day/ton U).

The criteria obtained for universal and loop research reactors can be easily calculated since they include quantities which characterize the properties of the concrete reactors and which can be determined without difficulty during operation. In most cases all of them are determined beforehand as planned values. Therefore, with the aid of the criteria it is possible not only to evaluate the economic effectiveness of one technical solution or other (e.g., in the construction of a new reactor or reconstruction of an existing one) but also to determine the economic gains or losses when the operating conditions of the reactor deviate from the planned conditions.

LITERATURE CITED

1. V. A. Tsykanov, At. Energ., 31, No. 1, 15 (1971).
2. V. A. Tsykanov, At. Energ., 33, No. 4, 849 (1972).
3. Technique (Main Rules) of Determining the Economic Effectiveness of the Use of New Technology, Inventions, and Innovations in the National Economy [in Russian], Ékonomika, Moscow (1977).
4. É. M. Torf, Economics and Organization of Pilot Plants [in Russian], Ékonomika, Moscow (1975).
5. M. L. Bashin, Planning of Work of Branch Scientific-Research Institutes and Design Bureaus [in Russian], Ékonomika, Moscow (1973).
6. V. A. Tsykanov and B. V. Samsonov, Technique of Irradiation of Materials in Reactors with High Neutron Flux [in Russian], Atomizdat, Moscow (1973).
7. V. A. Tsykanov and V. A. Kuprienko, NIIAR Preprint P-26 (320), Scientific-Research Institute of Nuclear Reactors (NIIAR), Dimitrovgrad (1977).
8. V. A. Tsykanov, At. Energ., 14, No. 5, 469 (1963).

PHYSICAL PRINCIPLES OF NEUTRAL OXYGENATED-WATER OPERATING CONDITIONS

E. P. Anan'ev and G. N. Kruzhilin

UDC 621.039.534.44

There is no doubt that a correctly staged and properly executed experiment provides the best basis for a theory. This clearly applies to complex technological processes that involve simultaneously occurring phenomena relating to various branches of science. Nevertheless, even here there is a need for a "pure" theory as a generalization of accumulated knowledge which would enable practical interpolation of experimental data, i.e., would make it possible to ascertain that no unforeseen excursions of investigated parameters take place with a given range. It is in connection with these considerations that we present here the conclusions reached in the process of putting the neutral oxygenated-water (NOW) operating condition into practice.

First of all, we want to note that the school of Academician A. N. Frumkin provided an extensive theoretical background for electrochemical processes including those relating to corrosion. These problems have been lately approached from an electrodynamic point of view as for example in the work of the department of O. I. Martynova of the Moscow Power Institute [1] and of the group of Yu. I. Blank of the Odessa Polytechnic Institute [2]. Here we touch upon certain microscopic or quantum aspects which are useful for understanding the nature of the problem and at the same time lead to certain conclusions of practical value. On the whole, the article is a brief review including an attempt to some qualitative generalizations.

First of all, recall that the neutral oxygenated-water operating conditions with addition of gaseous oxygen met at the time with considerable opposition since we all learned in good faith that oxygen dissolved in water is a potent corrosive agent. These new water operating conditions are based on two fundamental works carried out at the G. M. Krzhizhanovskii Institute of Power Engineering. The first was the work of K. A. Nesmeyanova who in 1964 established with the aid of an experimental circulating-water stand that the addition of gaseous oxygen into a flow of desalinated water causes formation of an oxide film on the walls of carbon steel or stainless steel tubes which practically stops corrosion. This result is illustrated in Fig. 1 [3]. The metal corroded off experimental plates turns into a dense oxide film and into loose oxide particles. Curves 3 and 4 indicate that when 3-5 mg/kg of dissolved gaseous oxygen is introduced into the flow the corrosion of the samples continues to increase for the first 250-500 h. The curves then become horizontal and parallel to the time axis. Thus, experimental data indicate that the quantity of corroded metal ceases to increase with time in this region meaning that for all practical purposes corrosion stops; the total loss of carbon and stainless steels at this point being ~ 5 and ~ 2 g/m^2, respectively. Additional resutls of this kind have been published in other works of Nesmeyanova [4, 5]. In 1974 the experiments have been repeated by M. E. Shitsman and L. S. Midler. They placed experimental carbon steel plates along the entire channel of a power unit oper-

Translated from Atomnaya Énergiya, Vol. 49, No. 1, pp. 6-11, July, 1980. Original article submitted August 20, 1979.

0038-531X/80/4901-0427$07.50

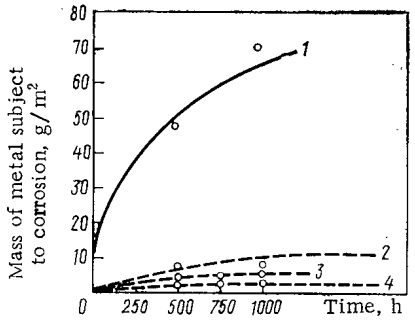

Fig. 1. Steel corrosion as a function of time for a water flow rate of 10 m/sec at 300°C: 1, 2) carbon and stainless steel, respectively, for an oxygen concentration 0.03 mg/kg; 3, 4) as before but with an oxygen concentration 3-5 mg/kg.

ating in NOW conditions. At all water temperatures from 30°C to critical temperature the results indicated a drastic drop in corrosion after an initial total corrosion of 5-6 g/m^2 [6]. These data are thus in total agreement with the results of K. A. Nesmeyanova mentioned above. Similar data on oxygen-water operating conditions have been published in Great Britain [7].

Obviously, the oxide film that protects the steel surface from corrosion also dissolves in water to some extent. The experimental results cited above are thus valid only to within the measuring accuracy. It must be noted that in the experiments of K. A. Nesmeyanova the samples were weighed with analytic balances with an absolute measuring error of ±0.2 mg. The total weight of corrosion products from the experimental 7 × 2.5-cm plates was up to 20 mg as found from the difference in metal mass before and after the experiments. The maximum relative error in corrosion products measurement was $\pm 2 \times 0.2/20 = \pm 2\%$. For a plate area $2 \times 7 \times 2.5 = 35$ cm^3 and an experimental time 5000 h [4] the error in corrosion rate measurement in the horizontal portion of the curve is $\pm 0.2/35 \times 10^{-4} \times 5000 = \pm 0.01$ mg/m$^2 \cdot$h. It can be thus reasonably assumed that the film dissolution rate is below this figure. As seen in Fig. 1 (curves 1 and 2), under purely neutral conditions the rate of carbon steel dissolution is about 100 mg/m$^2 \cdot$h and that of stainless steel, nearly 10 mg/m$^2 \cdot$h. One can thus assume that according to the above example the corrosion rate of carbon steel in oxygenated-water operating conditions is reduced at least 10^4 times and that of stainless steel at least 10^3 times.

The second fundamental work that prompted the use of NOW operating conditions in thermal electric power stations was that by Shitsman [8] who proved that in the rgeion of critical water temperature a low-density layer forms on the tube walls in high-thermal fluxes typical of fuel–oil steam generators. Considering this, M. E. Shitsman concluded in 1972 that in case of alkaline-water operating conditions there is no sufficient dissociation and OH^- anion production in the wall layer mentioned before so that there is no adequate alkaline protection of metal from corrosion. Thus, when a tube breakage occurred in 1974 at the Konakova Electric Power Station, the G. M. Krzhizhanovskii Institute of Power Engineering has recommended to replace the traditional alkaline hydrazine–ammonia operating conditions with the new neutral oxygenated-water operating conditions with addition of gaseous oxygen. Trials directed by the Chief Engineer Yu. I. Timofeev and M. E. Shitsman gave excellent results [9]. At the present time, NOW operating conditions are used in 45 supercritical-pressure units of thermal electric plants. Wider application of NOW operating conditions in all other units of this type is hampered by the need to replace the brass heater tubing with carbon steel tubing.

There are no principal obstacles for using these new NOW operating conditions in feed channels of atomic power plants including plants with high-power boiling reactors. The positive rseults expected can hardly be overestimated. As is well known, NOW operating conditions are already used for several years in Sweden [10]. In the USSR the first conversion to NOW operating conditions was crrried out in July 1979 in a 50-MW unit with a boiling-water reactor of the Dimitrovgrad Atomic Power Station. The use of NOW operating conditions in atomic power plants of the USSR was delayed because of the negative attitude of the classical school in power engineering [11].

Let us now discuss the process mechanisms. It is well known that corrosion of iron in a water flow is primarily an electrochemical process and is due to the fact that negative ions present in water tear away positive iron ions, i.e., iron atoms lacking one or two electrons. The latter are caused by the fact that in iron, as in other good conductors, one or two electrons of the outer shell are not strongly bound to the nucleus and are free to move in the metal lattice. From this point of view, the iron corrosion process is qualitatively the same in an alkaline medium in which there are sufficiently many negative ions in the form of OH^- as in neutral water because water molecules are polar, i.e., have an electric dipole and a corresponding equivalent negative electric charge. On the other hand, it is known that no corrosion at all takes place in steel vessels with mineral oil or kerosene since these liquids are not polar. No corrosion occurs also in vessels with pure acids in view of the fact that their molecules do not split into ions, such splitting taking place only in aqueous acid solutions in which under the action of polar water molecules the molecules of acid dissociate into H^+ hydrogen cations and Cl^- radical anions. Exactly the same mechanism acts in the interaction of pure water with porcelainlike dielectrics which unlike metals have no free electrons so that their atoms cannot turn into ions. The very low solubility of metal oxide films is due to the fact that being a semiconductor the film has an electron conductivity seven orders of magnitude lower than that of its parent metal. Consequently, its solubility in neutral water also is approximately seven orders lower than that of the metal. These figures and the fact that the rate of steel corrosion in the case of NOW operating conditions is three-four orders of magnitude lower substantiate K. A. Nesmeyanova's conclusion that practically no corrosion should take place in these operating conditions. The very high resistance of iron oxide films to corrosion was pointed out by such an authority as T. Hoare who observed that certain oxides, e.g., Al_2O_3 or Fe_2O_3, can be stored for long times without significant changes in acid solutions [12].

Such an approach, however, leads to paradoxes. One of them is that, as shown in K. A. Nesmeyanova's experiments, steel corrosion proceeds at a much higher rate in pure water than in alkaline water. Curve 1 in Fig. 1 indicates that the rate of carbon steel corrosion is 70 $mg/m^2 \cdot h$ in pure neutral water and only 10 $mg/m^2 \cdot h$ in alkaline-water operating conditions. The dipole moment of a water molecule ($1.84 \cdot 10^{-18}$ esu $\cdot$ cm) can be found in physical tables and taking into account its diameter ($3.2 \cdot 10^{-10}$ m) one can calculate the equivalent electric charge as being equal to 0.12e, i.e., less than the elementary electric charge $e = 1.6 \cdot 10^{-16}$ C. At the same time, the charge of OH^- is exactly e. This paradox can be probably most fully explained by the results of M. Pourbaix who on the basis of thermodynamic considerations proved that certain chemical and electrochemical reactions take place on steel walls at high pH and correspondingly high concentrations of OH^- ions in which a protective oxide film forms on the wall surface [13]. It should be noted, incidentally, that according to his calculations such a protection mechanism reveals itself most fully at 10-13 pH [13]. No such film can form or exist in neutral deaerated water.

At low pH values and correspondingly small OH^- concentrations, at which film formation is difficult and the effect of tearing away of iron cations by OH^- anions is most pronounced, the rate of corrosion is higher than at 7 pH. Hence also follows that the presence of oxygen would be desirable in desalinated water in alkaline operating conditions and high pH values so that introduction of hydrazine to suppress oxygen now practiced in alkaline-water operating conditions is not justified.

The second paradox is the relatively low rate of steel corrosion in water flow. The dissolution in water, e.g., of NaCl is quite fast. The point is, apparently, that charges of Na^+ and Cl^- ions do not change in time so that the forces of interaction of water molecule dipoles with ions of the crystalline lattice of NaCl salt remain more or less constant. A different situation exists in the case of dissolution of iron since its atoms remain a relatively short time without electrons. The equivalent charge of water molecule dipoles at the point of contact with iron atoms also varies with time (see Fig. 2). As a result, the probability that iron atoms will be torn away by water molecules should be higher than the probability of tearing away salt ions. The above-mentioned paradox can be approximately interpreted in this way. At least in principle, this approach offers a way to calculate the rate of dissolution of iron in pure water.

Passivation of a metallic wall by oxygen is very effective. The passivation process has been well described by Ulig [14]. Various investigations, including diffraction of slow electrons, proved that the interaction of oxygen with a metal surface begins by physical adsorption of metal molecules and is followed by chemisorption of its atoms helped by the electron affinity of oxygen which is quite high and equal to 1.465 eV. Because of this, O_2 molecules touching the walls greedily attach themselves to free metal electrons "adhering" to the metal surface and providing protection from corrosion by aggressive water dipoles.

Another possible mechanism takes place when O_2 attaches to itself one or two electrons from less strong anions and then "adheres" to the walls where the processes of chemisorption and metal oxide formation also take place.

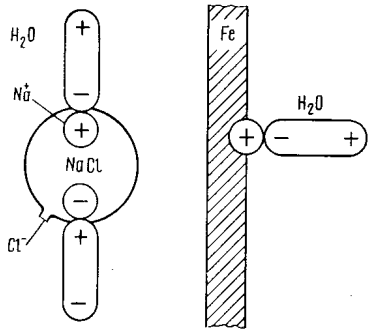

Fig. 2. Interaction of water molecule dipoles with Na^+ and Cl^- ions of the NaCl crystalline lattice and with iron ions at the interface with the steel wall.

Because of the relatively high electron affinity of oxygen (1.465 eV), its interaction with metal walls is temperature independent in the operating conditions of power generating units. As is well known, the kinetic energy of particles is ~0.04 and 0.08 eV at 300 and 600°K, respectively. The temperature effects are thus quite insignificant in comparison with the electron affinity energy of oxygen. Consequently, ther is no risk that the passivation of steel by oxygen dissolved in water will be affected by heat in the interval from room to critical temperatures. Experimental data of K. A. Nesmeyanova and of M. E. Shitsman and L. S. Midler lead to similar conclusions. More recent results [7] confirm this.

A significant question is the amount of oxygen to be added to the water flow. There is of course a minimum dose that produces the desirable effect. According to K. A.Nesmeyanova and to the results of [7], this minimum dose is 0.2 mg/kg. The maximum dose of gaseous oxygen in thermal power plants is limited by acting operating instruction to 0.5 mg/kg not by considerations of wall passivation but by practical operating conditions of the plants since the admission of gas into turbine condensers adversely affects their vacuum. There seem to be no other physical reasons to limit the concentration of dissolved oxygen in water. This is significant since in some practical conditions a relatively high oxygen concentration may prove to be desirable. To such conditions belong first of all preliminary passivation of steel surfaces of generating units before start-up and passivation after prolonged shutdown or after chemical decontamination and deactivation. Naturally, the passivation process should take as little time as possible and this can be achieved by increasing the oxygen concentration up to its solubility limit in water. A similar situation arises in atomic power plants with circulating natural-water reactors in which stagnation zones inevitably occur. Also in this case reliable passivation requires high oxygen concentration in water. The lower concentration limit can be here estimated by comparing the processes of diffusion and heat transfer. In good water circulation the heat transfer factor is of the order $20 \cdot 10^3$ kcal/m$^2 \cdot$h, while in a stagnant area the factor drops to $\approx 10^3$ kcal/m$^2 \cdot$h, i.e., by a factor of 20. Thus, for good passivation of steel walls in stagnant areas the oxygen concentration should be 20 times higher than the minimum value cited before, i.e., not less than 4 mg/kg.

Higher oxygen concentration must also be maintained in cases when there is a temporary increase of water conductivity of of chlorine ion concentration since, as is well known, the latter easily affects the oxygen film on steel surfaces. In a recent monograph on corrosion [15] this effect is ascribed to the fact that the negative charges of chlorine ions are concentrated in a narrow regions forming a sort of "spear" thus increasing the probability of their penetration into the metal film. It is reasonable to assume that in oxygenated-water operating conditions the two processes of breaking up the oxide film by chlorine ions and of its "healing" by oxygen proceed in parallel. Thus, to ensure that the film remains intact under temporary high chlorine-ion concentrations one must add a proportionally higher amount of oxygen. Unfortunately, this important aspect of the problem has not been fully investigated even if a beginning was made in [7].

Thus, neutral-water operating conditions with an addition of gaseous oxygen are increasingly being used in thermal power plants in the USSR. In 1968 Freier [16] initiated the use of neutral operating conditions with an admixture of hydrogen peroxide in the Hamburg Electric Power System. It is important to note that between 1961 and 1968 the System was operating with purely neutral-water conditions [16] in which the rate of corrosion is ten times as high (see Fig. 1, curve 1) as in conventional alkaline conditions. Naturally, these operating conditions have been changes in 1968 to oxygenated-water conditions after the results of K. A. Nesmeyanova have been published in 1966. Freier did not, however, exactly follow the results of K. A. Nesmaynova but decided to add hydrogen peroxide to desalinated water.

The popularity of water operating conditions with an addition of hydrogen peroxide is due to the fact that peroxide has been initially assumed to give off atomic oxygen which is thought to be more active than molecular oxygen. It has been, however, soon found out that molecular oxygen O_2 and not atomic oxygen is liberated in the decomposition of hydrogen peroxide. Consequently, the positive effect of hydrogen peroxide on steel walls is no better than that of gaseous oxygen. Moreover, hydrogen peroxide decomposes easily only above 150°C so that in its use low-temperature regions of the plants remain without oxide film protection.

A similar conclusion has been reached by the authors of [17] who noted that molecular oxygen is a good substitute for hydrogen peroxide and does not involve any disadvantages. The authors point out that from the point of view of feeding equipment the use of gaseous oxygen is much simpler and safer than the use of hydrogen peroxide.

It is more interesting to note from a historical point of view that NOW operating conditions have been used probably for the first time in the circulation circuit of Physical and Technological Research Reactor which started operation in 1952 at the Institute of Atomic Energy [18]. The heat exchangers of this circuit were followed by a deaerator in which hydrogen, generated as a result of radioactive processes in the core, was released from the stream of distilled neutral water. The deaerator operated at atmospheric pressure at 20-30°C, hydrogen being removed from it by ventilation. Air was blown in by a fan and removed through a ventilation tube. Obviously, the stream of water was saturated by air including oxygen and in this state entered the reactor. The fuel elements and operating channels of the Research Reactor were made of aluminum and all its external units, of stainless steel. An exception were the valves used for controlling the operating channels mounted in horizontal collectors and made of carbon steel. Most prone to corrosion were the junction points between stainless steel and aluminum. Operating experience proved that no corrosion took place at these points and in other parts of the valves. It is significant to note that no corrosion products have been found on the fuel element surfaces of this reactor. Unfortunately, the actual rate of corrosion of carbon and stainless steel was never measured.

It should be noted that the pasivating effect of oxygen was first studied by Kolotyrkin, Florinovich, Petrov, Smirnova, and Vyazankin [19]. Unforntuately, their experiments were limited to autoclaves so that their results were not as effective and practically important as those of K. A. Nesmeyanova in strongly desalinated water.

In conclusion, the authors thank M. E. Shitsman and I. S. Dubrovskii for a discussion of the subject and for valuable advice.

LITERATURE CITED

1. O. I. Martynova et al., Teploénergetika, No. 3 (1976).
2. Yu. I. Blank et al., Teploénergetika, No. 9 (1978).
3. K. A. Nesmeyanova, E. B. Matskevich, and V. G. Kasatkina, in: Proceedings of the 3rd Int. Congress on Metal Corrosion [Russian translation], Vol. IV, Mir, Moscow (1966), p. 278.
4. K. A. Nesmeyanova, At. Energ., 29, No. 2 (1970).
5. K. A. Nesmeyanova et al., Teploénergetika, No. 11 (1973).
6. M. E. Shitsman et al., Teploénergetika, No. 5 (1977).
7. C. Tyzack and R. Berry, in: Conf. on Water Chemistry of Nuclear Reactor Systems, London (1977), p. 10.
8. M. E. Shitsman, Teplofiz. Vys. Temp., 1, No. 2 (1963).
9. M. E. Shitsman, Yu. I. Timofeev, and L. S. Midler, Énergetika, No. 5 (1976).
10. Von P. Fejes, VGB Kraftwerkstechnik, No. 2 (1977).
11. G. N. Kruzhilin, The Role of Various Reactor Systems in the Development of Atomic Power Plants in the USSR [in Russian], IAEA Int. Survey Course on Economic and Technical Aspects of Nuclear Power, Vienna (1969).
12. T. P. Hoare, in: Proceedings of the 3rd Int. Congress on Metal Corrosion [Russian translation], Mir, Moscow (1966), p. 25.
13. M. Pourbaix, Lectures on Electrochemical Corrosion, New York (1973).
14. H. Ulig, in: Proceedings of the 3rd Int. Congress on Metal Corrosion [Russian translation], Vol. 1, Mir, Moscow (1966), p. 25.
15. J. Sculby, The Fundamentals of Corrosion, Oxford (1975), p. 116.
16. R. Freier, VGB Speisewasser Taigung (1969), p. 11.
17. G. Resch and K. Zinke, VGB Kraftwerkstechnik, No. 3 (1979).

18. G. N. Kruzhilin, "Physical and technological research reactor," in: Proceedings of the 1st Geneva Conference [in Russian], Vol. 2, Fizmatgiz, Moscow (1958).
19. Ya. M. Kolotyrkin et al., in: Corrosion of Reactor Materials [in Russian], Atomizdat, Moscow (1960), p. 29.

MONITORING STRUCTURAL VIBRATIONS INSIDE REACTOR VESSELS

I. N. Andryushenkov, V. V. Bulavin, S. I. Vladimirtsev, F. V. Karmanov, and A. G. Smolyar

UDC 621.039.5.58

Safe operation of nuclear power plants requires protection of the reactor core from damage liable to disrupt heat removal in the core. One of the possible causes of such damage is excessive vibration caused by hydrodynamic forces in structural elements of the core or in other devices mounted within the primary circuit of the plant.

In spite of many research works [1, 2], many of the problems concerning elastic vibrations of poorly streamlined constructions have no satisfactory solutions. At the same time, the vibrations of core elements or of other devices placed within the primary circuit must be continuously or periodically monitored.

A reliable and comprehensive vibration monitoring method would make it possible to observe changes of the nature of vibration in time and to detect damage at the earliest stage preventing serious consequences.

The traditional visual (TV) inspection of in-reactor equipment, carried out as a rule once in several years of power plant operation, is obviously unable to provide a warning of vibration-caused damage. Strain-gauge measurements are now used to check vibrations of in-reactor requipment during hydrodynamic tests of nuclear power plants in start-up works. This method is quite effective as far as it concerns direct measurement of vibrations. However, its use during the plant operation is limited by the insufficient reliability of strain gauges in the corrosive medium of the primary circuit and by the difficulties associated with the introduction of a large number of gauges into the reactor and with providing reliable sealing.

Obviously, methods used to monitor vibrations must not interfere with the operation of the reactor and of the entire power plant. Such methods could be based, e.g., on passive analysis of neutron and acoustic noise. However, in normal operation nuclear power plants create many other sources of noise that affect their neutron and acoustic fields. The design of an efficient vibration monitoring system thus requires a solution of the difficult problem of separating out the weak random signal due to vibrations of a specific construction element from the background of high-amplitude interfering (parasitic) signals.

Despite these difficulties, the method of listening to acoustic noise by means of acceleration gauges (accelerometers) is recently used with some success. The gauges are mounted on the outside surface of the reactor vessel at points where its inside surface is in direct contact with in-reactor equipment to be checked. The method is simple to implement but the interpretation of results and quantitative estimation of vibration characteristics is very difficult.

A method based on the analysis of neutron flux noise by means of neutron ionization chambers located outside the reactor vessel is recently widely used for monitoring the frequency and amplitude of vibrations in the core. The method has been apparently for the first time used in the TRINO reactor in Italy [3]. Its possibilities are, however, quite limited. It does not allow to monitor the vibrations amplitude and frequency of individual core structures element and of various in-reactor devices that do not affect the neutron flux.

An interesting method of monitoring the vibrations of a specific control element, based on simultaneous processing of two different signals, has been proposed in [4]. In this method separation from the total neutron noise of a component associated with the vibrations of a given control element is made possible by the presence

Translated from Atomnaya Énergiya, Vol. 49, No. 1, pp. 11-14, July, 1980. Original article submitted November 27, 1979.

 0038-531X/80/4901-0432$07.50

of a second signal in which the contribution of vibrations due to the given element is dominant. An acoustic signal recorded by an accelerometer served as this reference signal. The accelerometer was mounted on the outside of drive protection tube of the element whose vibrations frequency was monitored. However, favorable conditions very important for this method are rarely met in practice. This is due to the fact that not all vibrations of any structural core element are dominant in the recorded reference signal.

Obviously, the method proposed in [4] also has limited possibilities. It should be noted that a common disadvantage of all the methods mentioned before is that the determination of vibrations amplitude of a specific in-reactor element is impossible and even its approximate estimation is associated with considerable difficulties.

Here we describe a method which, together withother methods mentioned before, expands the possibilities of monitoring the vibrations of in-reactor elements in the course of reactor operation. The proposed method solves the problem of eliminating the adverse effect of parasitic noise in the detected signal on the measured results.

The method of monitoring vibrations of in-reactor elements uses an ultrasonic radiator mounted on the outer surface of the reactor vessel to set up a definite acoustic field of fixed frequency. External radiation which passed through the internal multicomponent medium is recorded by a pickup also located on the external surface of the vessel. The detected signal passes through a narrow-band filter which separates the frequency of the external acoustic radiator. Most of the interfering parasitic acoustic signals are filtered out in this process.

In case of vibrations of various in-reactor elements the recorded signal will be amplitude-modulated by frequencies corresponding to the vibrations frequencies of each structural element. The time variation of the external acoustic field recorded in the receiving channel can be easily analyzed with the aid of existing instruments. These instruments make it possible to measure the frequency spectrum of the amplitude modulation of the external acoustic field due to the vibration of in-reactor elements at the detector location.

The modulation percentage of the external acoustic field of wavelength λ caused by vibrations of a specific in-reactor element depends on the relation between λ and the vibration amplitude Δ of the given structural element. Maximum modulation takes place when $\lambda = \Delta$. The vibrations frequency will appear in the spectrum as peaks whose magnitude bears a definite relation to the vibration amplitude of each individual in-reactor element.

This fact can be utilized for measurement of the amplitude of vibrations of any structural element inside the reactor vessel by means of devices placed outside the vessel.

Experimental Results. To check the validity of the above considerations we have carried out an experiment schematically shown in Fig. 1. A metal rod eccentrically mounted on a motor shaft is placed inside a metal vessel filled with water. The vessel is sealed by a top cover on which the motor is mounted. The motor turns a shaft passing through holes in the cover and in a disk of porolon which covers the entire liquid surface in the vessel. The shaft rotates at 96 rpm corresponding to a rotation of the rod in water at 1.6 Hz.

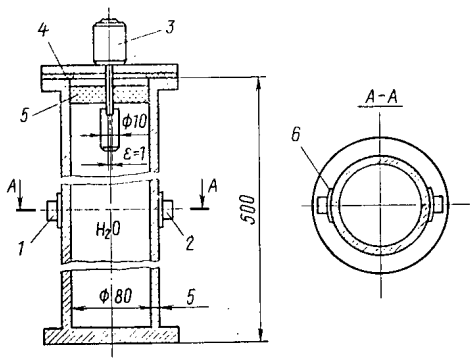

Fig. 1. Experimental setup for testing the proposed method of monitoring vibrations of in-reactor elements: 1) radiator; 2) pickup; 3) motor (96 rpm); 4) rubber gasket; 5) porolon disk; 6) indium.

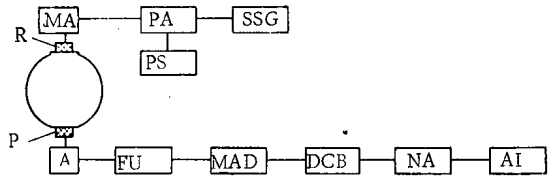

Fig. 2. Block diagram of the measuring circuit: PS) power supply; other notation explained in text.

The rod diameter is 10 mm and the eccentricity $\varepsilon = 1$ mm. Rotation of the motor causes the rod to vibrate thus simulating vibrations of an individual in-reactor element. The presence of a porous and soundproof porolon disk on the water surface prevents perturbations of the free water surface caused by a rotating rod from affecting the results of acoustic measurements. The acoustic radiator and pickup are mounted on the outside walls of the vessel. Because of the considerable curvature of the side surface of the vessel, the radiator and pickup are mounted on indium washer which closely encircles the vessel surface. This ensures a good acoustic contact of the piezotransducers with the vessel.

The block diagram of the measuring circuit used in the experiment is shown in Fig. 2. The sinusoidal reference signal generator SSG fed the ultrasonic radiator R at a frqeuency of ~500 kHz. The corresponding wavelength of the acoustic field in water was $\lambda = 3$ mm which is comparable with the eccentricity $\varepsilon =$ 1 mm. The sinusoidal SSG signal was applied to the ultrasonic radiator through a power amplifier PA and a matching amplifier MA. The acoustic signal received by the pickup P passed through a preamplifier A and through a filter unit FU with a center frequency of 500 kHz which could separate out from the signal any component within the frequency range from 470 to 530 kHz. The signal was then amplified and detected in the main-amplifier and detector unit MAD in which the envelope of the external ultrasonic field amplitude was separated. The amplitude was modulated by the rod rotations. After balancing out the dc component in the DCB unit and subsequent amplification in the normalizing amplifier NA the signal was recorded by the analyzing instruments AI: a magnetograph, a correlator, and a spectrum analyzer which made it possible to measure the spectral power density S_{AA} of amplitude modulation of the external acoustic signal.

An experimental curve of S_{AA} as a function of frequency f is shown in Fig. 3. Three peaks corresponding to f = 1.6, 3.2, and 4.8 Hz, i.e., to the fundamental and higher modes associated with the rotation of the rod in the vessel, can be easily observed in the figure. After the rotation stopped, S_{AA} was zero over the entire frqeuency range.

The described method of monitoring the vibrations of structural elements inside a reactor is, at first sight, simliar to that proposed in [5]. In the method [5] the acoustic transducer transmitted signal through the vessel walls and water to the surface of the vibrating element. The same transducer also served as an acoustic pickup which detected signal pulses reflected from surface of the investigated element. The time interval between the instant an acoustic pulse was transmitted and the instant it was received after a single reflection from the structural element, which was measured by special equipment, provided information on its displacement. The method makes it possible to measure the vibration frequency of a structural element only in the direction of a normal to its surface, drawn from the transducer. Moreover, unlike our method, the method [5] cannot in principle, measure the vibrations frequency of two or more elements located in the vessel at different distances from the transducer. This is due to the presence of multiple reflections of the acoustic signal from the surface of these elements.

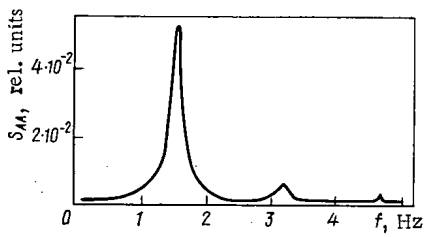

Fig. 3. Spectral power density S_{AA} of amplitude modulation of the external acoustic signal in relative units.

Conclusions. Let us consider certain aspects of the application of the proposed method of monitoring vibrations of in-reactor elements in an operating water-cooled–water-moderated power reactor.

As noted before, depending on their function, different structural elements of the reactor have different masses, sizes, and shapes and also are variously connected to other elements. This causes the frequency spectra of the vibrations of individual structural elements caused by hydrodynamic forces to differ from each other. Also different are the technological clearances between adjoining structural elements which determine the maximum vibrations amplitude in any direction when no mechanical damage occurred. For different structural elements of a given reactor type, these technological clearances usually vary from a fraction of a millimeter to several millimeters. Thus, taking into account the water temperature during reactor operation, the radiation frequency of the external ultrasonic transducer used with this method should exceed about 100 kHz.

Using the proposed method it is possible continuously or periodically to monitor the vibration of in-reactor elements and observe changes in the relative frequency and amplitude of vibrations of each individual structural element. This makes it possible to prevent any possible mechanical damage to in-reactor elements.

An advantage of the proposed vibrations monitoring method is the possibility of suppressing the undesirable effect of various acoustic interference of a technological nature which practically disappear at frequencies above 100 kHz. This can be achieved by selecting a suitable operating frequencies of ultrasonic radiators and ensuring high selectivity of the receiving channels.

An important drawback of the proposed method is the presence of low-frequency amplitude modulation of the field set up by the radiator caused by coolant temperature fluctuations. Additional physical information is needed to suppress this interference and to ensure reliable detection of the field modulation component associated with vibrations of a specific in-reactor element. Such information can by provided by noise signals of pressure and neutron flux transducers (both inside and outside the core) and by output signals of accelerometers mounted on outside surface of the reactor vessel and monitoring its vibrations. Measuring the relative spectral power density of one of the above-mentioned signals and of a signal proportional to the modulation of the field amplitude set up by the radiator it is sometimes possible to monitor the vibrations of a concrete in-reactor element. In choosing an additional information channel one must consider all the side effects associated with the vibrations of a given element.

LITERATURE CITED

1. M. Dubourg et al., Nucl. Eng. Design, 27, No. 3, 315 (1974).
2. V. V. Abramov et al., "Investigation of vibrations characteristic of the VVÉR-440 reactor shaft using a model," in: Proceedings of Canadian–Soviet Seminar on the Analysis of Vibrations in Nuclear Power Plants [in Russian], Toronto (1976).
3. A. Colling, in: Proc. Symp. Nuclear Power Plant Control and Instrumentation, Vienna, March 15-17 (1971), p. 141.
4. A. Graber et al., "Separation of single components from a complex noise signal by means of a modified averaging method," Zarbeitsbericht Rossendorf, ZFK RPP-14/76.
5. H. Runde and J. Kowies, Trans. Am. Nucl. Soc., 15, No. 1, 364 (1972).

COLLECTOR FEEDWATER SUPPLY AND STABILITY OF THE POWER DISTRIBUTION IN A PRESSURIZED-WATER REACTOR

V. I. Budnikov, S. V. Kosolapov, and A. Ya. Kramerov

UDC 621.039.56

To prevent damage to the core in an RMBK reactor if the pressurized collector fails, it has been suggested [1] that part of the feedwater should be supplied directly to the group collectors under normal working conditions. In that method of supplying the feedwater, any change in the flow rate in the group collectors influences not only the enthalpy of the water at the reactor input but also the total coolant flow in the reactor. This results in a feedback additional to that found when all the feedwater is supplied to the descending tubes, since the consumption of feedwater in the group collectors influences the flow of coolant in the reactor, and thereby the power level, thence the water level in the separator drum, and ultimately the flow of feedwater to the group collectors again. If there is a sufficiently large positive value for the steam coefficient of reactivity, the neutron pattern in the boiling-water reactor may become unstable with a short instability period [2], and it is therefore necessary to determine how the collector feedwater supply affects the disposition of the stability limits and the instability period for the power distribution in such a reactor.

We consider a nuclear power station with RBMK reactors in which the down tubes in the separator drum receive only part of the feedwater, with the rest passing to the group collectors (Fig. 1). For brevity, this method of feedwater supply will be called the second one, to distinguish it from the first, in which all the feedwater is supplied to the tubes from the separator drum.

The calculations were performed by the method of [2]. It was assumed that in the second method the flow of feedwater to the separator drum tubes was constant at 25% of the overall nominal value,* while the control of the feedwater flow was provided by adjusting the water flow to the group collectors, which are supplied by electric feed pumps. The transient response was calculated on the assumption that the characteristic of the level regulator for the water in the separator drum was linear near the state of equilibrium.

Stability of the Nominal State. For an average channel in an RBMK reactor with heat-transfer intensifiers [3], we show in Fig. 2 the transient response curves $\varepsilon_1(t)$ and $\varepsilon_2(t)$ calculated from the OKA program [4] for the first and second methods, respectively. There is a difference in behavior between $\varepsilon_1(t)$ and $\varepsilon_2(t)$ because the feed valve in the level regulator is more nearly closed in the second method than in the first. Also, over the section $t \in (0, 30)$ the form of $\varepsilon_1(t)$ is affected by the transport delay for the enthalpy of the coolant in the separator drum tube. In accordance with the method of [2], $\varepsilon_1(t)$ and $\varepsilon_2(t)$ were used to find the transfer functions, which were then substituted into the characteristic equation. The disposition of the roots of the latter was examined by the D decomposition method in the plane of the reactivity coefficients for the fuel $[a_f = -a_{ft}(\bar{t}_f^* - \bar{t}_c^*)]$ and the steam contant a_s. Here a_{ft} is the temperature coefficient of reactivity for the fuel, while $\bar{t}_f^*$, $\bar{t}_c^*$ are the stationary temperatures of fuel and coolant averaged over the core. Figure 3a shows part of the D curve and defines the fast instability limit due to the fast power coefficient of reactivity. The calculation was performed for a moderator reactivity coefficient $a_m = 5\bar{\beta}^*$ for the fundamental, neglecting xenon poisoning with the general-power regulator switched out. The broken and solid lines in Fig. 3a have been calculated for the first and second methods, respectively. The straight line representing the medium-period instability limit is due to the positive moderator coefficient of reactivity, but htis lies outside the limits of the figure. The special straight lines for the first and second methods coincide because the steady-state values of $\varepsilon_1(t)$ and $\varepsilon_2(t)$ are identical. The latter also indicates that the characteristic time of

*This flow of feedwater in the separator drum tube is required to provide cavitation-free operation of the principal pumps.

Translated from Atomnaya Énergiya, Vol. 49, No. 1, pp. 15-18, July, 1980. Original article submitted January 11, 1978; revision submitted January 8, 1980.

0038-531X/80/4901-0436$07.50

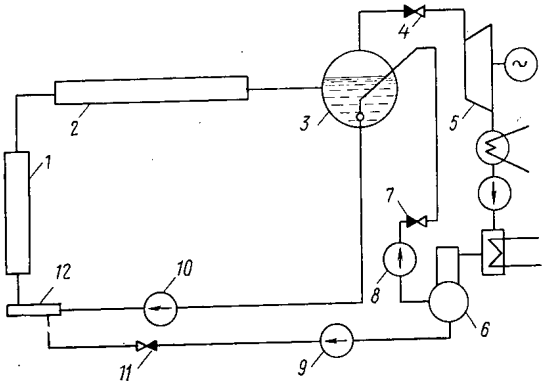

Fig. 1

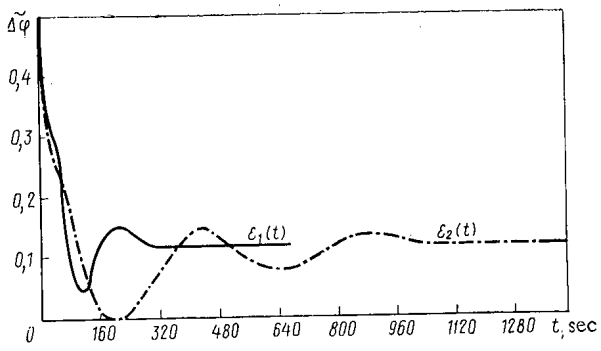

Fig. 2

Fig. 1. Simplified structural diagram of the coolant circulation loop in a nuclear power station containing RBMK reactors in the second method of feedwater supply: 1) heating channel; 2) steam–water pipe; 3) separator drum; 4) pressure regulator; 5) turbine generator; 6) deaerator; 7, 11) water-level regulators for the separator drum; 8, 9) feed pumps; 10) principal feed pump; 12) group collectors.

Fig. 2. Characteristic form of the transient response ε(t) for a nuclear power station with RBMK reactors in the first and second methods of feedwater supply.

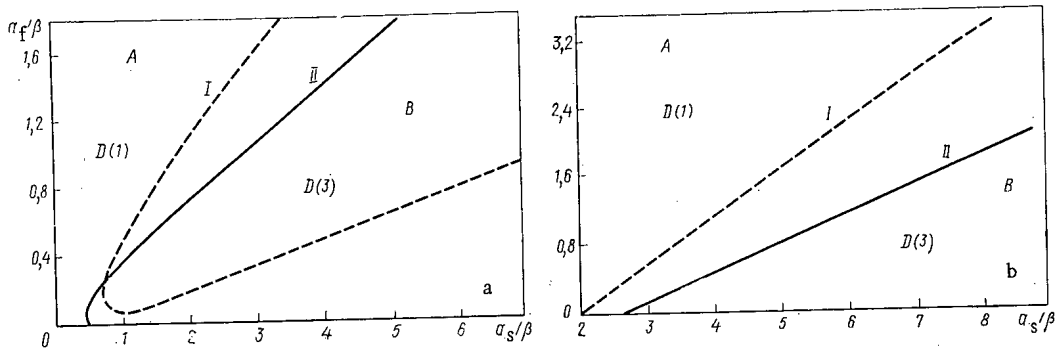

Fig. 3. D decomposition of the plane of reactivity coefficients a_S and a_f for the first and second methods of feedwater supply: a) fundamental; b) first azimuthal harmonic of right-left type; A) region of medium-period instability; B) region of fast instability.

the medium-period instability is the same for both methods. Figure 3a implies that the fast instability limit in the second method is shifted to somewhat higher values for the steam coefficient of reactivity. For example, for $a_f = \beta$ the difference in the values of a_S for these two methods is about equal to β. A similar picture applies for the first azimuthal harmonic of right-left type, where part of the D curve is shown in Fig. 3b. Here the difference in the limiting values of a_S is somewhat larger and is about 1.75β for $a_f = \beta$.* The deviation in the mean power is zero on the first azimuthal harmonic and consequently the overall power regulator does not operate.

The following conclusion may be drawn. If collector feedwater supply is used in a nuclear power station containing RBMK reactors, there is no change in the medium-period instability limit, and there is merely some increase in the margin with regard to the fast spatial instability.

Calculation of Transient Response. We have seen above that the change in feedwater flow to the group collectors in the second method influences not only the enthalpy of the water at the inlet to the core but also the coolant flow in the reactor. It is therefore of interest to examine the transient response in order to compare the two methods, particularly that arising from pressure change in the pressurized collector. Figures 4 and 5 show calculations on the transient response respectively for the two methods for a 2% step increase

*Here β is the overall proportion of delayed neutrons, $a_d = a_{mt}(\bar{t}^*_m - \bar{t}^*_o)$; a_{mt} is the temperature coefficient of reactivity for the moderator, and $\bar{t}^*_m$ is the stationary moderator temperature averaged over the core.

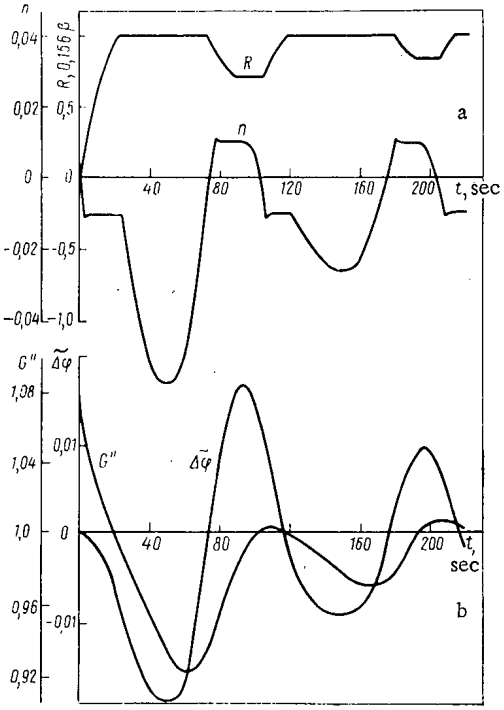

Fig. 4

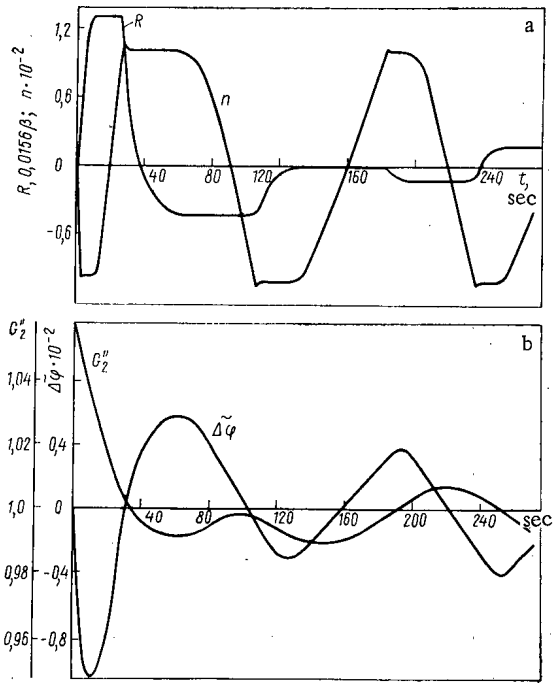

Fig. 5

Fig. 4. Transient response in a nuclear power station with RMBK reactors for the first method of feedwater supply arising from step increase in the pressure in the pressurized collector.

Fig. 5. Transient response in a nuclear power station with RMBK reactors for the second method of feedwater supply for a step increase in the pressure in the pressurized collector supplying 75% of the feedwater.

in the pressure in the pressurized collector above the nominal value. The calculations were performed via the OKA program with allowance for the overall power regulator. The overall weight assigned to the four automatic control rods was 0.312β; the reactivity coefficient were $a_f = \beta$; $a_s = 3\beta$; $a_d = 5\beta$. The heating time constants for the graphite and fuel were taken, respectively, as 4200 and 12 sec.

Figure 4a shows the relative deviation of the neutron flux n from the stationary value together with the reactivity R introduced by the automatic control rods. At 23 sec in the transient response, the automatic control rods reach the limit switches, and the deviation in the neutron flux goes outside the limits of the dead zone for the general power regulator. At 50 sec this deviation exceeds 5%. Then there are power-level fluctuations with a period of about 1.5 min. Figure 4b illustrates the variation in the relative feedwater flowrate G" and the increment in the mean steam content in the core $\tilde{\Delta}\varphi$. It is clear than an increase in pressure in the pressurized collector causes a virtually instantaneous increase in G" of about 5%. Then oscillation in the feedwater flow is set up with a period of about 1.5 min. There is a certain fall in $\tilde{\Delta}\varphi$ during the first 20 sec of the transient response, which is partly due to the increase in pressure in the separator drum as G" increases. From 20 sec onwards, there is a perturbation in the water enthalpy at the inlet to the core, which is due to the increase in G", and a sharp fall in $\tilde{\Delta}\varphi$ begins. Figure 5 shows the transient response in the second method. The relative feedwater flowrate in the group collectors is denoted by G_2''. Figure 5a shows that the power fluctuations in this method will lie almost entirely within the dead zone. The period of these fluctuations is about 2 min. The power-control system utilizes less than 7% of the total weight of the automatic control rods.

Figures 4 and 5 show that the deviations of the variables during the transient response in the response in the first method are appreciably larger than those in the second one. The only exception is the initial part of the transient response (about 30 sec). Here the difference in behavior for $\Delta\tilde{\varphi}$ occurs because the transport delay in the enthalpy at the inlet in the first method is substantially larger than that in the second. Also, in the latter method the change in flow rate to the group collectors influences the input enthalpy immediately.

There are fluctuations in feedwater flow rate in Fig. 4b and Fig. 5b; in general, these fluctuations can be caused by the operation of the general power regulator and by the water level in the separator drum. However, the main reason for the fluctuations in feedwater flow rate were shown by additional calculations with the general power regulator switched out to be due to instability on the fundamental in the neutron distribution. In fact, the power-level fluctuations are due to oscillation of the feed valve in the level regulator, and consequently to oscillations in the feedwater flow rate.

If collector feed is to be employed, it is desirable to improve the response of the pressure control system for the separator drum, because under certain emergency conditions (e.g., if the AZ-5 emergency protection is wrongly operated) there will be a considerable fall in pressure in the separator drum.* The deviation from saturation for the water in the separator drum tube is less in the second method than it is in the first, so the cavitation margin in the principal pumps may be reduced somewhat. Calculations show that this reduction will not occur if the time constant of the turbine synchronizer is about 10 sec. Also, the dynamic charteristics of the nuclear power station in these modes of feedwater supply are appreciably influenced by the parameters of the pressure-control system and the water-level control for the separator drum.

We are indebted to E. F. Sabaev for a discussion of the results.

LITERATURE CITED

1. I. Ya. Emel'yanov et al., At. Energ., 43, No. 6, 458 (1977).
2. V. I. Budnikov et al., At. Energ., 45, No. 5, 331 (1978).
3. A. P. Aleksandrov and N. A. Dollezhal', At. Energ., 43, No. 5, 337 (1977).
4. V. I. Budnikov and S. V. Kosolapov, Dep. No. 2841-78, VINITI, Moscow (1978).

*Calculations show that the time constant of 50 sec for the turbine synchronizer may result in a pressure fall in the separator drum of about 1.5 MPa.

MEASUREMENTS OF ^{239}Pu AND ^{235}U FISSION CROSS SECTIONS AND THEIR RATIO FOR NEUTRON ENERGIES FROM 100 eV to 50 keV

A. A. Bergman, A. G. Kolosovskii,
S. P. Kuznetsov, A. N. Medvedev,
A. E. Samsonov, and V. A. Tolstikov

UDC 539.173.4.162.3

The meaurement procedure was partially described earlier [1, 2]. We note only the experimental details which differ essentially from those reported previously. The measurements were performed in an isotopic neutron field formed in a lead cube during neutron moderation. The energy distribution of the neutrons is satisfactorily described by a Gauss function [1]. The corresponding relative width of the distribution function at half height is

$$\left(\frac{\tau_E}{\bar{E}}\right)=\left[\left(\frac{\tau_{E_0}}{\bar{E}_0}\right)^2\frac{\bar{E}}{\bar{E}_0}+(0.34)^2\left(1-\frac{\bar{E}}{\bar{E}_0}\right)+\frac{\bar{E}\ (\text{keV})}{183}\right]^{1/2},$$

where $\tau_E/\bar{E}=0.5$ at $E_0=30$ keV [3]. The quantity $\bar{E}$ (keV)/183 is due to the additional broadening of the spectrum resulting from the duration of the neutron burst Δt equal to 0.5 μsec.

Normalization measurements were performed by a nonstationary method with a period of 6100 μsec in a 120 × 80 × 100 cm graphite prism with a 20 × 20 × 40 cm cavity. The values were normalized to the thermal cross sections corrected for the deviation of the cross sections from the 1/v law in the region of the Maxwellian spectrum (Table 1).

Translated from Atomnaya Énergiya, Vol. 49, No. 1, pp. 19-21, July, 1980. Original article submitted August 20, 1979.

0038-531X/80/4901-0439$07.50

TABLE 1. Thermal Cross Sections Used for Normalization

Nuclide	σ_f (2200 m/sec)	Westcott factor	σ_f corr
^{239}Pu	742,0±2,1 b* [4]	1,052 [5]	780,6 b
^{235}U	585,7±1,1 b [4]	0,977 [5]	572,6 b

*1b = 10^{-28} m^2.

Detectors. Fission fragments were recorded by identical ionization chambers with layers of ^{239}Pu (20 mg) and ^{235}U (40 mg) in a common volume. The chamber was filled with a mixture of Ar + 50% CH_4 at a pressure of $2 \cdot 10^5$ N/m^2. The collection time of charges on the electrodes did not exceed 35 nsec. The energy dependence of the neutron flux was measured with standard SNM − 20 and SNM − 3 boron counters. The measurement procedure with the boron counters was chosen so that the efficiency of counting ^{10}B (n, α) events did not depend on the neutron energy. The recoil atoms from neutrons produced in the counter gas were not recorded.

Measurements and Processing of Results. The ^{239}Pu and ^{235}U fission fragment counting rates − I_f^9 and I_f^5 − were measured simultaneously with the fission chambers. The counting rate I_f of ^{10}B (n, α) events was measured with the boron counter.

The fission cross sections and their ratio are determined from the expressions

$$\sigma_f(\bar{E}) = A \frac{I_f(\bar{E})}{I_B(\bar{E})} \frac{1}{\sqrt{\bar{E}}} \frac{1+\gamma(\bar{E})}{1+\delta(\bar{E})};$$

$$\frac{\sigma_f^9(\bar{E})}{\sigma_f^5(\bar{E})} = B \frac{I_f^9(\bar{E})}{I_f^5(\bar{E})} \frac{1+\delta^5(\bar{E})}{1+\delta^9(\bar{E})},$$

where $1 + \delta(\bar{E})$ is the correction for the spectrometer resolution; $1 + \lambda(\bar{E})$ is the correction for the deviation of the cross section from the 1/v law [6]; A and B are normalization factors.

Structure of Corrections and Measurement Errors. The mean square error for $I_f(\bar{E})/I_B(\bar{E})$ and $I_f^9(\bar{E})/I_f^5(\bar{E})$ does not exceed 1.5% for individual time channels, and results mainly from the statistical spread (90%). The combined errors of the reference thermal cross sections (Table 1) and the normalization for the ^{239}Pu and ^{235}U fission cross sections and their ratios is 0.7%.

An accurate correction for recycled neutrons contributed no more than 2%. The error arising from the production of background neutrons at times close to the time of a neutron burst was determined experimentally. For the fission cross sections and their ratio it was at most 0.3% for E ≈ 5-15 keV. The error resulting from the increase in the efficiency of counting ^{10}B (n, α) events for faster neutrons did not exceed 0.2% at $\bar{E}_m \approx 50$ keV.

An accurate correction (0.6%) was introduced for the absorption of thermal neutrons in the SNM-3 counter gas. Absorption in other structural materials of the detectors introduces an error of 0.2-0.3% into the fission cross sections and 0.1% into their ratio. A correction was introduced for the deviation of the ^{10}B (n, E) cross section from the 1/v law in accord with [6].

The error in determining the time of recording of events was determined mainly by the speed of response of the detectors. For the ^{239}Pu and ^{235}U chambers this inaccuracy did not exceed ±0.02 μsec, and for the boron counter ±0.03 μsec, which gives a maximum error of 1.8% in the determination of the fission cross sections at E ≈ 50 keV.

The error from the inaccuracy in determining the avreage neutron energy from the slowing down time is maximum in the region below 0.5 keV for ^{235}U and below 1 keV for ^{239}Pu. It does not exceed 2% for the ^{239}Pu fission cross section, 1.5% for ^{235}U, and 2% for their ratio. Corrections for the spectrometer resolution were introduced into σ_f (^{239}Pu) and σ_f (^{235}U) for neutron energies of 3-50 and 1-50 keV, respectively. At these energies the fission cross sections vary smoothly with energy, and are approximated by the expres-

TABLE 2. Data on ^{235}U Fission Cross Section

E_n, keV	Deviation from mean, %									A		B (present work)		B − A, %
	Lemley [7] 1971	Gayther [8] 1972	Blons [9] 1973	Perez [10] 1974	Mostovaya [11] 1975	Kononov [12] 1975	Gwin [13] 1976	Czirr [14] 1976	Muradyan [15] 1977	$\bar{\sigma}_f$, b [7–15]	error, %	$\bar{\sigma}_f$, b	error, %	
0,1—0,3	+0,6	—	+2,5	—	+1,6	—	−1,4	−3,1	−0,1	20,39	0,8	20,42	1,5	+0,2
0,3—1,0	−1,9	—	+3,5	—	+2,5	—	−2,0	−4,8	+2,8	11,31	1,4	11,65	1,1	+3,0
1—3	−6,0	—	+5,3	—	+3,9	—	−1,3	−4,2	+2,2	7,17	1,95	7,29	0,9	+1,6
2—5	−5,9	+5,6	+3,3	+2,1	+1,6	—	−4,4	—	−2,0	4,811	1,6	4,767	0,9	−0,9
5—10	−6,0	+2,5	+2,9	+2,4	+1,6	—	−4,3	—	+0,9	3,303	1,4	3,259	1,0	−1,3
2—10	−5,0	+5,0	+4,1	+3,3	+2,6	—	−3,4	−7,2	+0,6	3,830	1,6	3,824	1,0	−0,2
10—20	−4,6	+3,3	+3,7	+3,2	—	−3,8	+0,4	+4,5	+2,4	2,450	1,3	2,487	1,2	+1,5
20—30	−1,8	+1,2	+2,8	+1,7	—	+1,8	−1,4	−5,8	+1,4	2,140	0,65	2,085	1,4	−2,6
30—40	−3,9	−0,1	—	+4,3	—	+1,6	−2,0	—	—	1,980	1,4	1,906	1,6	−3,6
40—50	−2,3	+2,4	—	+5,6	—	+2,2	−1,5	−6,4	—	1,848	1,7	1,798	1,6	−2,6

sion E^{-p}. In this case $\delta(\bar{E}) \approx \frac{1}{2}(p^2 - 0.25)\ (1/8\ln 2)(\tau_E/\bar{E})$. The corrections to the fission cross section for the resolution do not exceed 1.3%, and for the ratio of the cross sections 0.2% in the energy ranges indicated above.

Discussion of Results.* Table 2 lists the average values of the data from [7-15] on the ^{235}U fission cross section averaged over the energy intervals indicated, and their mean square errors calculated on the assumption of equal weights (column A). Only their deviations from the mean are listed. Our results are listed in column B. The energy ranges are chosen so that the resolution does not affect the results because of structure in the cross section. It is clear that the results are in good agreement with the average values (column B − A) within the limits of error of the average values and the errors of our measurements. The data of Czirr are normalized to the thermal cross section as in the present work, but in the 2-50 keV range they are ≈6% lower than our values and the average data. The ratio of Kononov's data to ours is constant in and above the 20-50 keV range, but decreases by about 8% in the 10-20 keV range, and ≈6% in comparison with the average data.

The distortion of the energy dependence of the fission cross section reported in some papers for an appreciably relative change of energy appears to be the result of faulty corrections for effects related to neutron scattering. There are also possible normalization errors in those papers. The good agreement of our data with those of Muradyan [16] should be noted (Table 2). An analysis of his procedure shows that systematic errors may arise with increasing energy, but up to 10 keV these data are reliable (~1% error). In the 20-30 keV range his error increases to 3%.

The recommended data of Kon'shin [17] (1975) for ^{235}U at 1-keV intervals, renormalized in the 2-10-keV range to our data, are in good agreement with our results up to 50 keV, and show that in the 5-50-keV range there is no structure in the fission cross section which could lead to systematic errors in the determination of the cross sections averaged over standard intervals. It can be concluded from all the above that our data for ^{235}U are reliable, and consequently also the values for ^{239}Pu, since they were obtained by the same method and simultaneously.

The spread of all the existing data for σ_f (^{239}Pu) is large. Table 3 lists data for the indicated energy ranges with relative errors (column B). The intervals were chosen so that the spectrometer resolution did not affect the results because of the presence of structure in the cross section. Table 3 also lists values from papers by Gwin, Gayther, and Ryabov, their average values (column A), and the deviation of the average value from our data (column B − A). These data show nearly the same energy dependence except in the 0.7-1-keV range where Ryabov's data agree with ours, but Gwin's values are 8% lower. In the 0.1-6-keV range the average values reported by these experimenters are about 5% lower than ours; in the 6-20-keV range they are nearly the same, and in the 20-50-keV range they are ≈4% higher.

Our values for the ratio of the ^{239}Pu and ^{235}U fission cross sections over the energy intervals are in good agreement with Carlson's data [20] (Table 4). Carlson's data were normalized by the threshold method and also to Lemmel's data [21], which in turn were normalized to the thermal region. The totality of the data

*A more detailed discussion of the work with tables of data for all points and data over unconsolidated standard intervals will be published in the "Nuclear Constants" compilation.

TABLE 3. Data on the ^{239}Pu Fission Cross Section

E_n, keV	Gwin [13]	Gaither [18]	Ryabov [19]	$\bar{\sigma}_f^A$, b [13, 18, 19]	B (present work) $\bar{\sigma}_f$, b	B (present work) total error, %	B−A, %
0,1—0,3	17,93	—	18,022	17,98	19,29	1,9	+7,0
0,3—1,0	8,022	—	8,391	8,206	8,409	1,9	+2,5
0,7—1,0	6,09	—	6,599	6,340	6,612	1,8	+4,2
1—6	3,114	3,127	3,064	3,102	3,252	1,5	+4,9
6—10	2,09	2,054	2,080	2,075	2,078	1,3	+0,15
10—20	1,78	1,74	1,687	1,736	1,747	1,4	+0,6
20—30	1,64	1,615	1,597	1,617	1,560	1,5	−3,6
30—40	1,61	1,632	1,568	1,603	1,511	2,1	−6,0
40—50	1,54	1,552	1,519	1,537	1,490	2,1	−3,0

TABLE 4. Data on the Ratio of the ^{239}Pu and ^{235}U Fission Cross Sections

E_n, keV	A Carlson [20]	B (present work) σ_f^9/σ_f^5	B (present work) total error, %	B−A, %
0,1—0,3	—	0,939	1,3	—
0,3—1,0	—	0,715	1,6	—
0,7—1,0	0,697	0,688	1,5	−1,3
1—6	0,622	0,639	1,4	+2,7
6—10	0,656	0,664	1,4	+1,2
10—20	0,710	0,706	1,2	−0,6
20—30	0,749	0,749	1,4	0
30—40	0,818	0,794	1,6	−3,0
40—50	0,834	0,829	1,6	−0,6

listed on the ^{235}U fission cross section, Carlson's data, and our results for the ratio of the fission cross sections are inconsistent with the average energy dependence of σ_f (^{239}Pu) reported in recent papers by Gwin, Gayther, and Ryabov.

LITERATURE CITED

1. F. Shapiro, in: Tr. Fiz. Inst. Akad. Nauk, 24, 3 (1964).
2. A. A. Bergman et al., Nuclear Constants [in Russian], No. 7, Atomizdat, Moscow (1971), p. 50.
3. A. A. Bergman and A. Malikzhonov, Kratk. Soobshch. Fiz., No. 4 (1972), p. 71.
4. H. Jackson et al., Review of Standard Reference Data and Important Cross Section Discrepancies, ANL, Argonne, Ill., Nov. (1976), p. 63.
5. J. Donald, Neutron Effective Cross Sections [Russian translation], Moscow (1959).
6. M. Sowerby et al., J. Nucl. Eng., 24, 323 (1970).
7. J. Lemley et al., Nucl. Sci. Eng., 43, 281 (1971).
8. D. Gayther et al., in: Proc. Conf. Second Panel on Neutron Standard Reference Data, IAEA, Vienna (1972).
9. J. Blons, Nucl. Sci. Eng., 51, 130 (1973).
10. R. Perez et al., Nucl. Sci. Eng., 55, 203 (1974).
11. T. A. Mostovaya et al., in: Proc. Conf. on Neutron Physics [in Russian], Vol. 6, TsNIIatominform, Moscow (1976), p. 76.
12. V. N. Konov, At. Energ., 38, 82 (1975).
13. R. Gwin et al., Nucl. Sci. Eng., 59, 79 (1976).
14. J. Czirr et al., Nucl. Sci. Eng., 60, 383 (1976).
15. T. V. Muradyan et al., in: Proc. Conf. on Neutron Physics [in Russian], Vol. 3, TsNIIatominform, Moscow (1977), p. 119.

16. T. V. Muradyan et al., ibid., p. 113.
17. G. V. Antsipov et al., Nuclear Constants [in Russian], No. 20, Part 2, Atomizdat, Moscow (1975), p. 3.
18. D. Gayther [11], p. 49.
19. Yu. V. Ryabov, At. Energ., 46, 154 (1979).
20. G. Carlson and J. Behrens, Nucl. Sci. Eng., 68, 205 (1978).
21. H. Lemmel, in: Proc. Conf. on Nuclear Cross Sections and Technology, NBS Special Publ. 425.1-286, Washington, D. C. (1975).

BRITTLE FRACTURE OF STEEL ELECTROLYTICALLY SATURATED WITH HYDROGEN*

G. Biggiero, A. Borruto, and F. Marafini

UDC 621.039.531

Earlier investigations of the behavior of steel when it is saturated with hydrogen have shown that embrittlement takes place, especially in specimens containing inclusions. Therefore, in order to determine the fracture parameters, we used steel from an experimental melt which had a minimal inclusions content. The results obtained were compared with data on fracture analysis by means of a "Stereoscan" scanning microscope and were examined on the basis of the nature of the distribution of the inclusions.

In the experiments, at various current densities, we observed a wide dispersion of the data, the reason for which may be assumed to be the large fluctuations in the amount of inclusions in the specimens. Fractographic investigation revealed "lines of rest" very similar to those observed in fatigue fracture. However, in the case of fatigue fracture these lines reflect the existence of ductile and brittle fracture, whereas in the case of hydrogen saturation they occur because of longitudinal cracks which apparently depend on the current density.

Steel Investigated. We used standard heat-treated 38NiCrMo4 steel (Table 1). The specimens used for corrosion tests under load were made from a single ingot and had the shape of rods with a polished surface on the working segment (Fig. 1). The large-grained ferrite–pearlite structure is typical of rolled steel subjected to prolonged annealing.

Because of the instability of martensite, for the purpose of obtaining a structure most sensitive to hydrogen embrittlement, we used the following treatment to produce low-temperature bainite: austenitization at 860°C for 30 min; bainite transformation at 350°C for 40 min; cooling in air to room temperature. After the heat treatment of the specimens, the surface layer of salts and oxide was removed by polishing with No. 600 abrasive paper. The properties of the specimens are shown in Table 2.

Apparatus. The scheme of the apparatus for loading the specimens in the process of electrolytic saturation with hydrogen is shown in Fig. 2. The test specimen, loaded by means of a system of pulleys, serves as the cathode of the electrolytic cell. The anode consists of a platinum wire spiral placed around the specimen at a distance of 3 cm. The electrolyte used was a 0.1 N or 0.3 N solution of sulfuric acid. Before testing, the specimens were covered with a layer of Teflon, so that the only part left open for hydrogen saturation was the working segment, whose surface area was calculated by Guldino's method. The specimens were stored in paraffin oil and washed with acetone before being placed in the test apparatus.

*The article was written especially for our journal. Translated from English by L. N. Ryabchikov.

Metallurgical Institute of the University of Rome, Italy. Translated from Atomnaya Énergiya, Vol. 49, No. 1, pp. 22-25, July, 1980. Original article submitted May 28, 1979.

0038-531X/80/4901-0443 $07.50

TABLE 1. Brand Composition and Chemical Analysis of the Steel

Steel	Composition, mass %							
	C	Si	S	P	Ni	Cr	Mo	Mn
38NiCrMo4	0,34—0,42	⩽0,40	—	—	0,70—1,00	0,70—1,00	0,15—0,25	0,50—0,80
Specimen	0,38	0,32	0,024	0,01	0,81	0,72	0,16	0,76

TABLE 2. Mechanical Properties of Specimens after Heat Treatment

Composition of specimen	H_V, kgf/mm² (1 kgf/mm² = 9.8 MPa)	σ_b, kgf/mm²*
Completely annealed	194	67
After austenitization at 860°C and aging at 350°C	410	134

*Mechanical tests were conducted on the specimens to study corrosion under load.

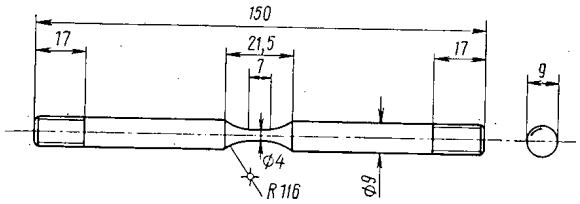

Fig. 1. Specimen for corrosion tests. The surface area of the working segment is equal to 3.72 cm².

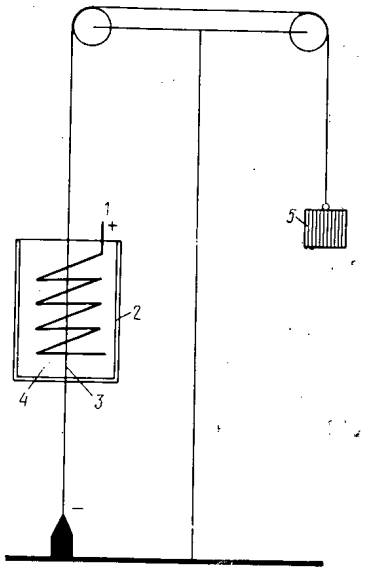

Fig. 2. Apparatus for loading the specimen: 1) platinum anode; 2) glass cup; 3) specimen serving as cathode; 4) electrolyte; 5) load.

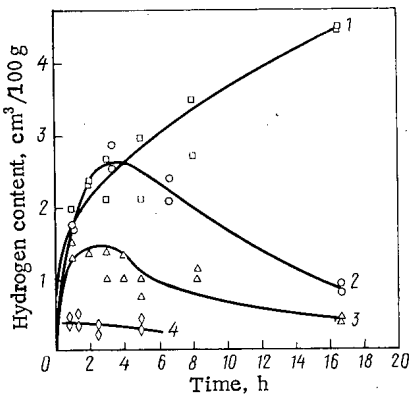

Fig. 3. Total hydrogen content in KhS80 steel as a function of duration of electrolysis and current density (1, 2, 3, and 4 correspond to current densities of 10, 5, 2.5, and 1 mA/cm^2; 2, 3, and 4 were obtained with blackening of the specimen).

Method of Investigation. During the prolonged tests the specimens became covered with a black film, the formation of which was accompanied by the dissolution of Fe^{2+}, so that the fracture took place not because of hydrogen embrittlement but because of the reduction in the specimen cross section. The time of onset of this blackening depends on the current density and the purity of the steel (Fig. 3). After the blackening of the specimen the rate of dissolution is independent of the current in the electrolytic cell, and for steel of the specified composition it approximates the rate of dissolution of the metal at its corrosion potential.

The results of the tests were affected not only by the reduction in the cross section of the specimen but also by the sharp drop in the hydrogen content of the steel, which was clearly noticeable at a current density of 1-2 mA/cm^2, when after several hours of exposure the specimen became completely blackened, but it was fractured only several days later because of the reduction in the cross section and not because a crack had developed. This behavior may be explained by two factors: in the first place, the considerable increase in time before fracture at low values of current density and, in the second place, the reduction (almost to zero) of the hydrogen content in the metal after exposure for a short time.

The electrochemical explanation of the blackening of the specimen is based on the effect of the potential acting on it, which lies between the corrosion and equilibrium values [1]. In order to eliminate this extraneous phenomenon, it is sufficient to increase the current in the electrolytic cell. At a current density of 4 mA/cm^2 the blackening was observed for about 40 h, whereas at 10 mA/cm^2 it began, in a very weak form, only after 60 h. In order to obtain the most reliable results, we used current densities at which the fracture occurred much earlier than the phenomenon described above.

Results of the Tests. Under identical test conditions, some specimens fractured very rapidly, while others resisted prolonged loading. Because of the wide scatter of the data, it was impossible to draw any conclusions concerning the effect of the current density on the limit of long-term corrosion resistance. The data available in the literature indicate that there is no such effect.

An analysis of the fracture surface using the scanning electron microscope showed that for a current density of 16 mA/cm^2 the specimen exhibited a number of large cavities localized primarily around the external surface (Fig. 4). At first it was assumed that the dispersion of the test results was due to the formation and localization of pores under the influence of the rapid penetration of hydrogen into the metal. However, this assumption was not confirmed, since the dispersion did not disappear even at lower current densities, although there were marked changes in the morphology of the fracture. Earlier, in the investigation of the mechanical properties of high-purity steel, it was noted that the deviation of the results may be due to a nonuniform distribution of small quantities of phosphorus. This gives reason to believe that the observed dispersion in the experimental data is also due to the nonuniform distribution of a very small number of inclusions in the matrix of the steel [2, 3]. It may even be asserted that for every specimen there exists a particular value of the long-term corrosion resistance limit, which depends on the number and distribution of inclusions. To corroborate this assertion, we used a method similar to the one generally used in tests of long-term resistance. Each specimen was subjected to the action of fixed, gradually increasing loads, and by

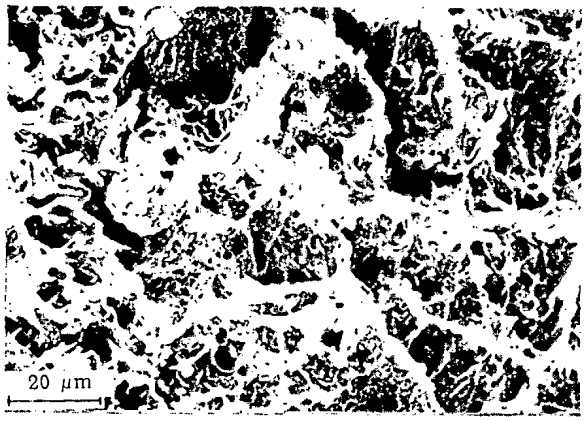

Fig. 4. Fracture of a specimen which failed after 0.7 h at 60 mA/cm^2 and a stress of 696 MPa.

Fig. 5. Fracture of a specimen which failed after 1.1 h at 16 mA/cm^2 and a loading of 627 MPa.

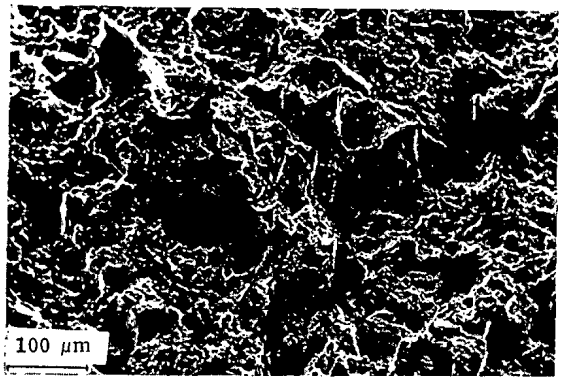

Fig. 6. Formation of micropores and microcracks in a specimen which failed after 1.6 h at 4 mA/cm^2 and a stress of 696 MPa.

maintaining each load for a sufficiently long time, we were able to guarantee that the stress acting on the specimen remained below the long-term corrosion resistance limit as determined by the usual tests. The long-term corrosion resistance limit calculated by the new method apparently will not coincide with the value obtained by the conventional method for absolutely identical specimens having exactly the same distribution of inclusions, but it will not differ too much from the value found by the same method for the other specimens of the given series. Thus, we can ascertain the effect of unequal values of inclusions content in different specimens.

Fractography. The specimens for fractographic analysis were cut from the test specimens at distances of about 0.5 cm from the point of fracture. An analysis of the fracture surface enabled us to establish three main properties of the structure: the presence of a series of lines, which may be called "lines of rest" and are extraordinarily similar to the widely known fatigue lines; the presence of longitudinal cracks in the central zone of the fracture; and the variation of the nature of the fracture as a function of the current density. The lines of rest are traces of regions in which the development of the failure terminated. This termination in the present case is due to the presence of longitudinal cracks formed by the action of hydrogen. Such longitudinal cracks reduce the concentration of the stresses, as a result of which there is a halt in the development of the crack at the applied loading. The arc-like shape of the crack indicates its symmetric development from the initial point and also the uniform arrangement of the longitudinal cracks. After the propagation of the crack stops, there is further hydrogen embrittlement of the area around the end of the crack, enabling it to grow again until its next intersection with another longitudinal crack. This intermittent propagation of the crack can be clearly seen in a fractograph of the specimen (Fig. 5).

Under the action of this mechanism, there is formed a crack which is microscopically very similar to a fatigue crack but is distinguished by certain features characteristic of ductile fracture, e.g., the presence of separate fibers subjected to tension.

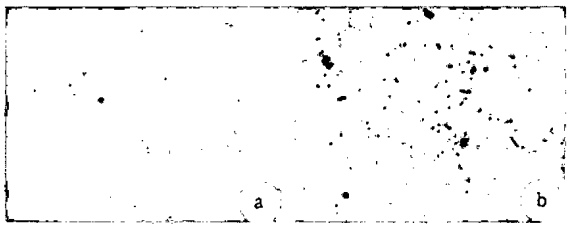

Fig. 7. Inclusions in the steel investigated. a) Specimen which did not fail; b) specimen which failed, ×100.

The formation of micropores and microcracks, clearly visible in the specimen shown in Fig. 6, can be attributed to the recombination of atomic hydrogen on the surface of the inclusion. The distribution of the hydrogen content within the specimen is very nonuniform, and the maximum concentration must obviously appear at the surfaces at which the failure begins. Confirming this, we observed the maximum concentration of molecular hydrogen at the surface of the inclusions and that of atomic hydrogen at the boundaries of the grains. The observed longitudinal cracks and cavities are the result of internal bubbles of hydrogen. From this it follows that the molecular hydrogen exerts pressure on the fibers of the material in a direction perpendicular to the direction of the applied tensile stress. If the fibers in the specimen are oriented in the direction of the loading, then the ratio of the ultimate strength to the long-term corrosion strength limit must reach very high values (for the steel investigated it amounts to about 2.23). At high current densities the hydrogen pressure has a favorable effect on the coalescence of the pores that are formed (see Fig. 4).

Analysis of Inclusions. The specimens for analysis were selected from those in which the tests revealed a maximum deviation of the properties. Most of the tested specimens did not fail. The observed large dispersion in the test results should be attributed to the effect of the inclusions present; the inclusions content varied sharply (Fig. 7). The data obtained must be further verified by other methods, but they provide a way of explaining the observed dispersion in the results and to confirm the theories based on a study of the role of inclusions [2-4].

LITERATURE CITED

1. H. Margot et al., Mém. Sci. Rev. Mét. (1976).
2. C. Briant et al., Metall. Trans., 9A (May, 1978).
3. S. Banerji et al., ibid., February.
4. De Vito et al., private communication.

CERTAIN THERMODYNAMIC PROPERTIES OF URANIUM NITRIDE UN_y

Yu. F. Khromov and R. A. Lyutikov

UDC 536.422.15

The vaporization and thermodynamic properties of uranium nitride have been the topic of many investigations [1-10]. It seems to us however that most of these investigations suffer from certain methodological deficiencies. For example, in an investigation of the vaporization of uranium nitride corresponding to the $UN_{sol} + U_{liq}$ phase range [2-7], the thermodynamic properties of the boundary alloy have been estimated without taking into account their changes in the homogeneity range. Vapor pressure over UN has been measured for one component only (either nitrogen or uranium). Moreover, the content of UN due to solid-phase interaction with the crucible material and predominant vaporization of nitrogen shifts rapidly from the homogeneous to the two-phase range.

Accordingly, we have undertaken to measure the equilibrium partial vapor pressure of both UN components using the technique [11] based on the integral Knudsen method, and to calculate certain thermodynamic properties of UN_g. The cell material was zirconium nitride, the investigated uranium nitride serving as a reflector.

The results of measuring the equilibrium uranium and nitrogen pressures for UN of various composition in the 1750-2250°K temperature range are shown in Fig. 1.* The figure also shows analogous data for ZrN and certain other published data [3, 9, 10]; the values of nitrogen pressure over UN [10] obtained under conditions of solid and gas phase equilibrium have been extrapolated to temperatures encountered in our work.

The results have been processed using the Gibbs–Duheme equation. Since at equilibrium T = const and P = const, we have

$$C_U \delta\mu_U + C_N \delta\mu_N = 0,$$

where C is the number of moles of nitrogen and uranium and μ is the chemical potential. Introducing a new variable $y = C_N/C_U$ and passing to component pressures, we have

$$d \ln P_U/P_U^0 + y d \ln P_N = 0,$$

where P_U^0 denotes vapor pressure of pure uranium.

The constant of the reaction $2N \rightarrow N_2$ has the form

$$K_p = P_{N_2}/P_N^2,$$

whence

$$\ln P_{N_2} = \ln K_p + 2 \ln P_N.$$

After substituting we find the desired equation:

$$\ln \frac{P_{1U}(y_2)}{P_{2U}(y_1)} = -\frac{1}{2}\int_{y_1}^{y_2} y d \ln P_{N_2}.$$

This equation was used to plot the variation of partial pressures of uranium and nitrogen (Fig. 2) over UN_y uranium nitride in the homogeneity region; the ratio N/U was determined to within ±0.0005.

*1 mm Hg = 133.322 Pa; 1 atm = 101,325 Pa.

Translated from Atomnaya Énergiya, Vol. 49, No. 1, pp. 25-28, July, 1980. Original article submitted April 10, 1979.

0038-531X/80/4901-0448$07.50

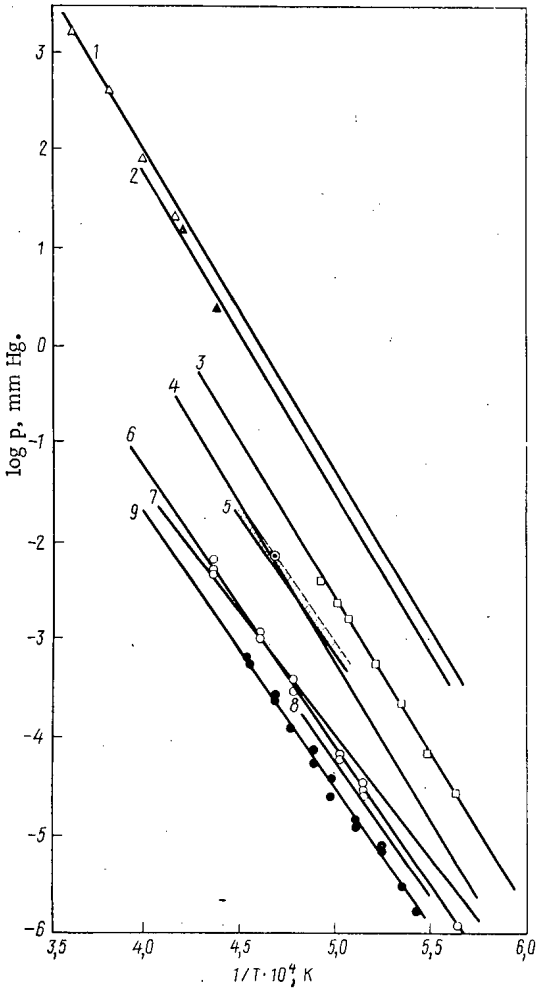

Fig. 1. Temperature dependence of partial nitrogen and uranium pressures over nitrides of different compositions: 1) $\log P^{N_2}_{UN_{0.996}} = 14.6 - (3.19/T)\cdot 10^4$ [10]; 2) $\log P^{N_2}_{UN_{0.992}} = 14.43 - (3.2/T)\cdot 10^4$ [10]; 3) $\log P^{N_2}_{U(NOC)_{0.990}} = 13.26 - (3.17/T)\cdot 10^4$ (our experiments); 4) $\log P^{N_2}_{UN+U_{liq}} = 12.75 - (3.2/T)\cdot 10^4$ [9]; 5) $\log P^{N_2}_{TiN} = 10.844 - (2.785/T)\cdot 10^4$ [11]; 6) $\log P^{U}_{U(NOC)_{0.986}} = 10.98 - (3.05/T)\cdot 10^4$ (our experiments); 7) $\log P^{U}_{U_{liq}+UN} = 8.77 - (2.55/T)\cdot 10^4$ [3]; 8) $\log P^{N_2}_{ZrN} = 9.45 - (2.74/T)\cdot 10^4$ (our experiments; 9) $\log P^{U}_{UN_{0.990}} = 10.95 - (3.1/T)\cdot 10^4$ (our experiments).

Using the obtained values of $1/2 \log P_{N_2}$ and $\log P_U$ at 2000 and 1800°K we have obtained analytic relations that describe partial pressures and activities of the components of various UN_y compositions (Table 1).

Table 1 indicates that $\Delta H^{S}_{U;\ 1/2N_2}$ depends weakly on N/U. It can also be noted that the chosen lower boundary of the homogeneity range corresponds to the composition $UN_{0.985}$ which is close to the mean of $UN_{0.996}$ [10] and $UN_{0.96}$ [3].

The upper boundary has been assumed to correspond to the composition $UN_{1.0}$ [9, 12]. Vapor pressure for pure uranium has been determined from [13]

$$\ln P^{0}_{U} = 5.77 - \frac{2.55}{T}\cdot 10^4.$$

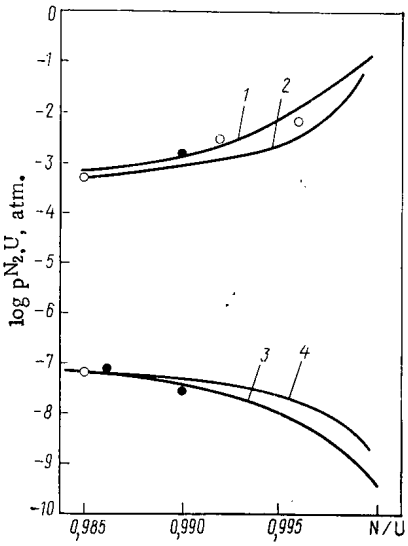

Fig. 2. Partial pressure of nitrogen and uranium over UN_y nitrides in the homogeneity range at 2000°K:
1) $\log P_{N_2}^{1/2}$ (experiment); 2) $\log P_{N_2}^{1/2}$ [9, 12] (calculated);
3) $\log P_U$ (experiment); 4) $\log P_U$ [3, 12] (calculated);
●) our data; ○) data adopted from [3, 9, 10].

TABLE 1. Temperature Dependence of Partial Pressure and Heat of Sublimation of Nitrogen and Uranium for UN_y Nitrides Corresponding to the Homogeneity Range

Composition	$1/2 \log p_{N_2}$ atm $= A - B/T \cdot 10^4$		$\Delta H_{1/2\,N_2}$, kcal * / g·atom	$\log p_U$ (atm) $= A - B/T \cdot 10^4$		$\log a_U = A - B/T \cdot 10^4$		ΔH_U^s, kcal / g·atom
	A	B		A	B	A	B	
$UN_{1,0}$	7,27±0,15	1,60±0,02	73,2±0,5	3,39±0,25	2,54±0,03	−2,38	−0,01	120,8±1,5
$UN_{0,996}$	6,14±0,15	1,60±0,02	73,2±0,5	4,47±0,25	2,54±0,03	−1,30	−0,01	120,8±1,5
$UN_{0,995}$	5,96±0,15	1,60±0,02	71,8±0,5	4,65±0,25	2,54±0,03	−1,12	−0,01	120,8±1,5
$UN_{0,992}$	5,38±0,15	1,57±0,02	71,8±0,5	5,02±0,25	2,54±0,03	−0,75	−0,01	120,8±1,5
$UN_{0,990}$	5,14±0,15	1,57±0,02	71,8±0,5	5,20±0,25	2,54±0,03	−0,57	−0,01	120,8±1,5
$UN_{0,986}$	4,84±0,15	1,56±0,02	71,8±0,5	5,40±0,25	2,54±0,03	−0,37	−0,01	120,8±1,5
$UN_{0,985}$	4,79±0,15	1,56±0,02	71,8±0,5	5,60±0,25	2,54±0,03	−0,17	−0,01	120,8±1,5

*1 cal = 4.1868 J.

TABLE 2. Values of the Constant Kp for the Reaction $UN_{1.0} = U_g + 1/2N_2$

T, °K	$\lg K_p = 10,66 - \frac{4,115}{T} \cdot 10^4$	$\lg K_p = 11,16 - \frac{4,30}{T} \cdot 10^4$ [3]	T, °K	$\lg K_p = 10,66 - \frac{4,115}{T} \cdot 10^4$	$\lg K_p = 11,16 - \frac{4,30}{T} \cdot 10^4$ [3]
1750	−12,84	−13,35	2100	−8,93	−9,32
1850	−11,54	−12,06	2150	−8,47	−8,84
1950	−10,40	−10,86	2200	−8,04	−8,39
2000	−9,91	−10,34	2250	−7,64	−7,98
2050	−9,26	−9,69			

It is interesting to discuss the obtained data and to compare certain thermodynamic characteristics of $UN_{1.0}$ with published data. The monotonic dependence of nitrogen and uranium pressures on N/U (see Fig. 2) proves that the compatibility of obtained results is acceptable in spite of considerable errors in the determination of the compositions. An analysis of the data of Table 1 and Fig. 1 also indicates that no congruent vaporization of UN can take place over the entire homogeneity range.

The value of the reaction constant (K_p) found for $UN_{1.0}$ is in good agreement (Table 2) with published data [3], particularly if one considers that the techniques used for investigating the vaporization were quite different. The heat of vaporization of UN_y [$UN_{y,\,sol} = U_g + y/2\,N_{2,\,g}$] was found to be $\Delta H^{ST}_{UN_{1.0}} = (194 \pm 5)$ kcal/g·atom which is close to the data of [3]. Good agreement has been obtained also in estimating the heat of vaporization from the relation

$$\Delta H^{S,\,298}_{UN_{1.0}} = T\left\{-R\ln K_p - \frac{\Delta (G_T - H^0_{298})}{T}\right\}.$$

For pure uranium $\Delta H^0_{298} = 125 \pm 2.5$ kcal/g·atom [14], the heat of formation of UN in the reaction $1/2N_{2,\,g} + U_{sol} = UN_{sol}$ amounts to 68.5 ± 3 kcal/g·atom which is close to the value (70.7 to 71.5) ± 1.1 kcal/g·atom obtained in [15, 16] by calorimetric measurements.

The data on the pressure of nitrogen and uranium over homogeneous nitride are quite reliable as indicated by the good agreement between certain thermodynamic characteristics obtained. These data can be compared with theoretical ones obtained on the basis of the well-known thermodynamic model proposed by Kaurman [2] using the relations

$$\bar{F}_N = F^0_N - F_{N+} + RT\ln\frac{y}{1-y};$$

$$\bar{F}_U = F^0_U - F_{U+} + RT\ln\frac{1-y}{4\alpha^2},$$

where $\bar{F}_U$ and $\bar{F}_N$ are partial free energies of nitrogen and uranium in the homogeneity range of UN_y; F^0_N and F^0_U, free energies of 1 g·atom of pure components (at normal pressure and T = 0°K); α, concentration of thermal vacancies in the nonmetallic sublattice (as compared to the total number of sites in the lattice); and F_{N+} and F_{U+}, free energies of formation of nitrogen and uranium vacancies in UN_y. At a constant temperature F_{N+} and F_{U+} are constant over the entire existence domain of UN_y; they were determined from available data [3, 9] for a two-phase domain and were found to be: $F_{U+} = -320.4 \pm 24.985\,T$ and $F_{N+} = 73200 - 14.18\,T$.

As seen in Fig. 2, the calculated values of partial pressure of nitrogen and uranium are in fair agreement with experimental ones differing by not more than a factor of five. Thus, the statistical thermodynamic model can be used for calculating temperature dependences of pressure and activity of nitrogen and uranium in the range of homogeneity of UN.

LITERATURE CITED

1. R. A. Andrievskii et al., At. Energ., 26, No. 6, 494 (1969).
2. K. Gingerich, J. Chem. Phys., 51, No. 10, 4433 (1959).
3. C. Alexander et al., J. Nucl. Mater., 31, 13 (1969).
4. W. Olson and R. Milford, J. Phys. Chem., 67, 953 (1963).
5. P. Yozzella and M. Crescente, "Thermodynamic properties of uranium mononitride." Tech. Rept. NPWAC-47918, October 1965.
6. D. Keller, "Development of uranium mononitride," 1st Quarterly Progress Report- Jan-March 1964. USAE-Euratom Report BM-1-x-10083, Eurals-10331 BM-1 Apr. 1964.
7. H. Inouye and I. Leitnaker, J. Am. Ceram. Soc., 51, No. 1, 6 (1968).
8. C. Hoenig, J. Am. Ceram. Soc., 54, 391 (1971).
9. H. Tugawa, J. Nucl. Mater., 51, 78 (1974).
10. R. Benz and W. Hutchison, J. Nucl. Mater., 36, 135 (1970).
11. Yu. F. Khromov et al., Zavod. Lab., 44, No. 3, 296 (1978).
12. L. Kaufman and E. Clougherty, Metallurgy of High Pressures and Temperatures, New York (1964), p. 322.

13. E. K. Storms, Refractory Carbides, Academic Press (1967).
14. J. Drowart, A. Pattoret, and S. Smoes, J. Chem. Phys., 42, 2629 (1965).
15. F. Oetting and H. Leitnaker, J. Chem. Thermodyn., 14, 199 (1972).
16. P. O'Hare et al., in: Thermodynamics of Nuclear Materials, IAEA, Vienna (1968), p. 265.

THERMODYNAMIC ANALYSIS OF THE INTERACTION OF $UO_{2\pm x}$ WITH CARBON

Yu. F. Khromov and R. A. Lyutikov

UDC 536.422.15.639.882

The interaction of $UO_{2\pm x}$ with carbon is of both scientific and practical interest [1, 2]. The degree of interaction and the type of equilibrium in the U–C–O system are determined by the conditions of the reaction flow, the composition of the reagents, and the ratios in the initial mixture. One of the characteristics of the equilibrium is the pressure of CO (P_{CO}), in the reservoir. Thus, the change of the carbon's activity considering the displacement of the compound from one area of the phase diagram into another, may change the CO pressure by a factor of about 10^5 [3, 4]. The corresponding displacement of equilibrium might cause a change in the UO_2 composition during the reaction as the oxygen potential of UO_2 in the region of homogeneity may be changed by more than a factor of four [5]. Up to now, many works have been published which are devoted to an analysis of equilibrium in separate areas of the U–C–O diagram [3, 4, 6, 7] and also to the changes of the oxygen potential of $UO_{2\pm x}$ [8]. However, the narrow intervals of temperature and composition considered make these data difficult to utilize under other conditions. Therefore, it would be expedient to determine, on the basis of the knowledge at hand, the functional dependence of ΔG_{O_2} (UO_2) on the temperature and the composition in order to carry out the supplementary measurements of the oxygen potential of $UO_{2\pm x}$ for an elaboration of the dependence obtained and to analyze the conditions for equilibrium in the U–C–O system.

In this work we present the results of measurements of the CO equilibrium pressure for the UO_2 + C system with an excess of carbon. The changes of the oxygen potential in the region of homogeneity of the $UO_{2\pm x}$ [2, 5, 8-10] are analyzed. We also calculate P_{CO} for the UO_2–UC_2–C system at 1500-2500°K. These results might be used to evaluate the possible growth of pressure in the microfuel elements with a core sample of $UO_{2\pm x}$ and a pyrocarbon coating. The equilibrium oxygen pressure is determined by the Knudsen method using direct mass-spectrometer measurements [11] of the equilibrium pressure P_{CO} for the system $UO_{1.9995}$ + C.

The omegatron transmitter RMO-4S was calculated using pure CO with supplementary recording of the ratio of the peaks, $I_{^{12}C}/I_{CO}$, which allowed for the reliable separation of the close peaks of the remaining nitrogen and CO. To ensure reliable contact of the solid reagents with the surface of the UO_2 particles with diameter 0.2 mm, a pyrocarbon coating was introduced by precipitation from the gas phase [12]. Previous experiments have shown that the carbon activity in the coating is close to unity. Approximately 5 g of the UO_2 particles were loaded into the Knudsen cell, which had a diameter 15 mm and a height of 25 mm. About 1/3 of the particles dod not retain the pyrocarbon coating. The equilibrium between the solid and gas phases was established after one minute. Desorbtion of the absorbed gases (CO, N_2, and others) was achieved by outgassing of the particles studied at 1273°K for 10-12 h. After the intensity of the CO peak was reduced below that of the background, the dependence of $P_{CO} = f(T)$ was measured in the range 1473-1723°K for 5-10 min. The uncertainty in our measurements of P_{CO} due to systematic calibration errors was ±35%. The composition of the UO_2 being studied was determined following the rapid cooling of the Knudsen cell. It has been established by the emf [3] method and by the values of the crystal lattice parameter (a = 5.4710 Å*) [10], that equilibrium in the $UO_{2\pm x}$–UC_2–CO system corresponds to the value O/U = 1.9995 ± 0.0005.

*1 Å = 10^{-10} m; 1 atm = 101,325 Pa; 1 mm Hg = 133,322 Pa.

Translated from Atomnaya Énergiya, Vol. 49, No. 1, pp. 28-30, July, 1980. Original article submitted May 14, 1979.

0038-531X/80/4901-0452$07.50

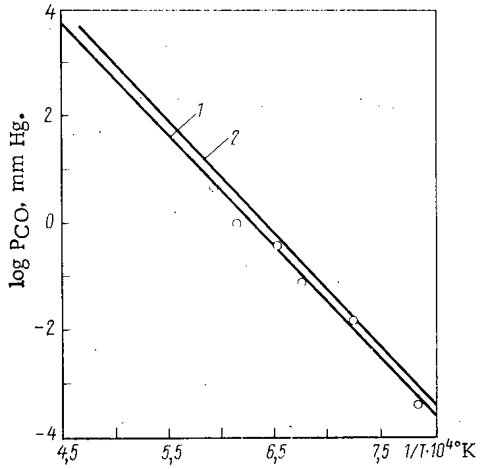

Fig. 1. Dependence of the pressure of CO in the UO_2-UC_2-CO system on the temperature: 1) data of the present work, $\log P_{CO}$ (atm) = $9.726 - (1.998/T) \cdot 10^4$ (○ – experiment); 2) published data [14].

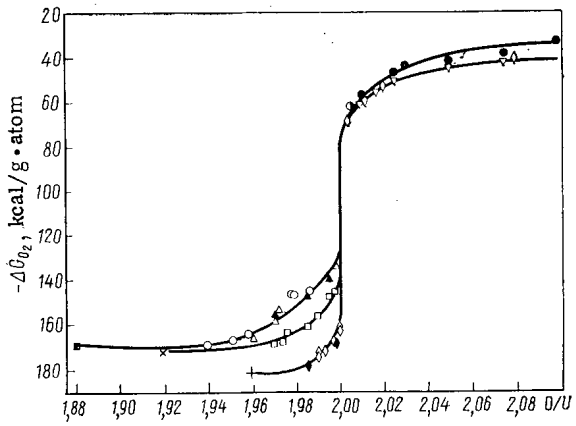

Fig. 2. Concentration dependence of $\Delta G_{O_2} = f(O/U)$ on the temperature of uranium dioxide. At a temperature 1873°K: +, ◇) data [8] and [5]; ◆, ▽) results of the extrapolated data [5] and [9]; at 2073°K: ×, □) data [8] and [10; at 2200°K: ■, ○, △) data [8], [5], and [10]; ▲, ◑, ●) results of data [10], [9], and [5, 9].

The results of the measurement of the CO pressure in the UO_2-UC_2-CO system were analyzed by the least-squares method with the analytic dependence on the temperature shown in Fig. 1, together with the published data [14]. The proximity of the present and published values of P_{CO} shows that in the previous experiments [14] studying equilibrium in the UO_2-UC_2-CO system at 1373-2100°K, the ratio O/U changed, moving closer to the value ~2.00 which was found after analogous measurements. The analytic dependence obtained was used to evaluate $\Delta\bar{G}_{O_2}$, assuming that reduction of UO_2 would occur, as was found earlier [15] by the following mechanism:

$$UO_2 + 2C = UC_2 + 2O_{[U_2O]}; \quad (1)$$

$$2O_{[UO_2]} + 2C = 2CO, \quad (2)$$

i.e., by the equation

$$UO_2 + 4C = UC_2 + 2CO. \quad (3)$$

TABLE 1. Value of the Constants A and B Defining the Temperature Dependence of the Equilibrium Pressure of Oxygen for Several Compositions of $UO_{2\pm x}$

Ratio O/U	$\log P_{O_2}(atm) = A - \frac{B}{T}\cdot 10^4$		Ratio O/U	$\log P_{O_2}(atm) = A - \frac{B}{T}\cdot 10^4$	
	A	B		A	B
1,970	18,56	7,52	2,000 min*	14,72	6,08
1,975	17,36	7,20	2,000 min*	−0,08	1,88
1,980	18,88	7,44	2,020	−0,48	0,98
1,985	19,32	7,48	2,050	1,92	1,30
1,990	22,00	7,92	2,100	2,96	1,40
1,995	22,08	7,84			

*Interval $UO_{2\pm x}$ where $x \leq 0.0005$.

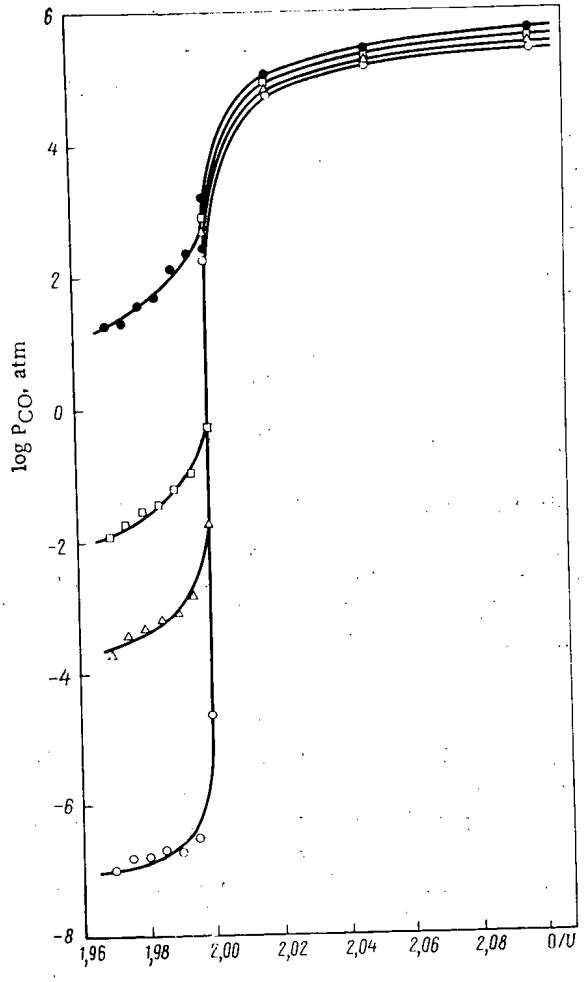

Fig. 3. Calculated equilibrium pressure of CO in the UO_2-UC_2-C system for 1500 (○); 1800 (Δ); 2000 (□) and 2500°K (●).

If stage (2) has equilibrium constant K_p, one may write

$$P_{O_2}^{1/2}[UO_{1.9995}] = P_{CO}/a_C K_p,$$

where $\log K_p = 4.68 + 0.5794/T \cdot 10^4$ [16]; $a_C = 1$ and P_{CO} is the measured equilibrium pressure of CO (see Fig. 1).

The temperature dependence of the partial pressure of oxygen obtained for $UO_{1.9995}$ can be described by the equation

$$\log P_{O_2\,(atm)}^{UO_{1.9995}} = \frac{5.1548}{T} \cdot 10^4 - 10.092.$$

An analogous dependence for the system $UO_2 + U_{liq}$ is [8]:

$$\log P_{O_2}^{UO_2+U\,liq} = 9.16 - \frac{56.260}{T}.$$

The dependence obtained for P_{O_2} for the region UO_{2-x} together with linear extrapolations conform to the recorded composition in the area of homogeneity of UO_2 [2, 5, 9, 10*] which allows one to construct a concentration dependence $\Delta\bar{G}_{O_2} = f(O/U)$ (Fig. 2) and a temperature dependence $\log P_{O_2} = f(T)$ for the separate values of O/U and also to define the coefficients of A and B in the equation $\log P_{O_2} = A - B/T \cdot 10^4$ (see Table 1). One should note the nonidentical influence of temperature on the equilibrium pressure of CO in the cases of pre- and post-stoichiometric composition (see Fig. 2). A stronger temperature dependence of P_{CO} for the prestoichiometric compositions in the presence of temperature gradients in the contact zone between UO_2 and carbon might be the reason for carbon transfer.

The equations for the equilibrium pressure of oxygen (see Table 1) and the equilibrium constants $K_p = f(T)$ allow us to obtain a general analytic dependence

$$\log P_{CO\,(atm)} = \log K_p + 1/2 \log P_{O_2(UO_{2\pm x})}$$

and construct a graph of the calculated values of the equilibrium pressure of CO for the $UO_{2\pm x}-UC_2-C$ systems at temperatures between 1500-2500°K and values of O/U from 1.97 to 2.10 (Fig. 3). The nonidentical influence of the temperature on the equilibrium pressure CO in the cases of pre- and post-stoichiometric compositions of UO_2 (see Fig. 3) is evidently connected with the various natural defects in these two areas of homogeneity and requires further study.

LITERATURE CITED

1. M. Ugajin, T. Arai, and K. Shiba, J. Nucl. Sci. Technol., 14, No. 2, 153 (1977).
2. V. Wheeler and I. Jones, J. Nucl. Mater., 42, 117 (1972).
3. A. Heiss, ibid., 55, 207 (1975).
4. R. Stoops et al., J. Am. Ceram. Soc., 47, 59 (1964).
5. T. Markin, V. Wheeler, and R. Bones, J. Inorg. Nucl. Chem., 30, 807 (1968).
6. B. Steel et al., J. Nucl. Mater., 35, 1 (1970).
7. M. Donne and G. Schumacher, ibid., 40, 27 (1971).
8. R. Ackermann et al., in: Thermodynamics of Nuclear Materials, Vol. 2, IAEA, Vienna (1975), p. 3.
9. K. Hagemark and M. Broli, J. Inorg. Nucl. Chem., 28, 2837 (1966).
10. N. Javed, J. Nucl. Mater., 43, 219 (1972).
11. Yu. Khromov et al., Zavod. Lab., 44, 296 (1978).
12. A. Naomidis et al., Reactortagung, 375 (1972).
13. V. G. Baranov et al., in: Second All-Union Conference on the Chemistry of Uranium [in Russian], Atomizdat, Moscow (1978), p. 18.
14. M. Rand et al., The Thermochemical Properties of Uranium Compounds, New York (1963).
15. T. Lindemer, H. Allen, and T. Leitnakes, J. Am. Ceram. Soc., 52, No. 5, 233 (1969).
16. M. Kh. Karapetyants, Chemical Thermodynamics [in Russian], Goskhimizdat, Moscow (1953), p. 421.
17. A. Pattoret, T. Drowart, and T. Smoes, in: Thermodynamics of Nuclear Materials, IAEA, Vienna (1968), p. 613.

*The data of [17] is not used since the results obtained for ΔG_{O_2} differ from the results of the enumerated works by 12-14 kcal/g-atom (1 cal = 4.1868 Joule).

LIFETIME OF PARAMAGNETIC E_1 CENTERS IN QUARTZ ROCKS

E. M. Medvedev

UDC 549:535.2:549.514.51

The study of E_1 centers in natural quartzes made it possible to approach the problem of determining the absolute age of the rocks [1-4]. An E_1 center is a non-impurity lattice defect (precenter) of quartz with an unpaired electron localized nearby [5-7]. The binding energy of an electron with a precenter is lower than the energy of disintegration of structural defects [4]. The initial stage of the change in the concentration of E_1 centers during heating of the specimens is determined by the motion of electrons in the quartz. With a fixed time for the process (e.g., 600 sec), heating the specimens to 573°K leads to an increase in the concentration of E_1 centers, i.e., thermal activation, while heating above this temperature results in annealing and a loss of paramagnetic properties by the E_1 centers.

To investigate the effect of the temperature on the rate of electronic processes in natural quartzes we selected a specimen which was uniform in size and contained elements of quartz sandstone with an initial E_1-center concentration of 10^{15} spin/g. The age of the sands stone is 650 ± 50 million years according to lead-isotope analysis.

Weighed specimens were kept under thermostatic control in quartz thin-walled ampuls inserted in a massive metallic body, heated by an electric spiral, with openings for specimens and thermometers. Before EPR analysis the specimens were cooled to room temperature. The plots of the isotherms of E_1-center activation are given in Fig. 1. The process of increasing the concentration is approximated by segments of straight lines at the coordinates $(C_E - C_0)/(C_{max} - C_0) - t^{1/2}$. The bands in the thermal-activation lines are due to two types of precenters, differing as to the electron binding energy. The E_1 centers formed are spectroscopically indistinguishable.

With a view to increasing the reliability of the extrapolation of the relations obtained in the range of ordinary temperatures at which the rocks occur one series of specimens was thermostated at 423°K for 10^8 sec (~3 years). The results of this experiment are given in Fig. 2. Figure 3 shows the dependence of the generalized rate of thermal activation of E_1-centers on the temperature of the specimen. Extrapolation of the dependence to the region of the usual temperature (293°K) permits the conclusion that under natural conditions the process of thermal activation of E_1-centers should be compoeted in $2.5 \cdot 10^{15}$ sec ($0.8 \cdot 10^8$ yr).

The low-temperature annealing of E_1 centers is concealed by the thermal activation process. Therefore, it was observed at 500°K or higher. The variation of the E_1-center concentration under isothermal annealing is shown in Fig. 4. The initial segments of the anneal are approximated will by straight lines. The lines then go over into ordinary exponential relations describing the anneal of the E_1 centers. The temperature dependence of the generalized annealing rate is shown in Fig. 5. Extrapolating the E_1-center anneal to the region of the temperature at which the rocks ordinarily occur (293°K), we find that for the electron system of E_1 centers this process should be completed in $2 \cdot 10^6$ sec ($6.4 \cdot 10^8$ yr).

Comparison of the thermal-activation time with the annealing time shows that in quartz rocks whose age exceeds 10^8 yr practically all E_1 centers should be activated under natural conditions and should be paramagnetic.

The detection of nonparamagnetic E_1 centers in sandstone quartzes, ~650 million years, indicates the existence of another mechanism which affects the electron system of the centers. The natural background of ionizing radiation is such a mechanism in rocks. The E_1-center concentration observed in quartz rocks by the EPR method is the result of the combined action of ionizing radiation and the thermal motions of electrons. When the action of the radiation is halted (by the radioactive elements being leached out of the rock) the E_1 centers in the paramagnetic state last for $\sim 6.4 \cdot 10^8$ yr.

Translated from Atomnaya Énergiya, Vol. 49, No. 1, pp. 31-33, July, 1980. Original article submitted June 26, 1979.

0038-531X/80/4901-0456$07.50

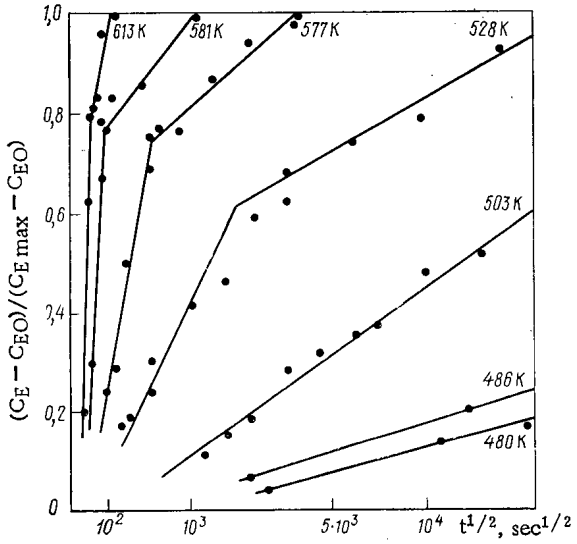

Fig. 1

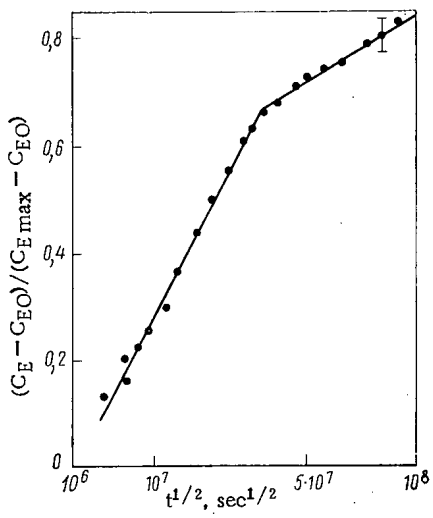

Fig. 2

Fig. 1. Isotherms of E_1-center activation: •) here, and in subsequent figures, experiment; the numbers next to the curves indicate the temperature in °K; $C_E - C_0$ and $C_{max} - C_0$ here and in Fig. 2 are, respectively, the increment and maximum increase in the concentration during heating.

Fig. 2. Isotherm of E_1-center activation at low temperature (423 ± 3°K).

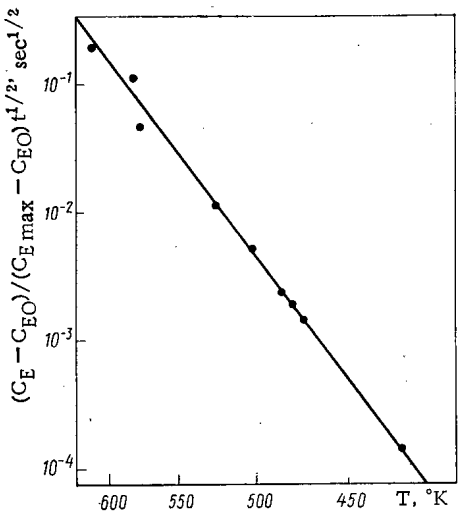

Fig. 3

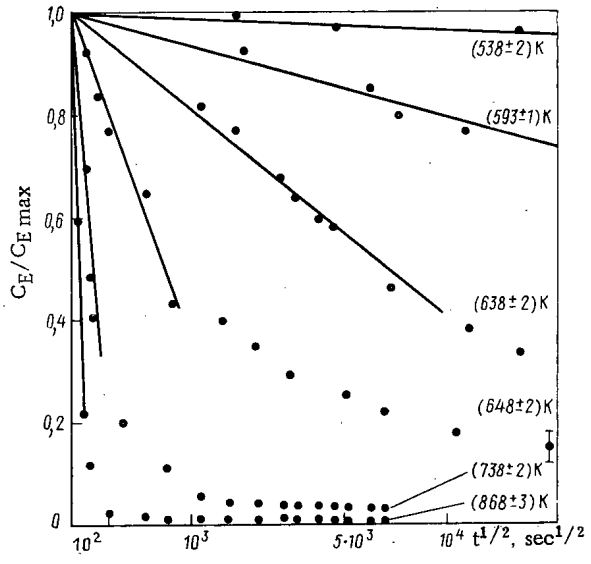

Fig. 4

Fig. 3. Rate of thermal activation vs absolute temperature of specimen.

Fig. 4. Variation of relative E_1-center concentration in quartz under isothermal annealing. The initial segments of the straight lines were drawn according to experimental points; the numbers next to the curves give the temperature in °K.

TABLE 1. Mean Values of High-Temperature Energy Parameters of E_1 Centers

Parameter	Thermal activation	Annealing
E, eV	0,95±0,06	1,4±0,1
B, sec	$1,5 \cdot 10^{-6}$	$5 \cdot 10^{-9}$

TABLE 2. Calculated and Experimental Values of τ

Mean lifetime	Temperature			
	623 K (350° C)		423 K (150° C)	
	calc.	expt.	calc.	expt.
τ_A, sec	60	60	10^5	10^7
τ, sec	10^3	10^3	10^8	—

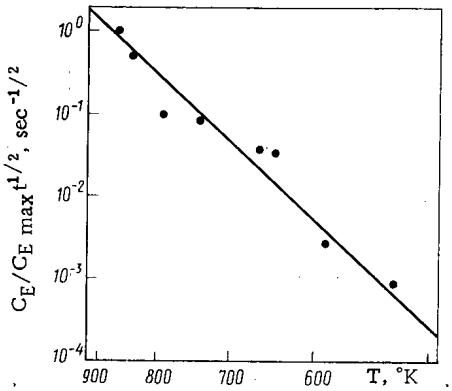

Fig. 5. Temperature dependence of annealing rate of E_1 centers.

Usually the characteristic time τ in which the E_1-center concentration changes by a factor of e is found from the well known formula

$$\tau = B \exp (E/kT), \tag{1}$$

where B is a frequency factor; E, activation energy of the process; k, Boltzmann's constant; and T, absolute temperature in °K.

By the method of gradual thermostating of quartz specimens in the temperature range from 573 to 773°K employing the technique described in [4], we found the mean values of the energy parameters of the E_1 centers during processes of thermal activation and annealing.

The parameters of E_1 centers given in Table 1 enable us to calculate τ at any temperature and to compare the calculated value with the experimental value. Table 2 gives the calculated and experimental values of τ for two values of temperature.

The τ_A value of 10^5 sec calculated from Eq. (1) at 423°K permits verification in a long experiment (see Fig. 2). The measured value of τ_A differs from the calculated value by two orders og magnitude. When the lifetime from Eq. (1) is extrapolated to the region of 293°K there may be even greater discrepancies between the theoretical and experimental values.

The proposed method of quasilinear extrapolation is based on the observation of the kinetics of thermal activation and annealing of E_1 centers in quartzes for a wide range of temperatures. The rate of the processes characterizing the drift mobility of spin carriers (electrons) in quartz at a temperature T is proportional to the factor

$$A(T) = \exp (-E_d/2kT), \tag{2}$$

where E_d is the drift activation energy.

Thus, for thermal activation and annealing of the spin system of E_1 centers over a wide range of temperatures, we can set up equations which describe the drift of spin carriers in the quartz lattice given local donor levels (E_1 centers) in the energy structure of the dielectric. The annealing of E_1 centers, which con-

tinues after the linear segments, is explained quite well by the barrier-activation theory and characterizes the recombination of point defects in the quartz at the temperature T.

The law considered in the paper was obtained for specimens of sandstone quartz of the upper Proterozoic Era. It requires further confirmation with a large number of specimens of different ages and genesis.

Conclusions. In quartz rocks E_1 centers are formed in both paramagnetic and nonparamagnetic states under the effect of the natural background of ionizing radiation.

Nonparamagnetic E_1 centers go over into the paramagnetic state under the effect of heat on quartz (thermal activation of E_1 centers).

The rate of thermal activation depends on the absolute temperature of the specimen.

Two subtypes of E_1 centers differing as to the rate of thermal activation were detected.

By quasilinear extrapolation in the coordinates $(C_E - C_0)/(C_M - C_0) - t^{1/2}$ it was found that thermal activation of E_1 centers of the first type, determined from the initial segments of the process, whould be completed at the usual temperature of 293°K (20°C) in $\sim 0.8 \cdot 10^8$ yr.

Annealing of E_1 centers of the first subtype in natural occurrence (at 293°K) is completed in $6.4 \cdot 10^8$ yr. The time for the completion of the thermal activation and annealing of E_1 centers of the second subtype is roughly an order of magnitude longer than in the case of the first subtype.

As a result of a long experiment (~3 yr) it was established that at 423°K (150°C) the method of quasilinear extrapolation inables the thermal activation time to be estimated more accurately than does the barrier-activation theory usually employed.

LITERATURE CITED

1. A. M. Danilevich and V. V. Pavshukov, in: Abstracts Second All-Union Radiogeochemical Meeting [in Russian], Dushanbe (1975), p. 215.
2. B. M. Moiseev and L. T. Rakov, Dokl. Akad. Nauk SSSR, 233, No. 4 (1977).
3. L. T. Rakov and B. M. Moiseev, At. Energ., 44, No. 2, 180 (1978).
4. A. M. Danilevich, V. V. Pavshukov, and É. M. Medvedev, At. Energ., 43, No. 3, 202 (1977).
5. L. V. Bershov, A. S. Marfunin, and A. V. Speranskii, Izv. Akad. Nauk SSSR, Ser. Geol., No. 11, 106 (1978).
6. V. P. Solntsev, R. I. Mashkovtsev, and N. Ya. Shcherbakova, Strukt. Khim., 18, No. 4, 729 (1977).
7. A. Ruffa, Phys. Rev. Lett., 25, No. 10, 650 (1970).

BEAM EXTRACTION FROM SYNCHROTRON WITH CYCLOTRON PREACCELERATOR

M. Yu. Novikov, V. S. Panasyuk,
Yu. K. Samoshenkov, V. V. Sanochkin,
Yu. M. Tereshkin, and V. B. Kromchenko

UDC 621.384.634.4

The construction and operating principle of a synchrotron with a cyclotron preaccelerator (CPA), operating as a generator of pulses of synchrotron radiation in the vacuum ultraviolet region, were considered in [1]. At present, studies are being conducted on multiturn undirected beam extraction for metrological purposes and one-turn beam extraction for research and industrial needs. This work broadens the range of application of the accelerator.

Let us consider multiturn undirected beam extraction.

Characteristics of Measurements of Charge of Particle Beam in CPA

The accelerating chamber of the CPA is filled with nondense plasma, formed when the microwave accelerating field ionizes the residual atmosphere. Under such conditions it is practically impossible to measure the beam charge with open probes. The slow particles set up in the probes currents which are commensurate with the beam current, as a result of which in this case we can speak only of qualititive measurements. Although it does cut off slow particles, a shielded probe greatly absorbs accelerated particles in its shield. They "stick" in it during repeated passages, approaching the probe with a very small step. Moreover, the use of any probes in general, and shielded probes in particular, in an accelerator of the type under consideration poses difficulties.

Velikanov et al. [2] described measuring the charge of a particle beam by comparing the intensity of the spectral line isolated from the synchrotron radiation in the visible region with a calibrated source of radiation. However, this method is comparatively complicated and, moreover, is applicable only at a quite high beam energy when the intensity and spectrum of the synchrotron radiation have the necessary parameters. It thus remains a timely problem to develop a method of making direct measurements of beam charge with a satisfactory degree of accuracy.

On the trailing edge of the pulse of the magnetic guide field after the microwave accelerating field is switched on the beam automatically expands to the walls of the accelerating chamber. Care must be taken only to ensure that the angles of approach of the beam to the chamber walls be as close to the normal as possible. In this case, absorption of electrons in the walls is minimal. Beyond the limits of the chamber the electrons strike a measuring electrode and are stopped in them. Since the capacitance of the measuring electrode is known, the beam charge can be determined from its potential.

Accelerator Design

The iron-free electromagnet (Fig. 1) consists of two turns connected in parallel to a current-pulse generator by means of current lead-ins. The inner space of the turns forms a microwave cavity resonator. To reduce the radiation of microwave power plates with outside cylinders are mounted on the ends of the electromagnet, the plates being transparent to the guide field. Inside the resonator is a glass accelerating chamber with a branch piece for evacuation and a plasma probe. Opposite the probe on the axis of the accelerator is a plasma injector. The annular measuring electrode, acting as a Faraday cylinder, consists of a massive toroid and an electrostatic screen and has a coaxial lead-out. The dimensions of the toroid guarantee complete absorption of the accelerated electrons. The electrostatic screen is a layer of graphite on a thin polyethylene substrate. Such a screen is transparent to the magnetic guide filed [3].

Translated from Atomnaya Énergiya, Vol. 49, No. 1, pp. 34-38, July, 1980. Original article submitted July 13, 1979; revision submitted January 11, 1980.

0038-531X/80/4901-0460$07.50

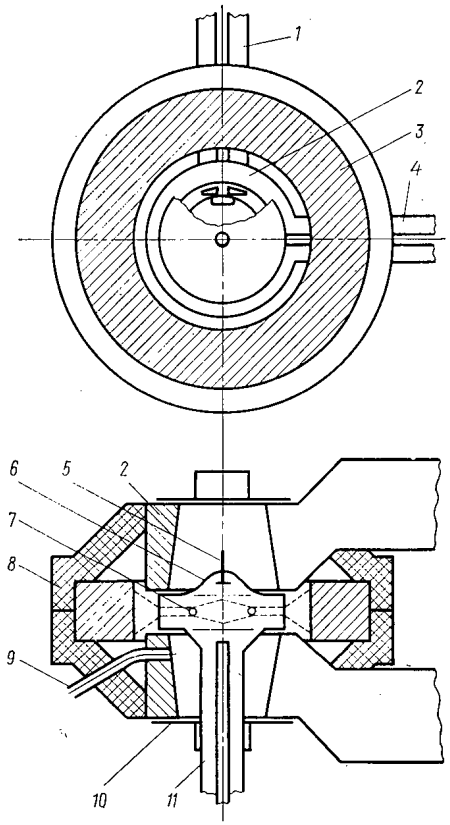

Fig. 1. Design of accelerator: 1) microwave power lead-ins; 2) turns of electromagnet; 3) annular measuring electrode; 4) current lead-ins; 5) plasma probe; 6) vacuum chamber; 7) section of beam in synchrotron orbit [---) envelope of beam in motion during preacceleration and extraction]; 8) housing; 9) lead-out of microwave probe; 10) shielding plates with outside cylinders; 11) injector.

The dimensions and shape of the electromagnet turns were chosen so as to obtain the necessary magnetic field configuration in the acceleration region and tuning of the resonator to the frequency of the magnetron microwave oscillator. The electromagnet power supply, resonator excitation system, injector, and vacuum system are similar to those described in [1] and are characterized by the following parameters: electromagnet current amplitude 1 MA, acceleration time 2 μsec, microwave oscillator frequency 3 GHz, injector intensity 10^9-10^{11} particles, and vacuum in accelerator chamber $7 \cdot 10^{-4}$ Pa.

Particle Dynamics

The main distinctive features of particle dynamics in the CPA are associated with the capture of electrons into acceleration from a region whose dimensions are comparable to the radius of the relativistic orbit [4, 5]. Moreover, the design features of the accelerator permit undirected multiturn extraction of the beam to be accomplished [3]. Let us consider the particle dynamics from the central region to the measuring electrode.

Influence of the Electric Field of a Turn. Acceleration in the CPA takes place in the presence of a quasi-stationary (in relation to the microwave period) electric field as the result of the potential difference over the electromagnet turn. The solution of the nonrelativistic equations of motion of a charge in uniform fields describes the trajectory in the first several turns and shows that the acceleration regime is possible with satisfaction of the inequality $0.5E_{rf} > E$, where E_{rf} is the amplitude of the microwave field and E is the strength of the quasistationary field of the electromagnet turn. Let us note that in actual fact this field is attenuated by radio-frequency plasma filling the accelerating chamber.

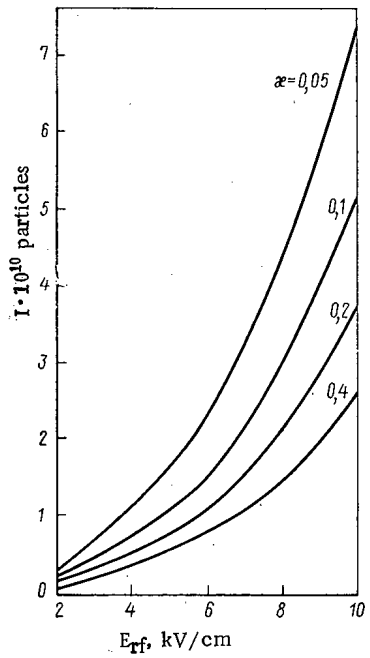

Fig. 2. Intensity vs amplitude of microwave field.

Capture Region. In a real accelerator the magnetic guide field depends on the axial coordinate z:

$$H(z)|_{r=0} = H(0)[1 + \varkappa (z/\rho)^2], \tag{1}$$

where H is the strength of the magnetic guide field; r, radial coordinate; $\varkappa$, dimensionless coefficien; $\rho = c/\omega_{rf}$ (here c is the speed of light and ω_{rf} is the frequency of the microwave field). This inhomogeneity of the field leads to a limitation on the vertical size of the region from which particles can be captured into acceleration. Suppose that near cyclotron resonance the magnetic field varies slowly so that the adiabatic condition

$$\frac{T}{H}\frac{\partial H}{\partial t} \ll 1 \tag{2}$$

is satisfied. Here, T is the characteristic time which is equal to the period of cyclotron oscillations. Since in practice in order to increase the intensity an endeavor is made to satisfy the inequality $\cos\varphi_s \ll 1$, where φ is the phase of an equilibrium particle, condition (2) is satisfied as a rule. Then the equations of motion of the particle are of the form

$$\left.\begin{aligned} &\frac{d^2z}{dt^2} + \varkappa \frac{p_z^2}{m_0^2\rho^2} z = 0; \\ &\frac{dz}{dt} = \frac{p_z}{m_0}; \\ &\frac{d}{dt}\left(\frac{p_t^2 + p_z^2}{2}\right) = \frac{1}{2} eE_{rf}\, p_t \cos\varphi; \\ &\frac{1}{\omega_{rf}}\frac{d\varphi}{dt} = \varkappa\left(\frac{z}{\rho}\right)^2 - \frac{p_t^2 + p_z^2}{2(m_0c)^2}, \end{aligned}\right\} \tag{3}$$

where m_0 is the rest mass of the electron and e is the electron charge. The mutually independent variables chosen were the longitudinal momentum p_z, the transverse momentum p_t, the axial coordinate z, and the particle phase φ. These nonlinear equations are analyzed by the method of averaging [6]. Two cases are distinguished: the first is when the frequency of the longitudinal oscillations on average substantially exceeds the frequency of the variations of the transverse momentum and the second, is the inverse of the first case. In the first case, upon averaging Eqs. (3) over the period of longitudinal oscillations we get abbreviated equa-

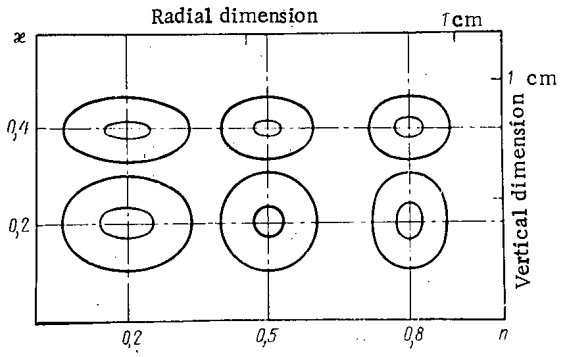

Fig. 3. Dimensions of capture region for various $\varkappa$ and n at $E_{rf} = 4$ kV/cm; the inner circles are the beam sizes in relativistic orbit for $\gamma = 9$.

tions and it is possible to find their first integral, i.e., the equation of phase trajectories. It is of the form

$$\varkappa \frac{A_z^2}{\rho^2}\left(\frac{p_t}{m_0 c}\right)^2 - \frac{1}{3}\left(\frac{p_t}{m_0 c}\right)^3 = \frac{eE_{rf}}{m_0 c \omega_{rf}} \sin\varphi, \tag{4}$$

here, A_z is the amplitude of longitudinal oscillations. It is seen from this formula that closed phase trajectories exist only when $A_z \leq A_{max}$, where

$$A_{max} = \frac{\rho}{\sqrt{\varkappa}}\left(\frac{3eE_{rf}}{2m_0 c\omega_{rf}}\right)^{1/3}. \tag{5}$$

The second case is considered similarly and in the right member of Eq. (5) we get a factor of $1/\sqrt{2}$. Thus, the maximum half-height of the capture region is determined by Eq. (5) while the total intensity I of the accelerator (Fig. 2) can be estimated from the formula $I = 2A_{max}N$, where the value of N is taken from [4].

Another important characteristic of the accelerator is the radial size R_{max} of the capture region. Considerations similar to those which led to Eq. (5) make it possible to obtain

$$R_{max} = \frac{\rho}{\sqrt{h}}\left(\frac{3eE_{rf}}{2m_0 c\omega_{rf}}\right)^{1/3}, \tag{6}$$

where the dimensionless coefficient h appears in the law of variation of the magnetic field in the median plane,

$$H(r)|_{z=0} = H(0)[1 - h(r/\rho)^2] \tag{7}$$

and is related to the field index n on the relativistic orbit by $n = 2h/(1-h)$.

Let us also point out that the dimensions of the accelerated beam can be found from Eqs. (5) and (6). Since the betatron oscillations are damped adiabatically with a rise in temperature, A_{max} and R_{max} must be divided by $\sqrt{\gamma_s}$, where γ_s is the Lorentz factor of the equilibrium particle. The beam dimensions at various values of $\varkappa$ and n are shown in Fig. 3. The limitations on the beam intensity owing to longitudinal Coulomb repulsion of particles were presented in [4].

Extraction of Beam to Measuring Electrode. When the particles reach the maximum energy γ_0 at some moment of time, henceforth as a matter of convention taken to be the zero time, the microwave field is switched off. The magnetic guide field decreases according to a given law determined by the current-pulse generator. Since there is satisfaction of the condition

$$\partial H/\partial t \ll \omega(t) H, \tag{8}$$

where $\omega(t)$ is the electron revolution frequency, which initially coincides with ω_{rf}, we can consider the dynamics in the adiabatic approximation. As is known [7], p_t^2/H is an adiabatic invariant. From this we find

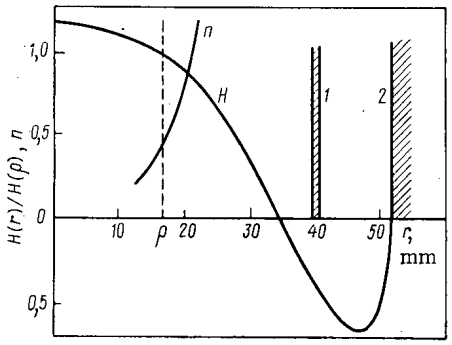

Fig. 4. Measurement of H(r) and n(r) in median plane of accelerator: 1) chamber wall; 2) measuring electrode.

the law of variation of the Lorentz factor with time:

$$\gamma(t) = \sqrt{1 + (\gamma_0^2 - 1)\frac{H[r(t), t]}{H(\rho, 0)}}. \tag{9}$$

Here r(t) is the radial coordinate of the electron at the time t and it can be found from

$$\left[\frac{r(t)}{\rho}\right]^2 \frac{H[r(t), t]}{H(\rho, 0)} = 1. \tag{10}$$

Thus, from

$$\frac{\omega(t)}{\omega_{rf}} = \frac{\gamma_0}{\gamma(t)} \frac{H[r(t), t]}{H(\rho, 0)} \tag{11}$$

we can calculate the electron revolution frequency $\omega(t)$ and find the behavior of the amplitude $A_z(t)$ of the vertical oscillations which is of interest to us [8]:

$$\frac{A_z(t)}{A_z(0)} = \left\{\frac{H(\rho, 0)}{H[r(t), t]}\right\}^{1/2} \left[\frac{\omega_{rf}}{\omega(t)}\right]^{1/2} \left\{\frac{n(\rho)}{n[r(t)]}\right\}^{1/4}, \tag{12}$$

where n[r(t)] is the field index of the magnetic guide field at the point r(t).

Equation (10) cannot be solved for all t. A a point r(t) quite far from the center the adiabatic condition is violated and the approach described above becomes inapplicable. Therefore, the trajectories were calculated numerically for certain concrete laws of variation of the field H(r, t). It turned out that the numerical results differ from the analytic results by no more than 10% right up to the critical point, after which the radial motion becomes unstable.

Clearly, the wall of the vacuum chamber should be in the region of unstable motion since only in this case are the angles between the particle trajectories and the wall sufficiently large. The transition to the unstable regime for particles with nonzero amplitudes of betatron oscillations occurs at a radius where n(r) = 1. An equilibrium particles loses stability when the radius of curvature of its trajectory becomes comparable to the size of the region occupied by the magnetic guide field. The greater the magnetic field index n, the smaller the radius at which this occurs, i.e., the smaller the necessary dimensions of the vacuum chamber must be. Moreover, with an increase in n the electrons quickly reach the region of instability and lose less energy because of retardation by the vortex electric field of the electromagnet. The energy losses during extraction are, e.g., ~60% for n = 0.15 and ~35% for n = 0.5 with an energy of 4 MeV in the synchrotron orbit.

In order to increase the accelerator intensity it is necessary to enlarge the capture region and, therefore, to reduce n [see Eqs. (5) and (6); and h increases as n decreases]. With allowance for the parametric resonances n = 0.25 and n = 0.75, a field index of $n \approx 0.5$ in the relativistic orbit was chosen as optimal for the given design.

With a measuring electrode in the form of a closed annulus an H(r) dependence is obtained with a characteristic negative segment (Fig. 4) which ensures the best extraction trajectories for given dimensions of of vacuum chamber and measuring electrode, which has been confirmed by numerical calculations, shows that

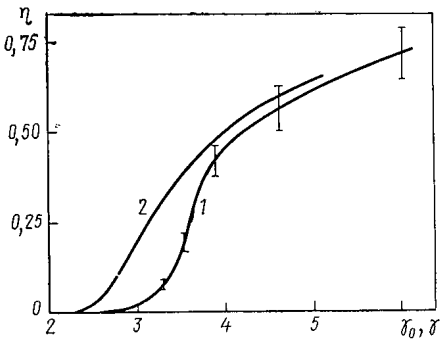

Fig. 5

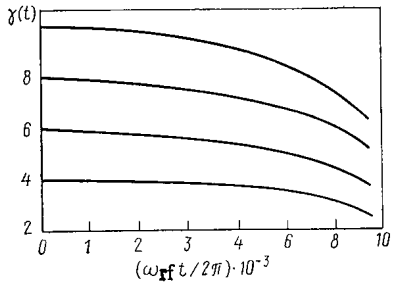

Fig. 6

Fig. 5. Energy losses during motion of beam from synchrotron orbit to vacuum chamber wall (distance between curves along abscissa axis): 1) experimental curve of beam transmission coefficient $\eta(\gamma_0)$ vs energy in synchrotron orbit; 2) calculated $\eta(\gamma)$ curve for various energies at chamber wall.

Fig. 6. Lorentz factor vs time in microwave periods for various values of initial energy.

for a given field the vertical dimension of the beam increases during motion until stability is disrupted: $A_a(t)/A_z(0) = 1.1$.

In the course of acceleration the beam passes through resonance at n = 0.25, situated between the capture region and the relativistic orbit. To avoid losses of particles the allowable value of the first azimuthal harmonic of the field index is $\leq 10^{-3}$ [8].

Technique of Measuring Beam Parameters and Some Experimental Results

The beam charge was determined by measuring the voltage across a known capacitance. Electrons impinging on the measuring electrode charge the capacitance consisting of the electrode-screen capacitance and the input capacitance of the measuring circuit. The time constant of charge dissipation from the measuring electrode is more than 100 sec. The charge is conserved up to complete relaxation of the processes in the power circuits of the accelerator, which produce appreciable noise, and is then commutated to an amplifier input. The output voltage of the latter is measured with an oscillograph or pulse voltmeter. The sensitivity of the method is limited by the imperfections of the commutator employed and proved to be no worse than $4 \cdot 10^6$ electrons for a charged capacitance of 240 pF. The total error of determination of this capacitance, the transfer constant of the amplifier and the V4-17 pulse voltmeter is less than 10%; this is the accuracy of measurement of charge without allowance for losses of particles in the chamber walls. Secondary emission from the aluminum measuring electrode, which constitutes 6% at a beam kinetic energy of 3 MeV [9], is suppressed in the given design by the magnetic field of the electromagnet. The measured value of the accelerator intensity at a microwave accelerating field of $4 \cdot 10^5$ V/m is 10^9 per acceleration cycle. The stability of the number of particles accelerated in this case is ±10%.

The energy losses caused by the vortex electric field as the beam moves between the synchrotron orbit and the wall of the accelerating chamber were evaluated from the displacement of the experimental plot of $\eta(\gamma_0)$ relative to the calculated $\eta(\gamma)$ curve [10]. Here η is the coefficient of beam transmission through the chamber wall, equal to the ratio of the number of particles transmitted through the wall to the number of particles incident on it, γ_0 is the energy of the beam in the synchrotron orbit, and γ is the energy of the beam at the inner surface of the chamber. Coefficient η was found from the decrease in intensity at a given γ_0 relative to the intensity for $\gamma_0 > 10$. From known values of η and the thickness of the vacuum chamber wall we calculated γ. The energy in the synchrotron orbit was determined from the ratio of the maximum induction of the magnetic guide field in the region of the orbit to the induction corresponding to cyclotron resonance at the frequency of the accelerating field. It is seen from Fig. 5 that the energy losses by particles during extraction are lower than those calculated (Fig. 6).

The time taken by the beam to travel from the synchrotron orbit to the measuring electrode was determined from the delay of the pulse of γ-ray bremmstrahlung relative to the trailing edge of the microwave pulse. The bremmstrahlung was recorded by a photoscintillation detector set up outside the accelerator in

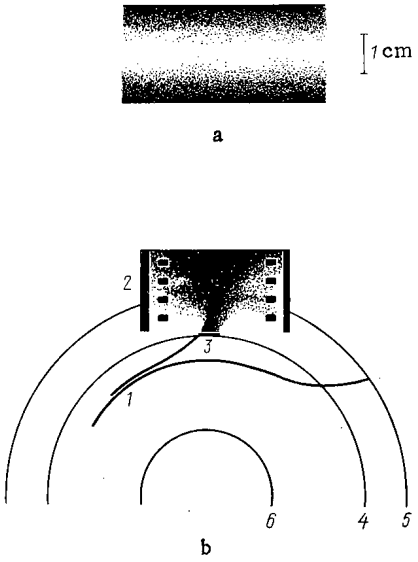

Fig. 7. Trace of extracted beam on photographic film wrapped around accelerating chamber (a) and diagram of experiment on determining the angles of beam exit into the air in the plane of the orbit (b): 1) calculated exit trajectory and wall 43°, between trajectory and surface of electrode 69°; 2) photograph of shadow on photographic film; 3) lead plate; 4) chamber wall; 5) surface of measuring electrode; 6) synchrotron orbit.

the plane of the beam trajectory. The measured delay time of the γ-ray pulse maximum is 1.2 ± 0.1 μsec while calculation gave 2.0-2.2 μsec.

It should be pointed out that the decrease in the extraction time and the energy losses in comparison with the calculated values is not unexpected and is due to the following cause. It follows from numerical calculations that the larger the amplitude of the betatron oscillations of the particle, the more quickly it is extracted and the less energy it loses. During extraction of the beam there is radial parametric resonance at $n = 0.75$. The resonance band is at a distance of 2.5 mm from the synchrotron orbit. The particles therefore "set into oscillation" almost at the very beginning of the extraction process, as a result of which the process is accelerated. This circumstance was not taken into account in the calculations.

The geometric characteristics of the beam were found from the image on a photographic film exposed to the beam. The axial and aximuthal distribution of the particles during extraction was imaged on the film wrapped around the accelerating chamber. Figure 7a shows a print of a segment, exposed at a particle energy of 3 MeV and an accelerating field of $1.5 \cdot 10^6$ V/m. The vertical beam size tt the accelerating chamber radius does not exceed 10 mm, which is in good agreement with the calculated value of $2.2A_{max}/\sqrt{\gamma_s} = 10$ mm [Eq. (5), $\varkappa = 0.37$]. The aximuthal distribution of the particles is uniform. The electron exit angles from the chamber wall into the air were found from the boundaries of the shadows left by the lead plate on the photographic plate placed in the plane of the orbit (Fig. 7b). A print of the film exposed by the beam is given together with the diagram. Comparison of the calculated trajectory 1 with the boundaries of the shadow 2 indicate good agreement between experiment and theory.

The authors express their gratitude to B. M. Stepanov for his constant interest in the work.

LITERATURE CITED

1. S. P. Velikanov et al., At. Energ., 41, No. 2, 113 (1976).
2. S. P. Velikanov et al., Izm. Tekh., 9, 34 (1979).
3. V. S. Panasyuk, A. A. Sokolov, and B. M. Stepanov, "Use of strong magnetic fields to accelerate charged particles" Paper read at Second International Conf. on Generators of Megagauss Magnetic Fields, Washington, May 29-June 1 (1979).
4. M. Yu. Novikov et al., At. Energ., 41, No. 2, 125 (1976).
5. A. V. Gryzlov et al., Zh. Tekh. Fiz., 42, 13 (1972).
6. I. N. Bogolyubov and Yu. A. Mitropol'skii, Asymptotic Methods in the Theory of Nonlinear Oscillations [in Russian], Fizmatgiz, Moscow (1958).

7. L. D. Landau and E. M. Lifshitz, The Classical Theory of Fields, Pergamon Press, Oxford (1971).
8. A. A. Kolomenskii and A. N. Lebedev, Theory of Cyclic Accelerators [in Russian], Fizmatgiz, Moscow (1972).
9. A. A. Vorob'ev, Applied Nuclear Spectroscopy [in Russian], No. 6, Atomizdat, Moscow (1976), p. 79.
10. V. F. Baranov, Dosimetry of Electron Radiation [in Russian], Atomizdat, Moscow (1974).

DOSE CHARACTERISTICS OF HIGH-ENERGY ELECTRONS, MUONS, AND PHOTONS

G. I. Britvich, G. I. Krupnyi,
V. N. Peleshko, and Ya. N. Rastsvetalov

UDC 539.1.074

Absorbed doses from high-energy leptons and photons in tissue-equivalent phantoms have been calculated for electrons and photons with initial energies E from 0.1 to 20 GeV in a water phantom [1, 2], and for muons with E up to 1000 GeV [3-5].

Experiments on absorbed doses [4, 6, 7] have been performed for a beam of electrons with E = 1 GeV (water absorber, anthracene scintillator), a beam of electrons with E = 5.2 GeV (water phantom, ionization chamber), a narrow beam of positrons with E = 2.9 GeV, and muons with E = 920 and 2800 MeV (polystyrene absorber). These results on energy release in tissue-similar media are very disconnected or encompass a narrow range of primary particle energies; practically no experiments have been performed on the dose characteristics of high-energy muons and photons. In our opinion the inadequacy of the experimental data does not permit the selection of the most reliable calculational method, suitable for determining dose characteristic standards of leptons and photons. In the recommendations of the ICRP on an estimate of the radiation hazard of electrons with energies E from 0.1 to 20 GeV [8], higher values of the maximum depth dose of electrons are assumed [1], which reflect "the general tendence of this international organization in unclear situations to recommend a certain excess protection of personnel" [9]. The present article presents results of experiments on the radiation hazard of high-energy leptons and photons.

Experiment. The experiments were performed with beams of secondary particles from the IFVÉ accelerator. Positrons with energies from 0.2 to 3.3 GeV were separated in the aligning channel [4]; positrons with E = 2.5, 5, and 9 GeV, muons with E = 2.4, 4.9, 8.9, and 10.9 GeV, and photons with $\bar{E}$ = 3.6 GeV in the positive particles channel [10]; a beam of electrons with E = 31 GeV in the electron channel [11]; electrons and muons with E = 40 GeV in the negative particles channel [12].

Figure 1a shows a schematic diagram of the arrangement of detectors in beams of secondary particles. In order to separate a positron (electron), the beam of particles was passed through a telescope of scintillation counters $S_1S_2S_3$, gas threshold Cerenkov counters $\check{C}_1$, $\check{C}_2$, adjusted to record positrons, a shower spectrometer L, a scintillation counter V_1 with a central aperture, connected in an anticoincidence circuit separating a 1.2-cm-diameter beam.

In addition, the counter S_3 with supplementary pulse-height discrimination does not permit the recording of more than one particle per event. This substantially improved the "purity" of separation of positrons, since in separate tests up to 15% of the positrons were accompanied by high-energy δ-electrons. The shower spectrometer was made of lead glass 11 radiation lengths (r.l.) thick. It was included for extra discrimination against a possible admixture of muons and pions. A trigger signal $S_1S_2S_3\check{C}_1\check{C}_2LS_3'\overline{V_1}$ permitted the recording of positrons (electrons) in the energy release spectrometer E with an admixture of muons and pions of nor more than 1% in all experiments.

The spectrometer was 24 × 24 cm polystyrene scintillator 2.12 g/cm^2 thick connected to a photomultiplier (FÉU) by two light guides. The signals from the FÉU were summed. This arrangement gave a good uniformity of the light collection from the whole area of the scintillator: for the central region of the spec-

Translated from Atomnaya Énergiya, Vol. 49, No. 1, pp. 39-43, July, 1980. Original article submitted October 4, 1979.

0038-531X/80/4901-0467$07.50

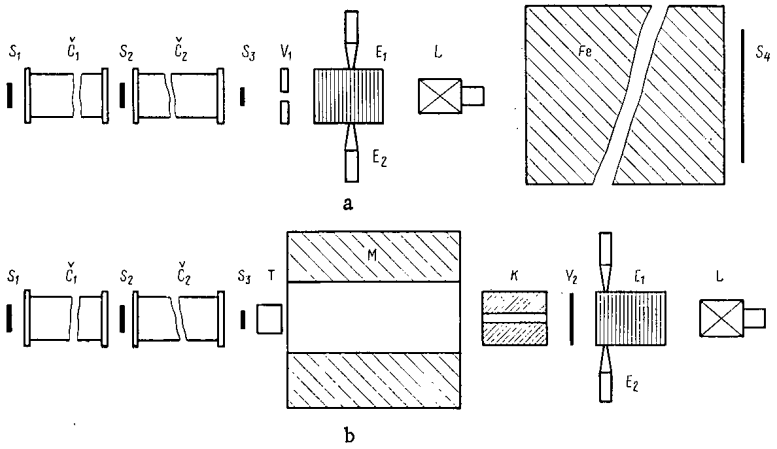

Fig. 1. Schematic diagram of location of detectors in experiments with a) electrons and muons; b) photons.

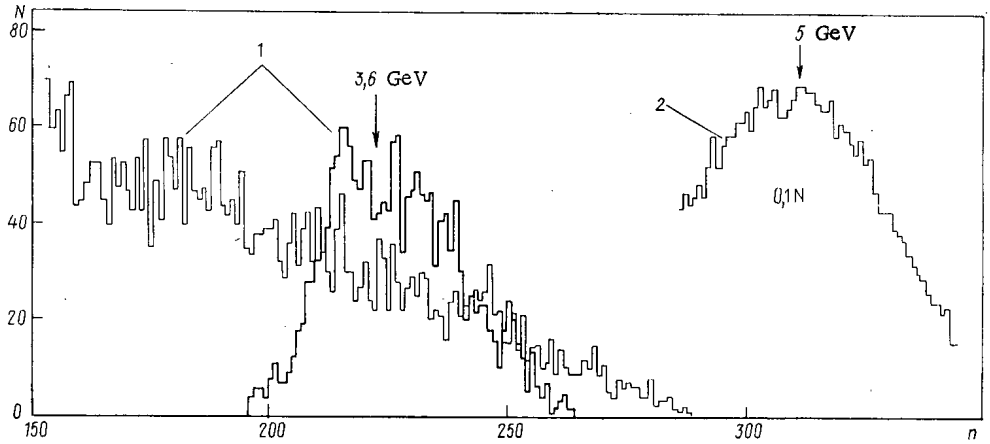

Fig. 2. Spectral distribution of photons (1) in beam. Dark histogram shows the spectrum in the 3.5-3.9-GeV range separated by the trigger signal. The arrow denotes the average value of 3.6 GeV obtained by calibration with a beam of 5-GeV positrons (2) indicated by the arrow.

trometer (~85% of the area of the scintillator) the spread of light output was no more than 5%. The spectrometer was placed between 24 × 24 cm absorbing plates. By interchanging the plates, the thickness X of the absorber in front of the spectrometer was changed while maintaining a constant total thickness of the absorber.

The arrangement of the detectors in the experiment with high-energy photons is shown schematically in Fig. 1b. Positrons, separated by two Cerenkov counters from a beam of secondary positive particles with a momentum of 5 GeV/sec, were incident on a Plexiglas target 0.6 r.l. thick. A clearing magnet was located beyond the target, and after it the following were set up on the axis of the beam: a lead collimator with a 4 cm aperture; a scintillation counter V_2 connected in an anticoincidence circuit to eliminate the recording of charged particles; an absorber with the energy release spectrometer E; a shower spectrometer L for recording photons, connected in a differential discriminator (DD) circuit. A trigger signal $S_1S_2\check{C}_1\check{C}_2L'\overline{V_2L''}$ permitted the recording in the spectrometer E of 3.5-3.9 GeV photons moving from the target at a zero angle in a solid angle of 60 μsr (Fig. 2).

In experiments with muons, a steel filter and counter S_4 (cf. Fig. 1) connected in the coincidence circuit with the trigger signal were set up beyond the shower spectrometer. The pressure in the Cerenkov counters was lowered to a level for recording muons, and the shower spectrometer, connected in the DD circuit, was adjusted to record muons. The hadron background was decreased by adding covers over the leading channel collimators.

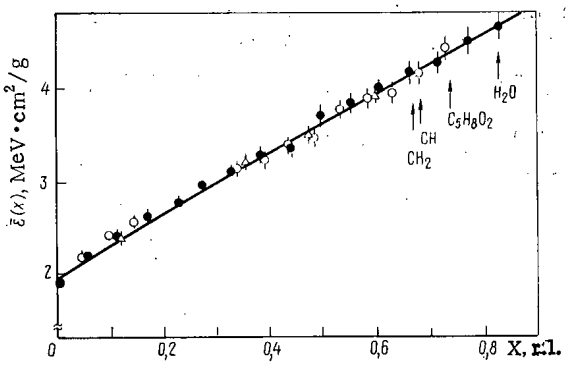

Fig. 3. Depth distribution of energy release $\bar{\varepsilon}(X)$ for positrons of initial energy 1.7 GeV in Plexiglas (●), polystyrene (○), and polyethylene (Δ).

TABLE 1. Characteristics of Absorbers

Material	Density, g/cm³	Radiation length [13], g/cm²	Thickness equiv. to 0.831 r.l., g/cm²	Thickness of plate, g/cm²
Water (H_2O)	1,00	36,08	30,0	—
Plexiglas ($C_5H_8O_2$)	1,18	40,55	33,7	2,23
Polystyrene, scintillator (CH)	1,06	43,8	36,4	2,12
Polyethylene (CH_2)	0,92	44,78	37,2	5,34

The tirgger signal developed provided resolution by pulse-height analysis. The average energy release $\bar{\varepsilon}$ was calculated from the spectral distribution $\varepsilon(W)$

$$\bar{\varepsilon} = \int_0^{W_{max}} \varepsilon(W)\, W\, dW \Big/ \int_0^{W_{max}} \varepsilon(W)\, dW$$

to determine the absorbed dose. The methods of calibrating the spectrometer, processing the experimental data, and analyzing the statistical and absolute errors of the measurements were described in [4].

Results. The energy release of 1.7-GeV positrons was measured in Plexiglas, polystyrene, and polyethylene (Table 1). The dependence of the energy release on the thickness of the absorber is shown in Fig. 3. A comparison shows that within the limits of statistical error of 3%, the values of the energy release in layers whose thicknesses in r.l. are equal coincide and do not depend on the material of the absorber ($C_5H_8O_2$, CH, CH_2). At the same time, the energy rlease in various absorbers 30 g/cm² thcik (indicated by arrows in Fig. 3) are different. For example, for polyethylene and water this difference is 20%. Since the experiments were performed mainly with Plexiglas and polystyrene absorbers, in order to compare with the data of [1, 2] and ICRP [8], the depth distributions of absorbed dose were interpolated to values of the thickness of the absorber corresponding to 0.831 r.l., which is equivalent to 30 g/cm² of H_2O. As an example Table 2 lists values of the energy release in Plexiglas for beams of positrons and photons.

One of the spectral distributions of the energy release $\varepsilon(W)$ measured for a beam of positirons with E = 2 GeV is shown in Fig. 4. The Summary Table 3 lists data obtained in all the experiments and the experimental results of [4, 6, 7]. The energy dependence of the conversion factor for monoenergetic electrons and positrons published in the recommendations of the ICRP, and our experimental results are shown in Fig. 5.

TABLE 2. Depth Distribution of Energy Release in Plexiglas,* MeV cm^2/g

Thickness of absorber, g/cm^2	Positrons, GeV				Photons 3,5—3,9 GeV
	0,7	1,7	2,5	5,0	
0	1,86	1,95	1,99	2,02	0,59
2,23	—	2,18	—	2,24	0,82
4,46	1,95	2,48	—	2,36	1,06
6,69	—	2,67	—	2,57	1,24
8,92	2,16	2,81	—	2,87	—
11,1	—	3,00	2,97	3,12	1,54
13,4	2,47	3,14	—	3,16	—
15,6	—	3,34	—	3,40	1,90
17,8	2,64	3,39	—	3,61	—
20,1	—	3,71	—	4,03	2,23
22,3	2,87	3,86	4,28	3,97	—
24,5	—	4,02	—	4,29	2,43
26,8	3,18	4,18	—	4,74	—
29,0	—	4,27	—	5,03	2,58
31,2	—	4,49	—	5,35	2,75
33,5	3,64	4,64	5,45	5,62	2,92
33,7	3,58	4,49	5,37	5,51	2,87

*Absolute error of results 7%.

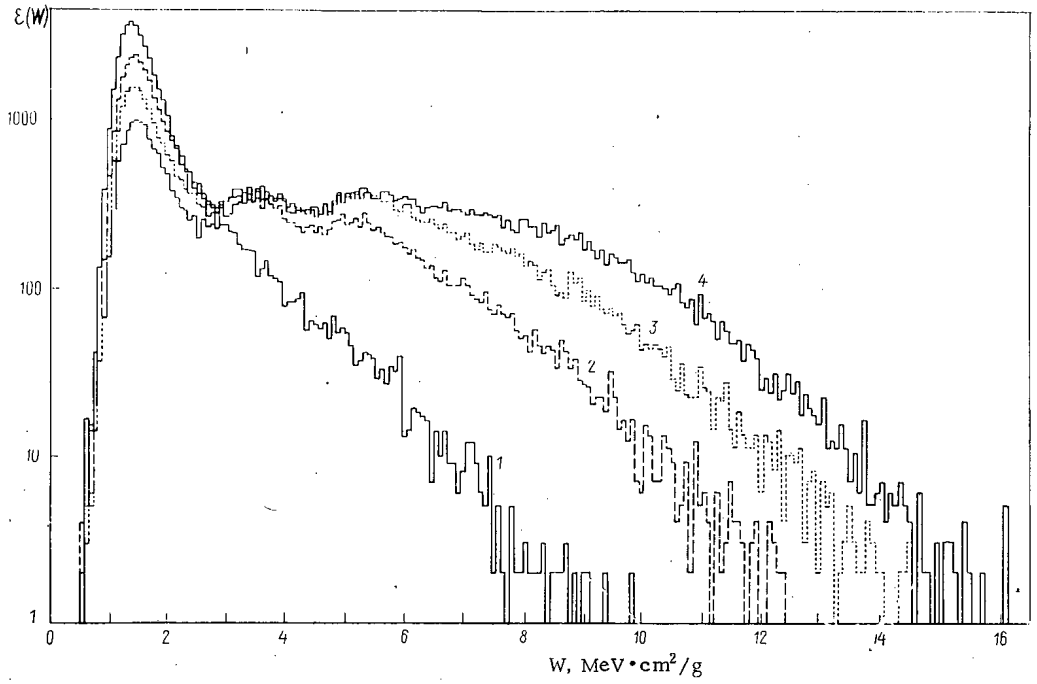

Fig. 4. Differential distribution of energy release ε(W) (the number of events in the interval 75 keV·cm^2/g) for positrons with an initial energy of 2 GeV: 1) at an absorber depth of 0 g/cm^2 for a total of 41130 events in the spectrum, $\bar{\varepsilon}$ = 1.97 MeV·cm^2/g; 2) 11.1 g/cm^2, 40280 events, $\bar{\varepsilon}$ = 3.06 MeV·cm^2/g; 3) 22.3 g/cm^2; 40330 events, $\bar{\varepsilon}$ = 4.16 MeV·cm^2/g; 4) 33.5 g/cm^2, 40270 events, $\bar{\varepsilon}$ = 5.30 MeV·cm^2/g.

Discussion of Results. Our measured values of the specific equivalent dose for electron radiation are systematically lower than those recommended by the ICRP [8] and the data of [9] over the whole range of energies investigated from 200 MeV to 40 GeV; for muons they practically coincide with the data of [3-5]. The values of the energy release in equal thicknesses of absorber, expressed in units of the radiation length, coincide and do not depend on the material (plexiglas, polystyrene, polyethylene).

The finite transverse dimensions of the spectrometer and absorber reduce the values of the energy release below those for an infinite plane absorber. Analysis of the data in [6] shows that under the conditions of our experiment the radiation leakage is ~1.6%.

TABLE 3. Summary Data on Dose Characteristics of High-Energy Leptons and Photons

Particle	Energy, GeV	Energy release in spectrometer,[1] MeV·cm²/g		Specific equiv. dose, mrem·cm²/particle²	Particle	Energy, GeV	Energy release in spectrometer, MeV·cm²/g		Specific equiv. dose, mrem·cm²/particle²
		$X = 0$	$X = (0,831 - \Delta X/2)$ p. u.				$X = 0$	$X = (0,831 - \Delta X/2)$ p. u.	
Positron	$0,20^{+0,6}_{-0,2}$	1,8±0,1	2,8±0,2	45±3	Positron[3]	2,9±0,2	2,0±0,1	5,7±0,4	91±6
The same	0,4±0,1	1,8±0,1	3,3±0,2	53±4	The same	3,1±0,2	2,0±0,1	5,4±0,4	86±6
" "	0,7±0,2	1,9±0,1	3,6±0,2	57±4	" "	3,3±0,2	2,0±0,1	5,5±0,4	88±6
Muon[3]	$0,9^{+0,2}_{-0,1}$	1,8±0,1	2,0±0,1	32±2	Photon	$3,6^{+0,3}_{-0,1}$	0,59±0,6	2,9±0,3	46±5
Electron[4]	1,0	1,8	4,3	—	Positron	5,0±0,1	2,0±0,1	5,6±0,4	91±6
Positron	1,2±0,2	2,0±0,1	4,7±0,3	76±5	Muon	4,9±0,1	1,8±0,1	2,1±0,2	34±2
The same	1,7±0,3	2,0±0,1	4,5±0,3	72±5	Electron[5]	5,2	3,6	13	200
" "	2,0±0,3	2,0±0,1	5,2±0,4	84±6	Positron	9,0±0,2	2,0±0,1	5,8±0,4	93±7
" "	2,1±0,2	1,9±0,1	4,8±0,3	76±5	Muon	8,9±0,2	1,9±0,1	2,1±0,2	34±3
" "	2,5±0,1	2,0±0,1	5,4±0,4	86±6	The same	10,9±0,2	1,8±0,1	2,2±0,2	35±2
Muon	2,4±0,1	1,8±0,1	2,0±0,1	33±2	Electron	31±1	2,0±0,1	6,3±0,4	101±7
Positron	2,8±0,2	2,0±0,1	4,5±0,3	73±5	The same	40±1	2,2±0,1	7,1±0,5	114±8
Muon[3]	2,8±0,2	1,8±0,1	2,2±0,1	34±2	Muon	40±1	1,9±0,1	2,5±0,2	40±3

[1]Averaged over thickness of detector $\Delta X = 2.12$ g/cm².
[2]1 rem = 0.01 J/kg.
[3]Data from [4].
[4]Data from [6].
[5]Data from [7].

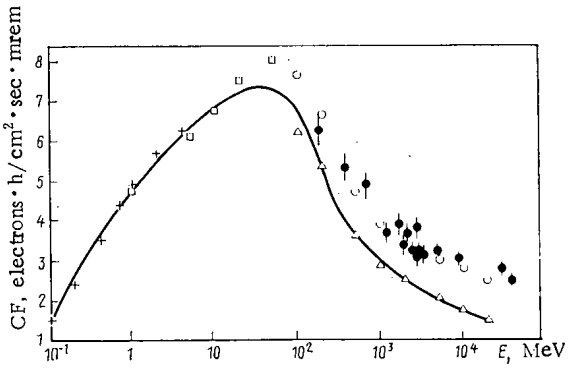

Fig. 5. Conversion factor (CF) for monoenergetic electrons and positrons: ——) +, □, ○, Δ, [8]; ●) our work.

The experiment with photons clearly cannot be considered sufficiently accurate in absolute normalization, since the long length t of the target (t = 0.6 r.l. was chosen from considerations of sufficient photon intensity) may permit the recording of more than one photon per event. Nevertheless, we consider this the simplest and most convenient method. The indeterminacy in the number of incident photons can be removed by using a target with $t \leq 0.1$ r.l.

In our opinion a comparison of the calculational methods with the experimental data on the differential distribution of absorbed dose (Fig. 4) represents a more accurate criterion of the correctness of the calculations. Such a comparison is probably possible only in calculations by the Monte Carlo method. In this case, it is desirable to use the experimental distribution $\varepsilon(W)$ for $X = 0$ as the function of random sampling of the energy release of a charged particle, since in this case the resolving power of the spectrometer is taken into account.

In conclusion, some characteristic features of the experiment should be noted.

It was shown that added discrimination of the scintillation counter in front of the phantom was necessary to eliminate the recording of δ-electrons accompanying the electron beam.

Unfortunately, the inclusion of the shower spectrometer behind the phantom for further selection and discrimination against background particles is possible only in electron beams with $E > 0.4$ GeV, since for lower energies the energy release in the phantom (~ 90 MeV) is comparable with the energy of the primary particle.

The experimental results obtained can be useful in estimating the radiation hazard for personnel working at high-energy accelerators, and in the design of new accelerator complexes.

In conclusion, we thank V. N. Lebedev for his support and interest in the work, V. F. Buchnev and S. M. Kupriyanov for an active part in preparing the apparatus, V. S. Lukanin and N. V. Mokhov for constant interest in the work and valuable advice on setting up and performing the experiment, V. M. Kut'in for kindly making it possible to perform the experiment in a channel, E. A. Belogorlov for providing for the processing of the results, and A. A. Mishina for preparing the manuscript for publication.

LITERATURE CITED

1. R. Alsmiller and H. Moran, Nucl. Instrum. Methods, 58, 343 (1968).
2. H. Beck, ibid., 78, 333 (1970).
3. A. A. Beschinskaya, E. L. Potemkin, and V. V. Frolov, in Dosimetry Problems and Radiation Shielding [in Russian], No. 14, Atomizdat, Moscow (1975).
4. G. I. Britvich and N. V. Mokhov, Preprint IFVÉ 75-120, Serpukhov (1975).
5. V. T. Golovachik et al., Preprint IFVÉ 74-58, Serpukhov (1974).
6. C. Crannel et al., Phys. Rev., 184, 426 (1969).
7. K. Tesch, Nukleonik, 8, 264 (1966).
8. ICRP Recommendations, Publication 21, Pergamon, Oxford (1973).
9. E. E. Kovalev et al., Atlas of Dose Characteristics of External Ionizing Radition [in Russian], Atomizdat, Moscow (1978).
10. S. A. Akimenko et al., Preprint IFVÉ 75-111, Serpukhov (1975).
11. S. S. Gershtein et al., Preprint IFVÉ 79-93, Serpukhov (1972).
12. F. Binon et al., Preprint IFVÉ 78-133, Serpukhov (1978).
13. C. Bricman et al., Review of Particle Properties. Particle Data Group CERN, Geneva (1978).

EXPERIMENTAL INVESTIGATION OF THE ^{137}Cs CONCENTRATION IN WATERS OF THE BALTIC SEA IN 1977-1979

D. B. Styro, G. I. Kadzhene, M. V. Lukinskene, A. P. Nemanis, and M. V. Aivarzhi

UDC 551.464.679

At the present time equilibrium has been established between the entrance of radionuclides from the atmosphere into the hydrosphere and their downward penetration from the water surface. The hazard of radioactive contamination is now a threat only in those regions where there is a discharge of radioactive waste, or fission products are carried by rivers into seas and oceans. An example of such a region is the North Sea in which the ^{137}Cs concentration has increased sharply in the last few years [1, 2]. The contamination of the waters of the Baltic Sea by radionuclides is due mainly to global fallouts, but there is the possibility of the entrance of waste from atomic industry plants located near its shore [3].

Many measurements have been made of the ^{137}Cs concentration in the Baltic Sea [4-9]. A uniform distribution of the concentration of the radionuclide in the surface waters is rarely observed, and its vertical profile is nonuniform also. There are characteristic changes of the absolute values of the concentration of

Translated from Atomnaya Énergiya, Vol. 49, No. 1, pp. 43-45, July, 1980. Original article submitted October 16, 1979.

 0038-531X/80/4901-0472$07.50

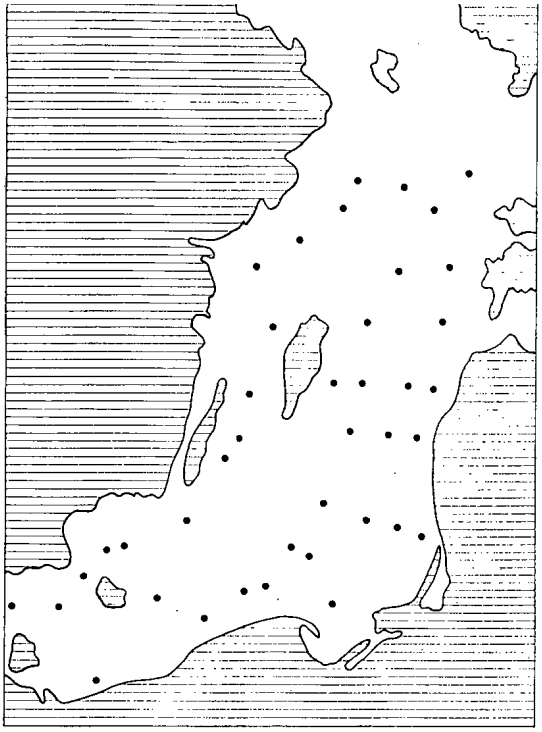

Fig. 1. Locations of samplings of seawater in the Baltic Sea.

the radionuclide at a depth of ~50 m, i.e., in the region of the layer of discontinuity in the density, below which there is mainly a decrease in the concentration of the radionuclide. Successive measurements of the ^{137}Cs concentration were made during trips of the ship Oceanographer in 1977-1979 at points marked on Fig. 1. The concentration was dettermined from 70-100 liters of seawater by a sorption method similar to that proposed in [10], and checked by a radiochemical method [11]; in certain cases only the radiochemical method was used. Saturated cesium sorbent or a concentration was measured with a γ spectrometer. The maximum error of the results did not exceed 25% [9]. The horizontal distribution of the ^{137}Cs concentration was nonuniform both on the surface and below. For example, in the autumn of 1977 the concentration of ^{137}Cs in the surface waters varied from 0.31 to 1.1 nCi/m^3 (1 Ci = $3.700 \cdot 10^{10}$ dis/sec) and in May of 1978 from 0.61 to 1.0 nCi/m^3. At a depth of 50 m the minimum and maximum values in October 1977 were 0.47 and 1.4 nCi/m^3, and in March 1978 the corresponding values were 0.42 and 1.3 nCi/m^3. At depths of more than 50 m the concentration generally decreased. The only frequently observed exceptions were in layers near the bottom in the southern part of the Baltic Sea, where at a few meters above the bottom a sharp increase in concentration was observed, aparently a result of the infiltration of this radionuclide from the waters of the North Sea [1, 2].

The horizontal distribution of the ^{137}Cs concentration was more uniform in the spring than in the fall, but in the spring the concentration on the average increases, especially in the surface waters, as shown by the data of Table 1. It must be assumed that the variations of the absolute values of the concentration of the radionuclide are to some extent related to the season of the year, i.e., to the intensity of fallout and the atmospheric activity [12].

TABLE 1. Average Values of the ^{137}Cs Concentration at Various Depths in the Baltic Sea in 1977-1979, nCi/m^3

Depth, m	Oct. 1977	Mar. 1978	May 1978	Nov. 1978	Feb. 1979
0	0,64	0,80	0,79	0,68	0,74
50	0,80	0,76	—	0,75	—
>50	0,63	—	—	—	—

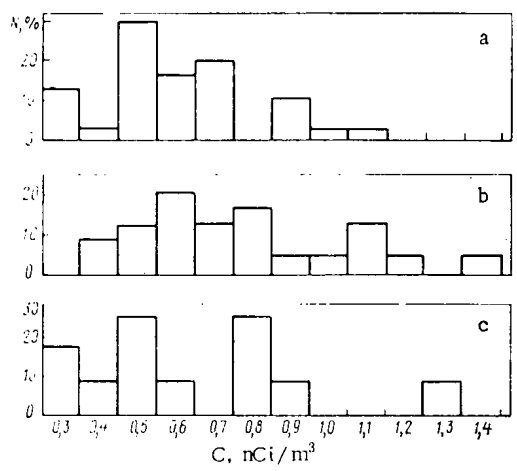

Fig. 2

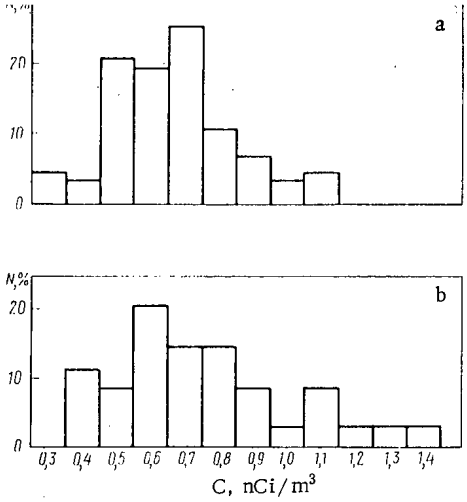

Fig. 3

Fig. 2. Relative reproducibility of results of measurements of ^{137}Cs concentration (autumn 1977) a) in surface waters, b) at a depth of 50 m, c) below 50 m.

Fig. 3. Relative reproducibility of results of measurements of ^{137}Cs concentration (data from 1977-1979) a) in surface waters, b) at a depth of 50 m.

Figure 2 compares the reproducibility of identical values of the ^{137}Cs concentration as a function of the number of measurements in October 1977 at various depths in the Baltic Sea. In the surface waters the most typical concentration was 0.5-0.6 nCi/m^3 (cf. Fig. 2a). At a depth of 50 m these values were somewhat higher: 0.6-0.7 nCi/m^3 (cf. Fig. 2b). At depths of more than 50 m in the Baltic Sea two intervals of maximum values from the total number of measurements were observed – at concentrations of 0.5-0.6 and 0.8-0.9 nCi/m^3 (cf. Fig. 2c). However, the last results can only be considered preliminary because of the scantiness of the data.

In the surface waters the ^{137}Cs concentration was 0.5-0.7 nCi/m^3 from October 1977 to February 1979, and the maximum of the measurements corresponded to values between 0.7 and 0.8 nCi/m^3 (Fig. 3a). In this period the ^{137}Cs concentration at a depth of 50 m varied over a wider range than in the autumn of 1977: from 0.4 to 1.4 nCi/m^3 (cf. Fig. 3b). The most typical values of the concentration at this depth were lower than the values of the concentration in the surface waters.

Conclusions. The nonuniform distribution of the ^{137}Cs concentration in the waters of the Baltic Sea is evidently due to variations in the intensity of global fallouts, the hydrologic behavior of the sea, storm activity which can result in an increase in bottom deposits having a larger excess of radionuclides, the effect of waters of the North Sea which have an increased ^{137}Cs content, and runoff of waters from the land.

The vertical profile of the ^{137}Cs concentration is characterized by a small increase at a depth of ~50 m, and then a decrease. Much more rarely there is an increase in the concentration at a depth of more than 50 m, which obviously is due to the presence of a layer of discontinuity in the density at a depth of ~50 m which prevents the penetration of ^{137}Cs into deeper layers. It should be noted particularly that there are layers near the bottom in the southern Baltic (at a depth of less than 50 m) where there frequently is observed a larger ^{137}Cs concentration than in layers above them as a result of the effect of waters of the North Sea. In the spring the absolute and average lalues of the ^{137}Cs concentration in the surface layer generally increase up to a depth of ~50 m, which probably is related to the spring maximum of atmospheric fallouts [12].

LITERATURE CITED

1. H. Kautsky, Dtsch. Hydrogr. Z., 6, 217 (1976).
2. D. B. Styro et al., in: Chemical and Radioactive Contaminants of the Atmosphere and Hydrospheres [in Russian], Mokslas, Vilnius (1978), p. 138.
3. A. M. Petros'yants, Atomic Power [in Russian], Nauka, Moscow (1976).
4. A. Salo and A. Voipio, Radioecological Concentration Processes, 19, 827 (1968).
5. A. Voipio and A. Salo, Nord. Hydrol., 2, 57 (1971).
6. S. M. Vakulovskii et al., At. Energ., 39, 177 (1975).

7. L. B. Styro et al., in: Radioactivity of the Atmosphere and Hydrosphere [in Russian], Mokslas, Vilnius (1977), p. 197.
8. D. B. Styro et al., in: Chemical and Radioactive Contaminants of the Atmosphere and Hydrosphere [in Russian], Mokslas, Vilnius (1978), p. 131.
9. D. B. Styro et al., At. Energ., 45, 201 (1978).
10. N. P. Dargene, M. V. Lukinskene, and D. B. Styro, in: Physical Aspects of the Contamination of the Atmosphere [in Russian], B. Styro, (Editor), Mokslas, Vilnius (1976), p. 248.
11. L. M. Ivanova, Radiokhimiya, 9, 622 (1967).
12. B. I. Styro, V. Yu. Luyanas, and K. K. Shopauskas, Radioactivity of the Atmosphere and Meteorology [in Russian], Mintis, Vilnius (1975).

PRINCIPAL COMPONENTS OF THE BACKGROUND COUNTING RATE OF A LARGE SCINTILLATION DETECTOR

Yu. V. Sivintsev, G. A. Nezhdanov, E. L. Koval'chuk, K. V. Voronin, and S. P. Pugachev

UDC 539.1.074.6

One of the main ways of increasing the sensitivity of the methods of radiometry and spectrometry of ionizing radiations is to lower the background counting rate (BCR) of the detector. It is known that htis quantity consists of three components, which are produced by cosmic radiation and the radionuclides contained in the passive shielding used and in the detector itself.

In recent years passive steel low-background shielding (SLB) no less than 20 cm thick in any direction* has been widely used. Such equipment, which has been developed at the I. V. Kurchatov Institute of Atomic Energy, is being used in scientific investigations as well as for the control of the BCR of scintillation detectors during their development and production. An attempt has been made in [1] to determine experimentally the contribution of cosmic radiation to the BCR of a large scintillation detector. The use of various passive shields on the surface of the earth and in connection with burial of the detector beneath the earth (for a significant reduction of the cosmic radiation flux) has stimulated the authors to repeat this work.

In the 1960s the material of the glass envelope of the FÉU-49 photomultiplier was replaced by potassium-free (sodium) glass to lower the fraction of the BCR produced by ^{40}K. This action significantly reduced the contribution of photomultipliers to the BCR of scintillation detectors [2]. A further reduction of the BCR is usually achieved by the exclusion of the cosmic component with the help of an anticoincidence circuit [3] or extensive (more than 100 m water equivalent) passive shielding [4].

In this paper the contribution of the FÉU-49 to the residual (after exclusion of cosmic radiation) BCR is experimentally determined, and the possibility of lowering the BCR after replacement of the glass envelope of the FÉU-49 by a quartz one is estimated.

Contribution of Cosmic Radiation. Measurements were made at the Baksansk Neutrino Observatory (BNO) in the ground-level (about 1700 m above sea level) and the underground (660 m water equivalent) low-background laboratories [5] in March of 1979.

The absolute value and spectral composition of the BCR of the scintillation unit (SU) developed at the I. V. Kurchatov Institute of Atomic Energy on the basis of a single crystal of NaI(Tl) 140 × 140 mm in diameter and an FÉU-49 was investigated. Both in the ground-level and in the underground laboratories we used an SLB apparatus. In addition the measurements in the underground laboratory were made in a low-background chamber shielded from the radioactive radiations of the bocks by 100 cm of dunite (an ultrabasic rock), 1 cm of steel, and 3 cm of tungsten† [5].

*Further increase in the thickness of the shielding does not result in significant reduction of the BCR.
†For the sake of brevity, we will write "tungsten shielding" below.

Translated from Atomnaya Énergiya, Vol. 49, No. 1, pp. 45-49, July, 1980. Original article submitted December 24, 1979.

0038-531X/80/4901-0475$07.50

TABLE 1. BCR of SU No. 23 (in pulses/sec) in the Ground-Level and Underground Laboratories of the BNO for Different Energy Ranges

Laboratory	Shielding	Energy range, MeV				
		0,1–0,8	0,8–1,2	1,2–1,8	1,8–3,0	0,1–3,5
Ground-level	No	1300±70	120±6	100±5	35±2	1600±80
" "	SLB	14,0±0,3	2,3±0,1	1,7±0,1	1,1±0,05	19±1
Underground	No	900±50	120±6	100±5	33±2	1200±60
"	SLB	4,6±0,2	1,2±0,1	0,80±0,05	0,30±0,02	7,0±0,4
"	Tungsten	3,5±0,2	0,70±0,05	0,56±0,03	0,16±0,01	4,9±0,3

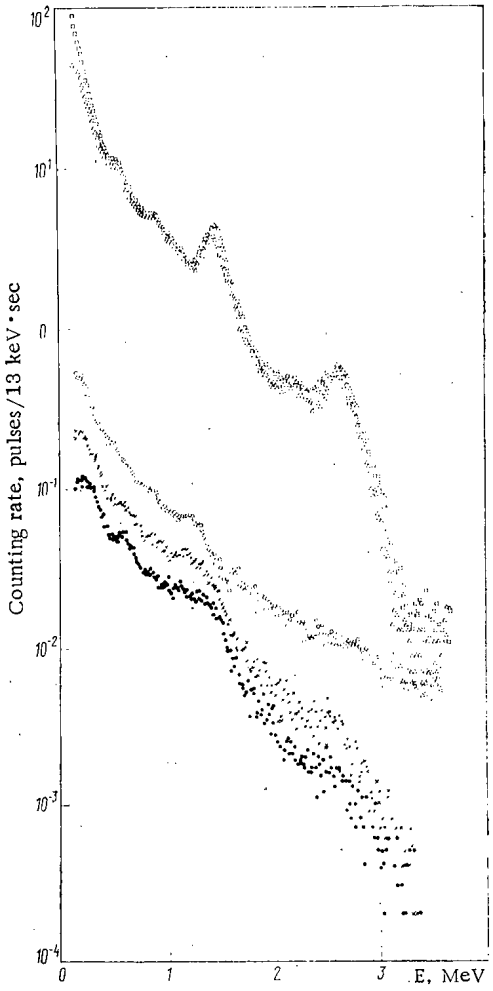

Fig. 1. Energy spectra of the background of SU No. 23 obtained in the ground-level laboratory without shielding (□) and in SLB (○) and in the underground laboratory without shielding (△), in SLB (×), and in tungsten shielding (●).

The instrumental spectrum of the pulse amplitudes was recorded by AI-1024-4 and UNO-1024-90 analyzers. The instrumental spectra of the BCR of SU No. 23 in tungsten shielding are given in Fig. 1. The peaks of the total absorption of ^{40}K (E = 1.46 MeV) and ^{208}Tl (2.62 MeV) are clearly evident in the graphs.

The results of the processing of the measured instrumental spectra of the BCR in different energy ranges are given in Table 1.

Since the muon flux in the underground laboratory is attenuated by a factor of $2 \cdot 10^3$ time [6], the contribution of cosmic radiation to the BCR is determined as the difference in the values of the BCR for the detector (shielded by one and the same passive shielding) recorded in the ground-level and the underground laboratories (Table 2).

TABLE 2. Contribution of Cosmic Radiation to the BCR of SU No. 23 for Different Energy Ranges

Energy range, MeV	Abs. contribution, pulses/sec	Rel. contribution, pulses/sec
0,1—0,8	9,4±0,5	67±4
0,8—1,2	1,10±0,05	48±3
1,2—1,8	0,90±0,05	53±3
1,8—3,0	0,80±0,02	73±4
0,1—3,5	12,2±0,5	64±4

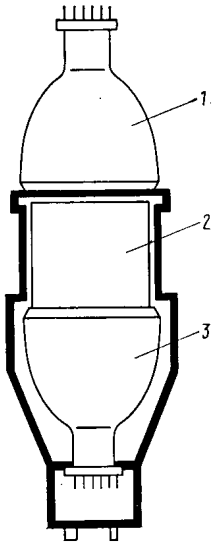

Fig. 2. Layout scheme of the investigated photomultipliers and glass envelopes: 1) investigated photomultiplier (or its glass envelope), 2) NaI(Tl) 140 × 140 mm in diameter, and 3) FÉU-49.

The increase of the contribution of cosmic radiation to the BCR of the detector in the 0.8-3.0 MeV range as the energy increases is explained by the abrupt reduction of that part of the background which is caused by natural radionuclides of the shielding and detector materials. The increase of the cosmic component of the BCR in the 0.1-0.8 MeV range can be related to the large value of the scattered cosmic radiation. All the results given are in agreement with the data of Refs. 3 and 4, in which similar measurements are described and the fraction of the cosmic component of the BCR is estimated to be equal to 60 and 72%, respectively. Such a large contribution of cosmic radiation to the BCR should be taken into account under ground-level conditions in connection with the determination of the intrinsic background of scintillation detectors in research on lowering it.

As has been noted, the widespread but not optimal SLB passive shielding was used in the measurement sequence described. Therefore, the BCR of SU No. 23 was determined in tungsten shielding, which is close to the optimal, in another series of measurements. These results permitted comparing the effectiveness of the passive shieldings used and also characterizing the radiation purity of iron and tungsten. The ratio of the BCR values of a detector recorded in the underground laboratory in steel (SLB) shielding and tungsten shiled-ing are given below:

Energy range, MeV	0.1—0.8	0.8—1.2	1.2—1.8	1.8—3.0	0.1—3.5
Ratio	1.3±0.1	1.7±0.2	1.5±0.1	1.9±0.2	1.4±0.1

TABLE 3. Contribution to the BCR of SU No. 22 Produced by the Photomultiplier and Glass and Quartz Envelopes*

Measured parameter	Energy range, MeV									
	0,1–0,8		0,8–1,2		1,2–1,8		1,8–3,0		0,1–3,5	
	pulses/sec	% inc.	pulses/sec	% inc.	pulses/sec	% inc.	pulses/sec	% inc.	pulses/sec	% inc.
Background	2,4	—	0,35	—	0,24	—	0,064	—	3,0	—
Photomultiplier	3,4	42	0,5	43	0,37	54	0,12	85	4,5	50
Photomultiplier env.	3,3	38	0,47	34	0,35	46	0,12	85	4,3	43
Quartz envelope	2,2	$\leqslant 5$	0,32	$\leqslant 5$	0,21	$\leqslant 5$	0,065	5	2,9	$\leqslant 8$

*The error is no greater than 5%.

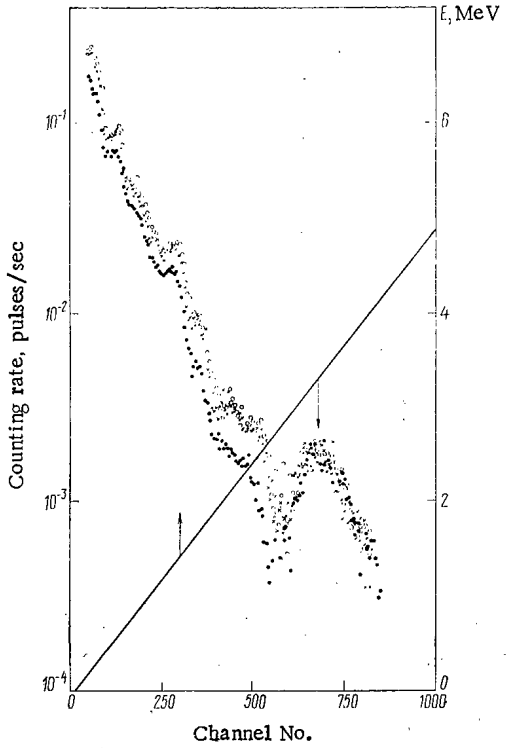

Fig. 3. Average instrumental spectra of the intrinsic background of the SU and also the background produced by the investigated photomultipliers and their envelopes (● – SU background, ○ – photomultiplier, and × – envelope). The results of the energy calibration of the SU are denoted by the straight line.

It is evident that in this case the steel shielding is inferior in radiation purity to tungsten by approximately a factor of 1.5 on the average, and by practically a factor of two in the range $E \geq 1.8$ MeV.

Contribution of the Photomultiplier and Its Glass Envelope. Measurements were made in the underground low-background chamber of the BNO. A detector (SU No. 22) based on a single crystal of NaI(Tl) 140 × 140 mm in diameter and an FÉU-49 were placed in tungsten shielding. The background counting rate of the detector was measured first, and then its increase due to the investigated FÉU-49, its glass envelope, and a quartz envelope geometrically identical to the glass envelope of the FÉU-49 (Fig. 2). Photomultipliers manufactured from November of 1970 through June of 1972 were used for these experiments. The average instrumental spectra of the intrinsic background of the SU and also the background produced by the photomultipliers and envelopes being investigated are given in Fig. 3, and the average data on the corresponding counting rates of the detector as a function of photon energy are given in Table 3. The error in the results caused by the statistical nature of the processes and the instability of operation of the equipment increased from 0.6 to 4% as the energy range increased. However, the mean-square error calculated from the data of seven series of BCR measurements varies from 1.5 to 5%. Evidently, the cause of the neglected error was a variation in the radon concentration in the underground laboratory. Therefore, all the results are given with an error of 5%.

A characteristic peculiarity of the data obtained is the significant increase in the BCR in connection with the measurement both of the photomultipliers and their glass envelopes. At the same time no variations of the BCR due to quartz envelopes were exhibited within the limits of error of the measurements. The contribution of the FÉU-49 to the BCR of the detector increases from 42 ± 2 to 85 ± 5% as the energy increases from 0.1-0.8 to 1.8-3.0 MeV, and the contribution produced by the envelopes of these same photomultipliers increased from 38 ± 2 to 82 ± 4%. This result can be explained by the fact that the content of radionuclides of the uranium and thorium series is significantly greater in the glass envelope of the photomultiplier than in the quartz envelope. According to our data, the replacement of glass envelopes of FÉU-49 by quartz ones should lower the BCR of SU with an NaI(Tl) crystal 140 × 140 mm in diameter by a factor of two to five, depending upon which one of the indicated energy ranges is being discussed. As the energy increases, this value increases. Thus, e.g., the BCR is lowered by no less than a factor of 20 due to the use of a photomultiplier in a quartz envelope for the recording range of the photopeak of ^{208}Tl (E = 262 MeV) with the boundaries 2.34 and 2.86 MeV.

For a photon energy $E \geq 3.0$ MeV, i.e., beyond the limits of the region of natural radioactivity, a peak is distinctly visible which is produced by the α particles of the uranium and thorium series. Since one and the same detector was used in all the measurements, the counting rate in this energy region agreed in all the measurements. Unfortunately, it is impossible due to the uncertainty in the ratio of the uranium and thorium concentrations to interpret this α-peak by indicating the uranium and thorium content in the material of the single crystal and its reflector.

Thus, one can close with the following conclusions:

1. The contribution of cosmic radiation for an SU based on a single crystal of NaI(Tl) 140 × 140 mm in diameter and an FÉU-49 under conditions of SLB shielding with a thickness of 20 cm of steel in every direction amount to from 48 ± 3 to 73 ± 4%, depending upon the energy range being recorded.

2. The amount of the contribution to the BCR of the large SU mentioned which is produced by the FÉU-49 and its envelope amounts to from 42 ± 2 to 85 ± 4% for the photomultipliers and from 38 ± 2 to 82 ± 4% for their envelopes as the energy increases from 0.1 to 3.0 MeV.

3. Within the limits of the measurement error no excess of the BCR of the SU is exhibited upon the placement on it of quartz envelopes geometriclaly identical to the FÉU-49 envelopes.

4. It has been estimated that the use of quartz glass envelopes lowers the BCR of an SU with an NaI(Tl) crystal 140 × 140 mm in diameter and an FÉU-49 by a factor of two to five, depending upon the energy range being recorded.

5. Comparison of the radiation purity of steel and tungsten upon their use as the materials of passive shielding has shown that in this case steel is inferior to tungsten in radiation purity by approximately a factor of 1.5 on the average, and by practically a factor of two in the region $E_\gamma \geq 1.8$ MeV.

LITERATURE CITED

1. G. A. Nezhdanov, Yu. V. Sivintsev, and V. M. Fomin, in: Prospects for the Development of the Technology and the Methods of Control and Production of Scintillators and Scintillation Detectors in the Tenth Five-Year Plan [in Russian], Vol. 2, Cherkassy (1977), p. 95.
2. Yu. V. Sivintsev et al., At. Energ., 22, No. 1, 60 (1967).
3. S. Tanaka et al., Nucl. Instrum., 56, No. 2, 319 (1967).
4. J. Kaye et al., ibid., 100, No. 2, 333 (1972).
5. E. L. Koval'chuk et al., in: Proc. Int. Conf. on Low-Radioactivity Measurements and Applications, Bratislava (1977), p. 23.
6. E. L. Koval'chuk, V. A. Luk'yanov, and A. A. Smol'nikov, Preprint of the Institute of Nuclear Physics, Academy of Sciences of the USSR P-0095, Moscow (1978).

SEARCH FOR AND IDENTIFICATION OF TRACKS OF FRAGMENTS FROM THE SPONTANEOUS FISSION OF NUCLEI OF SUPERHEAVY ELEMENTS IN NATURAL MINERALS

Kh. Murtazaev and V. P. Perelygin

UDC 546.799

The search for the effect of the spontaneous fission of superheavy elements by the method of dielectric detectors was first undertaken in 1968 [1], and since then much research has been performed in various countries [2-9]. The common approach was to try to observe an excess number of spontaneous fissions of atomic nuclei which could not be accounted for by the spontaneous fission of microscopic admixtures of uranium in the samples studied. The uranium concentration was measured by neutron activation analysis using the track method. The age of the samples either was known or was determined by the potassium–argon method [4, 5].

An appreciably excess density of fission fragment tracks was observed in certain samples of eighteenth and nineteenth century crystals and lead glasses [1,3]. However, direct measurements of the probability of fission of lead nuclei by cosmic radition [6] gave a value of 15 ± 4 fissions per gram per year, which in most cases accounted for the effect observed in the glasses. An excess density of spontaneous fission tracks was also observed in biotite from Tanzania [5], in micas from North America [7], at contacts of feldspars with the material of concretions [2], and quartz crystals with oxidized pyrite inclusions [5]. These samples were found deep underground or at a depth up to 5 km in the Pacific Ocean, which obviously eliminated any appreciable contribution from cosmic radiation. However, the observed effect could be due to the migration of uranium from the surfaces of contact in concretions and in contacts of quartz with oxidized pyrite or by cleavage cracks in micas – muscovite, biotite [5, 6].

One of the intrinsic faults of this method of searching for superheavy elements is its relatively low sensitivity. For reliable observation of the effect the number of tracks of spontaneous fission of superheavy nuclei should be at least equal to the number of tracks from the spontaneous fission of uranium nuclei in the sample. This means that the recording of spontaneous fission events in samples containing 10^{-6}-10^{-7} g per gram of uranium enables one to obtain an upper limit of the concentration of superheavy elements at a level of 10^{-12}-10^{-13} g/g.

In view of this, attempts were made to increase the sensitivity of the searches for spontaneously fissionable superheavy elements. One of the most promising ways of increasing the sensitivity was to use neutron coincidence counters, permitting the identification of superheavy nuclei by the multiplicity of neutrons emitted in spontaneous fission [8, 10, 11]. The sensitivity of the method permits the search for superheavy elements with a concentration down to 10^{-14}-10^{-15} g/g. By using this method the effect of spontaneous fission of an unknown element in meteorites of the carbonaceous chondrites type [12] and in thermal springs from the Cheleken peninsula [13, 14] was reliably established.

Other attempts to identify superheavy elements were based on the assumption that the average track length of fragments of the spontaneous fission of such nuclei in solid dielectrics is 20% longer than tracks of fission fragments of the actinides. However, samples of minerals (feldspars) of meteorites investigated in [15, 16] contained together with tracks of fission fragments also an appreciable number of tracks from cosmic nuclei of the iron group, producing tracks up to 25 μm long in feldspars. We note that in augite crystals from the Angra dos Reis meteorite [17], and in Whitlockite crystals from the Bjurböle meteorite [18] only one group of length 16-17 μm was observed in the spectrum of fission fragment lengths.

Out attempt to find superheavy elements is based on the assumption that such nuclei will undergo spontaneous fission into three fragments of comparable mass with a probability at least two orders of magnitude larger than that for the ^{238}U nucleus. This possibility of searching for and identifying fissions of superheavy

Translated from Atomnaya Énergiya, Vol. 49, No. 1, pp. 50-52, July, 1980. Original article submitted January 8, 1979; revision submitted January 24, 1980.

0038-531X/80/4901-0480$07.50

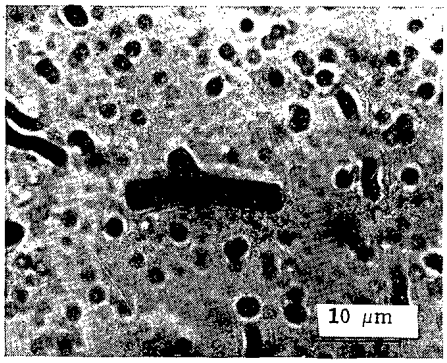

Fig. 1. Photograph of three-prong event observed in mica muscovite from East Siberia. One of the tracks appears on the mica surface.

elements is justified in detail in [18]. According to data in [19] the probability of the spontaneous fission of uranium nuclei into three fragments of comparable mass is $\leq 10^{-6}$ of the probability of binary fission. On the other hand, extrapolation of the probability ratio P_{3f}/P_{2f} for compound nuclei with Z = 108-110 formed in the reactions $^{40}Ar + Th$, $^{40}Ar + U$ at low excitation energies shows [18] that for the ground states of superheavy nuclei the ratio of the probabilities of spontaneous ternary fission and binary fission should be $\geq 10^{-4}$.

Thus, there is a possibility of identifying the effect of the spontaneous fission of superheavy nuclei by observing three-prong events in minerals of terrestrial and extraterrestrial origin. As a result of the increased probability of ternary fission of superheavy nuclei the sensitivity of the method is at least two orders of magnitude larger than in experiments seeking an excess density of spontaneous fission tracks. In addition, this method of search does not require independent measurments of the absolute age of the sample. We have searched for three-prong tracks indicating the spontaneous fission of hypothetical superheavy nuclei in micas – muscovites and biotites from various beds.

The muscovites were etched in 48% hydrofluoric acid for 1 h at 20°C, and the biotites in 10% hydrofluoric acid for 20 min at 20°C. Two samples of muscovite from East Siberia and India with track densities of $3.7 \cdot 10^3$ and $0.5 \cdot 10^3$ per cm^2, respectively, and Mam biotite containing $2.8 \cdot 10^3$ tracks per cm^2 were selected for further investigation. The micas selected were split along cleavage planes into plates 20-40 μm thick, etched, and scanned under a microscope from both sides simultaneously. A search was made for three-prong events with track lengths $L \geq 2$ μm and with angles φ between tracks $15° \leq \varphi \leq 175°$, which enabled us to eliminate the effect of random overlaps of single tracks. The total area of mica scanned (muscovite from the Mam bed) was 45 cm^2; it contained $3.7 \cdot 10^3$ tracks per cm^2, corresponding to $3.2 \cdot 10^5$ tracks more than 10 μm long. The area of the Indian mica scanned was 87 cm^2; it contained $0.5 \cdot 10^3$ tracks per cm^2, which corresponds to $7.5 \cdot 10^4$ tracks. Two three-prong tracks were observed in the sample of mica from East Siberia (Fig. 1) satisfying the criteria given above. It can be seen from the figure that one of the tracks appears on the mica surface. No such tracks were observed in the Indian mica. The three-prong tracks found can be accounted for by the eleastic interaction of a fission fragment with nuclei of elements with $Z \geq 12$ (e.g., Ar, K, Ca, Fe) contained in mica [20].

Elastic scattering of fragments from the spontaneous fission of uranium on nuclei of elements of the detector matrix can be discriminated against by measurign the lengths of all three tracks. In Fig. 2 the average length of tracks of fragments from binary and ternary fission of compound nuclei with Z = 108-110 is about the same, and is $\approx 10\%$ longer than the average length of tracks of fragments from the fission of actinides [21]. The three-prong events formed in the elastic scattering of uranium fission fragments have an average track length somewhat shorter than the tracks of fragments from binary fission [22]. However, in the case under consideration both recorded events had one track appearing on the mica surface, which made identication by etching length impossible. Only an upper limit of the ratio of the probabilities of binary and ternary fission in micas can be established at the level $P_{3f}/P_{2f} \leq 1 : 7.5 \cdot 10^4$.

The preliminary results presented in the present article on the search for the effect of ternary fission of superheavy elements enables us to establish a new value of the lower limit of the abundance of superheavy nuclei in the samples investigated at a level of sensitivity at least an order of magnitude greater than that achieved earlier by track methods. The uranium content in mica from East Siberia is about $3 \cdot 10^{-8}$ g/g, $P_{3f}/P_{2f} \leq 1.3 \cdot 10^{-5}$, and hence the upper limit of the concentration of superheavy elements in this sample is $\leq 4 \cdot 10^{-15}$ g/g.

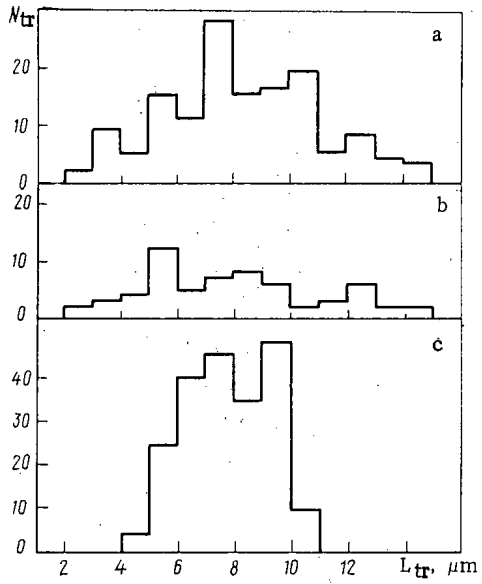

Fig. 2. Distribution of track lengths of fission fragments of nuclei formed in the interaction of 300 MeV ions of a) ^{40}Ca and b) ^{40}Ar with ^{238}U, and c) tracks of fragments from the spontaneous fission of ^{244}Cm in mica muscovite. The annealing and etching are identical for all samples [5, 22].

For further investigations it is expedient to develop tracks of ternary fission completely contained in the volume of the detector in order to be able to measure all the parameters of such three-prong events as the distribution of track lengths and the aximuthal angles between them. For micas and other minerals with very perfect cleavage, the procedure of partial splitting of the sample can be used, with subsequent etching and scanning of the contact surface. In other natural crystals tracks in the volume of the dielectric can be developed by producing artificial cracks, for example by the action of focused laser radiation [23].

In conclusion, the authors thank S. G. Stetsenko and D. Lkhagvasurén for help with the work.

LITERATURE CITED

1. G. N. Flerov and V. P. Perelygin, At. Energ., 26, 520 (1969).
2. O. Otgonsurén, V. P. Perelygin, and G. N. Flerov, Dokl. Akad. Nauk SSSR, 189, 1200 (1969).
3. É. Tses'lyak, JINR Report P15-4738, Dubna (1969).
4. P. Price and R. Fleischer, Phys. Lett., 30B, 246 (1970).
5. O. Otgonsurén et al., At. Energ., 32, 344 (1972).
6. G. N. Flerov, V. P. Perelygin and O. Otgonsurén, At. Energ., 33, 979 (1972).
7. D. Miller, Earth Planet. Sci. Lett. 4, 379 (1968).
8. G. N. Flerov, JINR Report P7-11097, Dubna (1978).
9. C. Herrman, Int. Rev. Sci., Inorganic Chemistry, 8, Ser. 2 (A. Maddock, Ed.) Butterworth, London (1975), p. 221.
10. G. N. Flerov et al., Yad. Fiz., 21, 9 (1974).
11. O. D. Maslov et al., JINR Report P6-8266, Dubna (1974).
12. I. Zvara et al., Preprint JINR P6-10589, Dubna (1972).
13. Yu. T. Chuburkov et al., Radiokhimiya, 16, 827 (1974).
14. G. M. Ter-Akop'yan, JINR Report D7-10129, Dubna (1977).
15. N. Bhandari et al., Nature, 230, 219 (1971).
16. R. Fleischer, P. Price, and R. Walker, Nuclear Tracks in Solids. Principles and Application. Univ. California Press, Berkeley (1975).
17. D. Lal, R. Rajan, and A. Tamhane, Nature, 221, 33 (1969).
18. V. P. Perelygin, S. G. Stetsenko, and N. Bkhandari, At. Energ., 42, 482 (1977).
19. M. Muga, C. Rice, and W. Sedlacek, Phys. Rev., 161, 1266 (1967).
20. V. Perelygin, in: Proc. Eighth Int. Conf. on Nucl. Photography and SSTD, Vol. 2, Bucharest, IFA (1972), p. 27.

21. V. Perelygin et al., Nucl. Phys., A127, 577 (1969).
22. L. Medveczky and C. Somogyi, in: Proc. of First Int. Conf. on Nuclear Track Registration in Insulating Solids, Vol. 2, Univ. Cleamont Press (1969), p. 65.
23. D. Lkhagvasurén et al., Paper presented at Int. Conf. on the Interaction of Heavy Ions with Nuclei and Synthesis of New Elements [in Russian], Dubna, Dec. 13-16 (1977).

EFFECT OF INDETERMINACY OF LIMITATIONS ON OPTIMIZATION OF BREEDING IN FAST REACTORS

A. S. Karabasov and G. B. Usynin

UDC 621.039.526

Optimization of the characteristics of advanced breeder reactors and the strategy for putting them into service is carried out under conditions where the initial information is indeterminate [1-4]. The purpose of taking the indeterminacy of the initial limitations is to obtain a single, entirely concrete set of reactor limitations and parameters characterizing its optimal design and based on available a priori information.

The initial stochastic problem of optimization in a probable formation is presented as follows:

find

$$\max_{\mathbf{x}} P\{f_0(\mathbf{x}, \omega) \leqslant 0\}$$

with the condition

$$P\{f_i(\mathbf{x}, \omega) \leqslant 0\} \geqslant 1 - \gamma_i;$$
$$i = \overline{1, m}; \quad 1 > \gamma_i > 0. \tag{1}$$

Here $\mathbf{x}$ is the vector of the optimized parameter; ω, vector of the parameters of the initial limitations; $f_0(\mathbf{x}, \omega)$, objective function; $f_i(\mathbf{x}, \omega)$, function of limitations; and $P\{f \leq 0\}$, probability of the condition $f \leq 0$ being satisfied.

In reactor optimization problems it is practically always possible to isolate the deterministic parts of the function of initial limitations. The initial problem (1) reduces to the following problem:

find

$$\min_{\mathbf{x}} g_0(\mathbf{x})$$

with the condition

$$g_i(\mathbf{x}) \leqslant y_i; \quad i = \overline{0, m}; \quad g_i(\mathbf{x}) = m_i / \sqrt{d_i(\mathbf{x})}, \tag{2}$$

where m_i is the mathematical expectation of the function $f_i(\mathbf{x}, \omega)$ and $d_i(\mathbf{x})$ is the variance of the function.

The values of y_i are found from $\gamma_i = W_i(y_i)$, $i = \overline{1, m}$, where $W_i(y_i) = P\{q_i(\omega) < y_i\}$ is the distribution of the random quantity

$$g_i(\omega) = \frac{f_i(\mathbf{x}, \omega) - m_i(\mathbf{x})}{\sqrt{d_i(\mathbf{x})}}.$$

In solving an optimization problem in this formulation, it is essential that the given probability of the initial limitations being satisfied by attained not at a conservative level but at a more optimistic level, which may lead to gains in the objective function.

Table 1 gives data on the inaccuracy of the fuel assembly parameters, whose indeterminacy has the most significant effect on the fast reactor characteristics. In determining the probability of the limitations being realized, we adopted the normal distribution law and assumed that the indeterminacy of all initial limit-

Translated from Atomnaya Énergiya, Vol. 49, No. 1, pp. 52-53, July, 1980. Original article submitted June 4, 1979; revision submitted January 14, 1980.

0038-531X/80/4901-0483$07.50

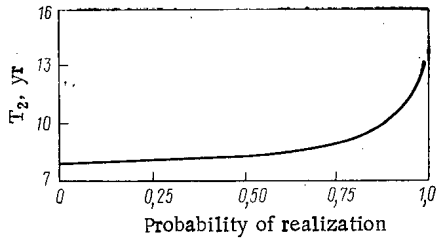

Fig. 1. Dependence of doubling time on probability of realization of limitations.

TABLE 1. Values of Initial Limitations

Parameter	Limitation	SD [6]	Level of initial limitations		
			conservative	mathematical expectation	probability (95%)
Fuel can thickness, mm	From below	0.013	0.35	0.4	0.367
Max. fuel can temp., °C	From above	10	660	700	675
Max. linear power, W/cm	From above	16	480	550	510
Steel swelling, rel. units	From below	0.13	1	0.5	0.83
Fuel-can thermal conductivity, kcal*/m²·h·deg	From above	0.08	0.2	0.6	0.4
Av. coolant heating, °C	From above	8	170	200	180
Pressure drop in reactor, kg-f/cm²*	From above	0.6	5	7	5.5
Plutonium critical mass, rel. units	From below	0.01	1	0.96	0.985
Breeding ratio, rel. units	From above	0.02	0.9	0.97	0.915
Probability of realization of level, %	–	–	100	0.2	95

*1 cal = 4.1868 J; 1 kgf/cm² = 98066.5 Pa.

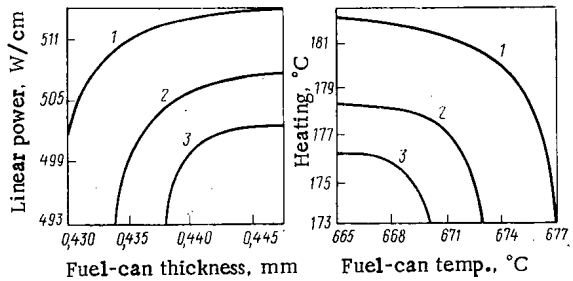

Fig. 2. Relations between reactor core characteristics, optimal in respect of doubling time, at various probabilities of their realization: 1) $1-\gamma = 95\%$, $T_2 \approx 9.6$ yr; 2) 97%, 10 yr; 3) 99%, 10.3 yr.

TABLE 2. Characteristics of Reactors Optimal in Respect of Doubling Time

Initial data	Level of initial limitations		
	conservative	mathematical expectation	probability (95%)
Fuel element diam., mm	6,8	7,2	6,9
Rel. spacing of fuel-element lattice	1,178	1,161	1,159
Height of reactor core, cm	100	96	98
Radius of reactor core, cm	168	164	164
Height of end shield, cm	30	45	33
Thickness of side shield, cm	39	58	45
No. of fuel ele. in assbly.	217	217	217
Thickness of assembly wall, mm	2,7	2,9	2,8
Height of gas cavity, cm	66	32	50
Gap betw. assemblies, mm	5,5	2,6	4,0
Sodium temp. at reactor inlet, °C	367	353	356
Thermal power, MW	3990	4140	4080
Electrical power, MW	1600	1600	1600
Breeding factor	1,20	1,35	1,29
Plutonium critical mass, kg	4050	3200	3410
Doubling time, yr	12,3	7,8	9,9

tations are independent. The results of the optimization of the characteristics of a fast breeder with a power W_{EL} = 1600 MW according to the doubling time with the aid of the model given in [5] are presented in Table 2.

The character of the dependence of the objective function and the limitations on the parameters being optimized results in the region of indeterminacy of optimal design solutions being linearly dependent on the corresponding region of indeterminacy of initial limitations (Fig. 1).

In the choice of a design solution for each combination of initial limitations, it is possible to find different technical variants of the solution, all with practically the same value of objective function. Possible combinations of reactor core characteristics which are optimal in respect of T_2 at various probabilities of realization are illustrated in Fig. 2. As some initial limitations are refined the region of optimal design solutions can be extended by ewakening the remaining limitations at the expense of reinforcing the refined limitations.

LITERATURE CITED

1. V. G. Ilyunin et al., in: Papers on Programs and Methods of Fast Reactor Design [in Russian], Izd. NIIAR, Dimitrovgrad (1975), p. 423.
2. A. M. Kuz'min, At. Energ., 39, No. 4, 269 (1975).
3. A. M. Kuz'min and Yu. V. Silaev, in: Nuclear Reactor Physics [in Russian], No. 5, Atomizdat, Moscow (1977), p. 54.
4. A. S. Karabasov and G. B. Usynin, in: Methods of Mathematical Modeling and Comprehensive Optimization of Power Plants under Conditions of Incomplete Determinacy of Initial Information [in Russian], Izd. Sib. Otd. Akad. Nauk SSSR, Irkutsk (1977), p. 117.
5. G. B. Usynin and A. A. Sennikov, At. Energ., 35, No. 1, 25 (1973).
6. A. A. Proshkin et al., Preprint FÉI-593, Obninsk (1975).

PERFORMANCE OF AUTOMATIC REACTOR-POWER CONTROL SYSTEM OF THE FIRST ATOMIC POWER PLANT WITH CORRECTION SIGNALS DERIVED FROM IN-REACTOR TRANSDUCERS

P. T. Potapenko, V. N. Sarylov,
F. F. Voskresenskii, V. G. Dunaev,
and A. P. Shulekin

UDC 621.039.566

The efficiency of ionization chambers (IC) as automatic control system transducers of high-power reactors is reduced by shielding of the chambers by control rods, by the considerable fluctuations of energy distribution caused by power variations, and particularly by spatial instability of energy distribtuion. At the same time, the presence of a comprehensive system of in-reactor monitoring based on direct-charge (DC) detectors offers a possibility of avodiing such deficiencies and of improving the accuracy and reliability of power control by basing it on the results of many measurements.

Potapenko et al. [1] describe an example of a control algorithm of the CANDU reactor which takes into account the sptaial neutron flux distributioh as measured by noninertial platinum detectors and inertial vanadium detectors (correctors).

Sarylov et al. [2] considered the application of only rhodium DC detectors in the automatic power control system of the First Atomic Power Plant. Experimental investigations proved that additional signal filtration is needed to improve noise immunity of the control system. This is due to the fact that while the use of a corrector to differentiate the DC detector signal improves the dynamic properties of the control system it also impairs its noise immunity in normal and emergency operating conditions.

Design calculations have been carried out of an automatic reactor power control system in which the ionization chamber (IC) current was calibrated against the signals of in-reactor DC detectors. An advantage of this method is the combination of the positive features of regular power controllers (fast response) and of the in-reactor monitoring system (accuracy and reliability) by using external and in-reactor transducers.

The power control signal is given by the equation

$$\delta = \frac{N_0 - [(N_{IC} + N_{DC}) - N_{IC-DC}]}{N_0},$$

where N_0 is the set-point signal.

As follows from the control algorithm, the ionization chamber signal N_{IC} is added to the signal of the DC detectors N_{DC} of the in-reactor monitoring system. Because of the considerable difference in the speed of response of the detectors, the reactor power is determined by the IC signal at the beginning of the transient process and by the DC detector signal, during the steady-state period. Subtraction of the IC signal multiplied by the filter transfer function, equal to the DC detector transfer function, (N_{IC-DC}), from the combined signal $N_{IC} + N_{DC}$ causes the contribution of the IC signal into the combined signal to decrease when the DC detector signal increases and to fall to zero at the end of the transient process (see Fig. 1).

The performance of the control system has been evaluatedon the basis of data and the mathematical model of the power control system used in the First Atomic Power Plant [2]. The mathematical model includes a point approximation of neutron kinetics with two groups of delayed neutrons, fuel temperature feedback, a description of DC and ionization chamber detectors and of other units of the reactor power control system.

Translated from Atomnaya Énergiya, Vol. 49, No. 1, pp. 53-54, July, 1980. Original article submitted July 23, 1979; revision submitted December 29, 1979.

0038-531X/80/4901-0486$07.50

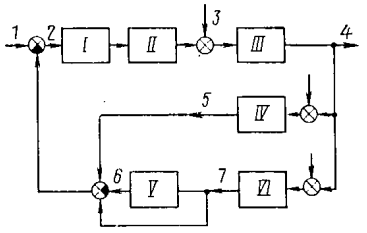

Fig. 1. Block diagram of composite automatic power control system: I) amplifier; II) final control element; III) reactor; IV) DC detector; V) filter with DC detector transfer function; VI) ionization chamber; 1) set point signal; 2) control signal; 3) reactivity perturbation; 4) power; 5) DC detector signal; 6) N_{IC-DC} signal; 7) IC signal.

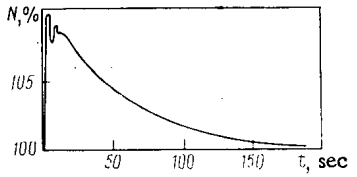

Fig. 2. Power control transient process for different DC detector and ionization chamber signals.

The composite control system has been analyzed for steady-state and dynamic operating conditions with equal and different signals generated by DC and ionization chamber detectors. The equation shows that when a reactivity perturbation occurs in the reactor, the control system rapidly compensates the perturbation in correspondence with the ionization-chamber signals and subsequently adjusts the power to the set point in accordance with the direct-charge detector readings. Of special interest is the analysis of transient processes taking place when the readings of ionization chamber and direct-charge detectors vary differently as a result of energy distribution fluctuations or ionization chamber shielding.

Assume that a change of reactor power due to internal or external perturbations is accompanied by considerable fluctuations of energy distribution (in elevation or azimuth) so that DC detectors and ionization chambers read different reactor powers. Such variations have been simulated by introducing different perturbations (power deviations from set point) into the DC detector and ionization chamber channels.

Figure 2 shows the transient processes in reactor power control taking place when 10% of N_0 perturbations are introduced into the ionization chamber channel and 0% perturbations, in the DC detector channel. Such a situation can occur, e.g., when only the height energy distribution changes while the reactor power remains constant resulting in a shift of the energy distribution peak and changing the ionization chamber readings. As seen in Fig. 2, the perturbations are rapidly processed in accordance with ionization chamber readings with a speed determined by the reactivity introduced by the control rods and result in a power increase of about 110%; the power then decreases to its rated value approximately after a time ($\sim$200 sec) determined by the inertia of direct-charge detectors.

Analysis of the transient process taking place when one of the four ionization chambers does out of order in the case of a power excess, indicates that the power surge reaches 125% of rated power and then returns to the nominal value after $\approx$200 sec. Thus, in contrast to the conventional power control structure, the steady-state reactor power returns to the 100% level when one of the ionization chambers fails to operate.

Theoretical analysis indicates that the composite reactor power control system bombines high accuracy due to the presence of many in-reactor direct-charge detectors with high speed of response characteristic of noninertial out-of-reactor neutron detectors. These advantages make to use of this algorithm desirable for controlling the power of large reactors.

LITERATURE CITED

1. P. T. Potapenko, V. G. Dunaev, and N. A. Kuznetsov, Atomic Engineering Abroad, No. 12, 3 (1977).
2. V. N. Sarylov, F. F. Voskresenskii, and A. P. Shulekin, Atomic Power Stations [in Russian], No. 2, Énergiya, Moscow (1978), p. 153.

WATER-IMPURITY CONTENTS OF POROUS DEPOSITS ON STEAM-GENERATING SURFACES

M. I. Ryabov

UDC 536.24:621.039.534.44

Measurements have been made [1] by means of ^{22}Na of the accumulation of impurities from water in porous deposits of iron oxides on steam-generating surfaces; the salt method [2] has also been used. The degrees of concentration were found to be, respectively, 10^4 and not more than 10. There are several models [3-6] used in estimating the degree of concentration. Here we suggest formulas for quantitative evaluation of the accumulation by the use of Macbeth's simple model [3], which are in quantitative agreement with experiment [1].

In Macbeth's model, steam escapes from the heating surface via the layer of deposit via steam tunnels, which have been identified by experiment [7-9], while water reaches the meniscus at the base of the steam tunnels by surface tension along feed capillaries in the porous structure. Impurities in the water accumulate in the feed capillaries. If we neglect curvature and nonuniformity in the cross section, we can represent such a capillary as a circular cylinder whose axis coincides with the X coordinate axis. At $x = 0$, the water evaporates in a steam tunnel; $x = \delta$ is the point of emergence of the capillary on the surface of the deposit.

The mean speed of water in a capillary is

$$W = qv'/ra, \tag{1}$$

where q is the heat flux at the heating surface; r, latent heat of evaporation; v', specific volume of water; and a, proportion of the volume of the deposit taken up by the feed capillaries.

In a state of steady mass transfer, the flow of impurity towards the base of the steam tunnel along the feed capillary is balanced by diffusion of the impurities against the water flow. The equation for convective diffusion applies to the impurity distribution along a feed channel, which takes the following form if we neglect the nonuniformity of the water velocity over the cross section:

$$-D\frac{d^2C}{dx}=W\frac{dC}{dx}, \tag{2}$$

where C is the impurity concentration in the water in the capillary and D is the diffusion coefficient of the impurity.

At $x = \delta$, the impurity concentration is equal to that in the initial water $C(\delta) = C_c$; at $x = 0$, the influx of impurity to the evaporation boundary is balanced by the outward diffusion (it is assumed that saturation is not attained and that the impurity is not deposited as a solid phase). Then we have

$$-D\frac{dC}{dx}\Big|_{x=0}=WC|_{x=0}. \tag{3}$$

The solution to (2) for these boundary conditions is

$$C(x)=C_c\exp\left[\frac{qv'}{raD}(\delta-x)\right]. \tag{4}$$

Translated from Atomnaya Énergiya, Vol. 49, No. 1, pp. 55-56, July, 1980. Original article submitted August 6, 1979.

0038-531X/80/4901-0488$07.50

The maximum impurity concentration is attained at the point of evaporation of water in the steam tunnel:

$$C(0) = C_c \exp\left(\frac{qv'\delta}{raD}\right) = C_c \exp\left(\frac{W\delta}{D}\right). \quad (5)$$

It follows from (4) and (5) that the impurity concentration rises very rapidly along the capillary and may be very high near the point of evaporation, i.e., at the surface of the metal. The extent of concentration in the pores ($\theta = C/C_c$) is exponentially related to the thermal loading and to the thickness of the deposits. The above formulas may be compared with isotope data [1]; (4) and (5) show that the impurity concentration is to be measured at a point, while in the experiments of [1] the mean degree of concentration was measured over the entire thickness of the deposit, which may be found from

$$\bar{\theta} = \frac{\bar{C}}{\bar{C}_c} = \frac{1}{C_c\delta}\int_0^\delta C(x)\,dx. \quad (6)$$

Substitution for C(x) from (4) into (6) gives

$$\theta = [\exp(y) - 1]/y, \quad (7)$$

where

$$y = \frac{K}{a}\,y_s = \frac{K}{a}\,\frac{sv'q}{Dr} \quad (8)$$

is the reduced length of a feed capillary; $y_S = sv'q/Dr$, reduced thickness of the deposit; s, actual thickness of the deposit; and $K = \delta/s$, coefficient representing the irregularity of the feed capillaries.

If $y \geq 3.5$, we can put (with an error of up to 3%) that

$$\exp(y) - 1 \approx \exp(y). \quad (9)$$

Then (7) with (8) and (9) gives

$$\log(\bar{\theta}y_s) = 0.434y_s\,\frac{K}{a} - \log\frac{K}{a}. \quad (10)$$

We see from (10) that the observations for $\bar{\theta}$ for the range $(K/a)y_S \geq 3.5$ should fit to a straight line in a plot with coordinates $\log(\theta y_S)$ and $0.434y_S$; then K/a is a numerically equal to the slope of the straight line. Also, the straight line should meet the ordinate axis with a negative intercept of $\log(K/a)$.

Figure 1 shows results from three experiments [1] processed in this way. Curves 1-3 characterize runs 2, 5, and 7 of [1] with heater 6 coated with magnetite deposits. The thickness of the coating was 25 μm. The observed points correspond to the maximum degrees of concentration recorded for each level of thermal load and so on. In the first two cases, the observed points fit closely to the straight lines derived by least-squares fitting. The correlation coefficient are, respectively, 0.992 and 0.95. In the region represented by the broken lines, the lines should not pass through the observed points, because (9) is not obeyed here.

Curve 1 corresponds to an experiment in which there was good quantitative agreement between theory and experiment, since the logarithm of the slope was 1.07, which is very close to the intercept of curve 1 on the ordinate axis, which is 1.01 in the negative region. In this experiment, the heat flux was successively increased, with recording of the accumulation of ^{22}Na in the deposits, which rose continuously. The maximum concentration recorded at each heat load was clearly close to the equilibrium value.

The points corresponding to curve 2 were recorded with a fixed heat load; only the pressure was varied, which affected v', r, and D in (8). Therefore, the observed points lie very close together. The logarithm of the slope is 1.19, while the intercept is 1.38 in the negative region. The agreement between these values is reasonably good, particularly since the points on curve 2 are close together and far from the ordinate axis.

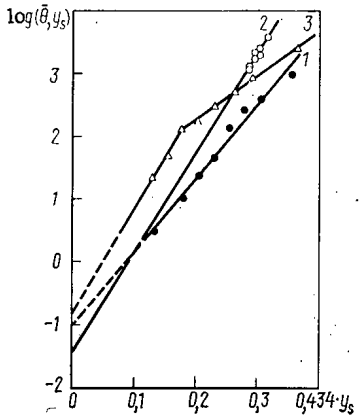

Fig. 1. Results from processing the experiments [1] on the accumulation of ^{22}Na in a layer of porous magnetite deposit.

In the experiment corresponding to curve 3, the heat flux was first increased and then decreased in sequence. It is likely that equilibrium values for the degree of concentration were not obtained, particularly at high heat loads. The above relationships will then not apply for these conditions, and it is clear that the curve 3 drawn through the experimental points has a kink. Nevertheless, the bottom three points correspond qualitatively to the theory, where the degree of concentration is least and is closest to equilibrium, since the straight line drawn through them meets the ordinate axis in the negative region.

Figure 1 shows that our quantitative relationships for the accumulation of soluble impurities in porous deposits are closely confirmed by the isotope data [1]. The undetermined quantity in calculations from (4) and (5) is K/a. In the experiments of [1], K/a was about 10-20, but it varied from experiment to experiment, although all the measurements were made at a single point on the tube. The inconstancy of K/a clearly occurs because there were no strictly fixed feed capillaries in the layer of corrosion products, but instead the paths of the water through the pores to the bases of the steam tunnels formed at random.

LITERATURE CITED

1. L. Picone, D. Whyte, and C. Taylor, WCAP-3731 (1963).
2. M. A. Styrikovich et al., Teplofiz. Vys. Tem., 15, No. 2, 353 (1977).
3. R. Macbeth, AEEW-R711 (1971).
4. P. Cohen, Am. Inst. Chem. Eng. Symp. Ser., 70, No. 138, 71 (1974).
5. M. A. Styrikovich, A. I. Leont'ev, and S. P. Malyshenko, Teplofiz. Vys. Temp., 14, No. 5, 998 (1976).
6. V. S. Polonskii et al., Dokl. Akad. Nauk SSSR, 241, No. 3, 579 (1978).
7. R. Macbeth, R. Trenberth, and R. Wood, AEEW-R705 (1971).
8. N. G. Rassokhin et al., Teploenergetika, No. 9, 12 (1973).
9. W. Huijbregts, G. Genlgersma, and A. Snel, KEMA Rapport No. III, 9884-74 (1974).

THE SCOPE FOR INCREASING THE SCALE OF THE FUEL CYCLE FOR VARIOUS FAST REACTORS

A. N. Shmelev and L. N. Yurova

UDC 621.039.5

The provision of fuel for developing nuclear power (NP) is related to the commissioning of fast breeder reactors (BR). However, the problem is not very simple, for various reasons, among which we may note the following:

1) BR are technically more complicated and require more capital investmant than do thermal-neutron reactors;

2) the engineering industry may be large oriented to rapid increase in the power of thermal-neutron reactors at the stage of construction of fast reactors; and

3) some uncertainty in estimating the reserves of cheap uranium may hold back the rapid commissioning of fast reactors.

It has been pointed out [1] that the general use of fast reactors in the 1990s would provide a sufficient amount of plutonium for developing nuclear power. Under these conditions, the design of fast reactors with low specific loading may result in delays in accumulating plutonium and in increasing the scale of the fast-reactor fuel cycle.

On the other hand, the use of fast reactors at this stage with elevated specific loading (but with a doubling time the same as for fast reactors with reduced loading) may lead to more rapid expansion of the fuel cycle by earlier utilization of the accumulated plutonium and subsequent breeding. This would require less capital investment and less engineering effort in the expansion of fast reactors. To illustrate this, we have performed calculations on increasing the scale of the fuel cycle for fast reactors.

We assume that at the start of commissioning of fast reactors with a rate $\omega_c(\omega_c > \omega_0)$ (where ω_0 is the inherent rate of growth of the fast-reactor system), the thermal reactors will have accumulated an amount of fuel G(0). A change in scale of the fuel cycle of fast reactors is indicated by the ratio G'_c/G_c, where G_c is the amount of fuel in the fuel cycle when one employs fast reactors with specific loag g_f at time T_0, when all the accumulated plutonium G(0) has been utilized, while G'_c is the amount of fuel in the fuel cycle at the same time T_0 when one uses fast reactors with specific load $g'_c > g_c$.

Table 1 gives calculations on G'_c/G_c for various values of $G(0)/g_c$ and various rates ω_0/ω_c of fast reactor commissioning. It is clear that if one uses fast reactors with elevated specific loading (ω_0 = const), then the scale of growth of the fuel cycle will be appreciably increased. This is due to earlier utilization of the accumulated plutonium and subsequent breeding during the time period. Table 1 also gives the relative power levels of the fast reactors with g'_f, viz., W(g'), and of fast reactors with g_f, viz., W(g). The use of fast reactors with $g'_f > g_f$ from the start enables one to increase the scale of the fuel cycle more rapidly with a lower level of energy output from the fast reactors, and therefore with less capital investment and less engineering effort. Even with a rate of commissioning of fast reactors of four times the natural growth rate, the fuel breeding may result in about 25% increase in the scale of the fast reactor fuel cycle.

It has been pointed out [2] that the fuel breeding in a fast reactor during the initial period of implementation is very important, and a formula was given relating the reduced costs for this period of developing nuclear power to the specific loading and the rate of excess breeding. If the present assumptions are made, this formula implies that the reduced costs will be somewhat less if elevated specific loadings are used in the initial period of fast-reactor commissioning by comparison with the use of fast reactors with reduced specific loading.

Translated from Atomnaya Énergiya, Vol. 49, No. 1, pp. 56-57, July, 1980. Original article submitted September 28, 1979.

0038-531X/80/4901-0491 $07.50

TABLE 1. Relative Increase in the Scale of the Fuel Cycle and Power Reduction on Using Fast Reactors with Elevated Specific Loading and Elevated Breeding

Parameter	$\frac{G_0}{g_f}$	$\frac{\omega_0}{\omega_c}$	g'_f/g_f		
			1	2	3
G'_c/G_c	10	0,5	1	1,374	1,626
$W(g')/W(g)$			1	0,687	0,542
G'_c/G_c		0,25	1	1,166	1,26
$W(g')/W(g)$			1	0,583	0,42
G'_c/G_c	20	0,5	1	1,404	1,689
$W(g')/W(g)$			1	0,702	0,563
G'_c/G_c		0,25	1	1,176	1,29
$W(g')/W(g)$			1	0,588	0,43

As the supply of fuel to thermal reactors at the stage of developed nuclear power engineering will be expressed in natural terms, not relative ones, it is desirable to express the scale of the fast-reactor fuel cycle in the same way, although this is not equivalent to expressing the rapid growth of the energy output of the fast-reactor system.

As there may be delays in commissioning, and also some reduction in the rate of commissioning of fast-reactor power at elevated loading, one can still expect a fast and persistent increase in the scale of the fuel cycle, which will facilitate the transfer of nuclear power to a balanced fuel cycle. The distribution of the capital investment shows that the main contribution will still be concerned with the construction of nuclear power stations, only about 20% going to the development of reprocessing facilities [1]. For this reason, the largest economy in capital investment will come from reducing the cost of building nuclear power stations. Power stations with fast reactors require elevated capital investment, and this position will clearly persist in the initial stage of large-scale commissioning. These features also indicate that it is now desirable to increase the energy output of nuclear power stations with fast reactors.

These estimates of the natural parameters of course cannot give an exhaustive answer on the relative performance from using fast reactors with elevated specific loading and high breeding ratios. This requires an all-round economic evaluation.

Conclusions. If one uses fast reactors with elevated loading and elevated breeding at the initial stage of large-scale implementation, there will be more rapid utilization of the plutonium provided by thermal reactors, and also breeding with less capital investment. This feature of such reactors can be used e.g., to reduce the rate of increase in the energy output, and therefore to reduce the rate of capital investment without adverse effect on the increase in the fuel cycle scale.

LITERATURE CITED

1. N. P. Dergachev et al., At. Energ., 43, No. 5, 365 (1977).
2. V. S. Kagramanyan and V. B. Lytkin, Preprint FÉI-449, Obninsk (1973).

ALLOWING FOR COUNTERFLOW IN A MASS-DIFFUSION ELEMENT

V. A. Kaminskii, O. G. Sarishvili,
G. A. Sulaberidze, G. A. Tevzadze,
V. A. Chuzhikov, and V. P. Nadolinskii

UDC 621.039.34

Earlier papers [1, 2] considered a model of a separating process in which reverse convective transfer of gas through a diaphragm did not exhibit any major influence on the elementary separation effect. This holds for diaphragms of short length which have been used in practice thus far [3, 4]. In this case the concentration of the light component c_f at the point of supply coincides with the concentration c_F in the supply flow and the common solution of the equation of longitudinal transfer and the equation of external balance immediately yields a relation for the enrichment factor; the influence of depletion of the concentration of the light component in flow along the diaphragm on the separation effect is taken into account by the dependence of ε on the gas-flow division factor θ.

In a real element a depleted flow and an enriched flow moving in opposite directions on either side of the diaphragm. The competetive action of the processes of molecular diffusion and reverse convective transfer results in the profile of flows inside the element shown in Fig. 1. These processes ensure that the components being separated are exchanged between the flows moving on either side of the diaphragm. The presence of a counterflow leads to an increase in the transverse elementary enrichment and, therefore, enhancement of the overall separation effect of the apparatus.

For a more exact description of the process of separation in a mass-diffusion element, in deriving the transfer equations, besides reverse convective gas transfer through the diaphragm, one must take account of the influence of the counterflow as well as the reverse longitudinal diffusion on either side of the diaphragm. Moreover, in solving the transfer equations it is necessary to take account of the specifics of the boundary conditions for the concentration of the component being extracted depending on how the elements are connected.

The equations of balance for the flows of gas and light component in any cross section of the counterflow element, including the terms which take account of the reverse longitudinal diffusion, take on the following form when the notation of [1, 2] is employed:

$$G_a = L'' + G_b, \tag{1}$$

$$G_a c_a + \Pi a n D_a \gamma_a \frac{dc_a}{dy} = L'' c^- + G_b c_b - \Pi b n D_b \gamma_b \frac{dc_b}{dy}, \tag{2}$$

where the values of the effective diffusion coefficients D_a and D_b were obtained from

$$D = D_{10}/[1 - (1 - D_{10}/D_{12})\,\gamma]$$

by the substitution of γ_a and γ_b, respectively. In the case of separation of isotopes, we have $\Delta c \ll c$ and, therefore, we can assume that

$$dc_a/dy \approx dc_b/dy. \tag{3}$$

Then, from Eqs. (1) and (2) for the concentration of the light component in the external gap we get

$$c_a = \left(1 - \frac{L''}{G_a}\right) c_b + \frac{L''}{G_a} c^- - \frac{1}{G_a}(\Pi a n D a \gamma_a + \Pi b n D_b \gamma_b) \frac{dc_b}{dy}. \tag{4}$$

Translated from Atomnaya Énergiya, Vol. 49, No. 1, pp. 57-59, July, 1980. Original article submitted October 4, 1979.

0038-531X/80/4901-0493 $07.50

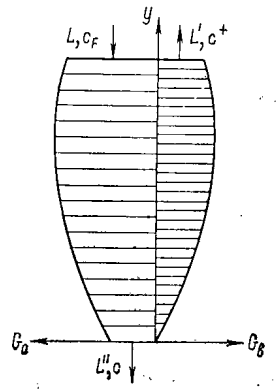

Fig. 1. Distribution of longitudinal flows in an element.

The equation of the differential balance of the light component in the cross section under consideration can be written as

$$G_b \frac{dc_b}{dy} + \frac{dG_b}{dy} c_b = \Pi \tau_{1x} \tag{5}$$

if terms of the second order of smallness are disregarded. The solution of the equation of transverse transfer of the light component through the diaphragm with allowance for the influence of the reverse convective gas transfer gives the relation

$$\tau_{1\mathbf{x}} = \tau_x \frac{1}{1-\delta} [c_a - \delta c_b + \alpha c_b (1-c_b)], \tag{6}$$

whre the functions α and δ are found from

$$\alpha = -\varepsilon_0 \int_0^{l_e} \frac{\partial \ln \gamma}{\partial x} \exp\left(-\int_0^x \frac{\tau_x}{nD\gamma}\, dx\right) dx;$$

$$\delta = \exp\left(-\int_0^{l_e} \frac{\tau_x}{nD\gamma}\, dx\right).$$

Substituting τ_{1X} from Eq. (6) with allowance for Eq. (4) in Eq. (5), we get the equation of transfer for the light component along the mass-diffusion element:

$$\left[(G_a - L'') + \frac{1}{1-\delta} \frac{\Pi\tau_x}{G_a} (\Pi a n D_a \gamma_a + \Pi b n D_b \gamma_b)\right] \frac{dc_b}{dy} = \frac{\Pi\tau_x \alpha}{1-\delta} c_b (1-c_b) - \frac{\Pi\tau_x}{1-\delta} \frac{L''}{G_a} (c_b - c^-). \tag{7}$$

After straightforward manipulations, Eq. (7) is put into a form characteristic of an equation of longitudinal transfer in apparatuses with enhancement of the primary effect because of counterflow:

$$\frac{dc_b}{dy} = \frac{H}{K} c_b (1-c_b) - \frac{L''}{K} (c_b - c^-), \tag{8}$$

where the kinetic coefficients H and K are calculated from

$$H = \alpha G_d; \tag{9}$$

$$K_d = \Pi a n D_a \gamma_a + \Pi b n D_b \gamma_b; \tag{10}$$

$$K_c = \frac{1-\delta}{\Pi\tau_x} G_a (G_a - L''); \tag{11}$$

$$K = K_c + K_d. \tag{12}$$

Integration of Eq. (8) over theheight of the separating zone of the element gives the value of the concentration of the light component in the enriched flow, i.e., $c_b(y = H_D) = c^+$. In order to determine c^+ it is necessary to know the concentration c_{b0} at the lower boundary of the inner cavity of the apparatus.

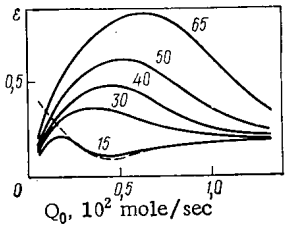

Fig. 2. Effect of total vapor flow on the enrichment factor (l_e = 1.4 cm).

Using Eq. (8), we can recast Eq. (4) in the form

$$c_a = c_b - \frac{L''}{G_a}\left(1-\frac{K_d}{K}\right)c_b - \alpha\frac{K_d}{K}c_b(1-c_b) + \frac{L''}{G_a}\left(1-\frac{K_d}{K}\right)c^-. \tag{13}$$

Then, bearing in mind that $G_a(y = 0) = L''$, for the concentration c_{b0} we get

$$c_{b0} = \frac{1}{2}\left[\sqrt{\left(\frac{1-\alpha_0}{\alpha_0}\right)^2 + 4\frac{c^-}{\alpha_0}} - \frac{1-\alpha_0}{\alpha_0}\right], \tag{14}$$

where $\alpha_0 = \alpha(y = 0)$.

Equations (8) and (14) contain three independent concentrations c^-, c_{b0}, and c^+. To complete the system we use the condition of external balance with respect to the element,

$$c_F = \theta c^+ + (1-\theta)c^-. \tag{15}$$

The solution of the system of equations (8), (14), and (15) makes it possible to calculate the values of the concentration of the light component in the depleted and enriched flows and the principal separating characteristics of the element, i.e., the enrichment factor

$$\varepsilon = \ln\left(\frac{c^+}{1-c^+}\Big/\frac{c^-}{1-c^-}\right) \tag{16}$$

and the separative power

$$\delta U = L[\theta\Phi(c^+) + (1-\theta)\Phi(c^-) - \Phi(c_F)]. \tag{17}$$

Figure 2 gives the characteristic dependence of the enrichment factor, calculated by the technique described above, on the total vapor flow for elements with various heights of the working part of their diaphragm (numbers next to curves). The enrichment factor in the regions of low values of Q_0 has a maximum. The existence of this maximum is attributed to the influence of two competing factors: enhancement of the primary separation effect as the result of the counterflow and longitudinal mixing of convections and reverse diffusion. The dashed line shows the plot of ε vs Q_0 without allowance for the counterflow. It follows from Fig. 2 that for a known type of elements (H_D = 15 cm) [3, 4] a difference in the dependences of ε on the total vapor flow, calculated by various techniques, is observed only in the region of low values of Q_0 when the element operates in a regime with internal circulation.

It must be emphasized that the influence of the counterflow leads to a dependence of ε on the height of the working part of the diaphragm. As seen from Fig. 2, with an increase in the height the total separation effect in the element grows. However, it must be borne in mind that along with this there is a decrease in the flow of the light fractions. Therefore, an increase in the length of the diaphragm is desirable only in special cases, e.g., when the elements are used in the fianl stages of the cascades.

To compare theory with experiment we studied the dependence of the separation factor on the total vapor flow in elements with a diaphragm length of 64 cm in the separation of neon isotopes (Fig. 3). The diaphragm, which was 0.3 mm thick, has 18 apertures of diameter 0.3 mm/cm^2, which corresponds to an effective diffusion resistance of 2.4 cm. The accuracy of the theoretical calculations was determined by the accuracy of the initial data and amounted to <1%. The experimental error was found by statistical processing of the re-

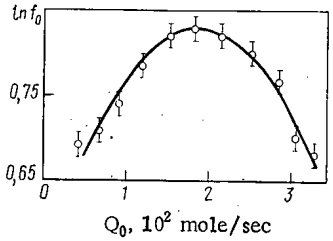

Fig. 3. Theoretical and experimental dependence of the separation factor on the total vapor flow: —) calculation; ○) experiment.

sults of the measurements [5]. Comparison shows satisfactory agreement between theoretical and experimental data, which confirms the substantiation of the assumptions and the applicability of the counterflow model of mass-diffusion element for practical calculations.

LITERATURE CITED

1. V. A. Chuzhinov et al., At. Energ., 40, No. 6, 471 (1976).
2. B. Sh. Dzhandzhgava et al., At. Energ., 45, No. 2, 129 (1978).
3. I. G. Gverdtsiteli et al., in: Proc. Second Geneva Conf., Soviet Scientists [in Russian], Vol. 6, Atomizdat, Moscow (1959), p. 69.
4. O. G. Sarishvili et al., At. Energ., 43, No. 3, 210 (1977).
5. R. S. Guter and B. V. Ovchinskii, Elements of Numerical Analysis and Mathematical Processing of Experimental Results [in Russian], Nauka, Moscow (1970).

EXPERIMENTAL INVESTIGATION OF ISOTOPE SEPARATION IN ASYMMETRIC MASS-DIFFUSION CASCADES

V. A. Kaminskii, O. G. Sarishvili, G. A. Sulaberidze, and V. A. Chuzhinov

UDC 621.039.34

The experimental investigation of asymmetric cascades is of considerable interest, particularly in connection with the conclusions of the theoretical paper [1] on the possibility of increasing their efficiency by connecting the stages asymmetrically. It should be noted, however, that since the calculation in [1] used a model of an element with a constant flow rate of the light fraction, the results obtained are not general.

The experimental arrangement consisted of a cascade of 10 steel mass-diffusion elements using mercury as an evaporator. The thickness, height, and diameter of the cylindrical barrier of the elements were 0.1, 150, and 58 mm, respectively. Each cm^2 of barrier surface had 11 openings 0.3 mm in diameter, which corresponds to an effective diffusion resistance of 1.27 cm. The gap between the barrier and the condenser wall was 3 mm. The upper supplementary condenser was 64 mm in diameter and 100 mm high, and was a direct extension of the separating part of the element. The light fraction from the supplementary condenser exits through a capillary 2.9 mm in diameter and 50 mm long. Table 1 shows the characteristics of such symmetrically connected elements as a function of the rate of flow of vapor into the apparatus.

Experiments were performed on the separation of neon isotopes at a working pressure of 70 mm Hg (1 mm Hg = 133.322 N/m^2). The flow rates of vapor into the main and supplementary condensers, Q_H and Q_L, respectively, were determined by heat exchange with the condensing surfaces, and then the coefficient of vapor distribution of the gas stream $\theta_V = Q_L/(Q_H + Q_L)$ was calculated. The Peclét diffusion number was

Translated from Atomnaya Énergiya, Vol. 49, No. 1, pp. 59-61, July, 1980. Original article submitted October 4, 1979.

0038-531X/80/4901-0496$07.50

TABLE 1. Characteristics of Mass-Diffusion Element

Q_0, 10^3 moles/	θ_v	ΔP*, mm H_2O	L', 10^4 moles/sec	ε	ln q	δU, 10^6 moles/sec
5	0,22	0,7	0,29	0,11	1,6	0,12
7	0,28	2,0	0,83	0,13	1,9	0,50
9	0,36	2,8	1,17	0,14	2,1	0,81
11	0,45	3,5	1,46	0,15	2,3	1,16

*Pressure drop across barrier (1 mm water equals 9.80665 N/m^2).

TABLE 2. Experimental Values of Enrichment Factor and External Flow Rates in Asymmetric Cascades

θ	ε	L', 10^4 moles/sec	L*, 10^4 moles/sec
1/4	0,127	0,54	2,17
1/3	0,133	0,75	2,25
1/2	0,150	1,46	2,92
2/3	0,183	2,08	3,12

*Flow rate of feed stage.

TABLE 3. Comparison of Calculated Characteristics of Symmetric and Asymmetric Cascades for the Production of ^{22}Ne with a 90% Concentration

θ	S*	P†, g/day	S/P
1/3	80	3,6	22,2
1/2	47	4,1	11,5
2/3	56	7,1	7,9

*No. stages.
†Output.

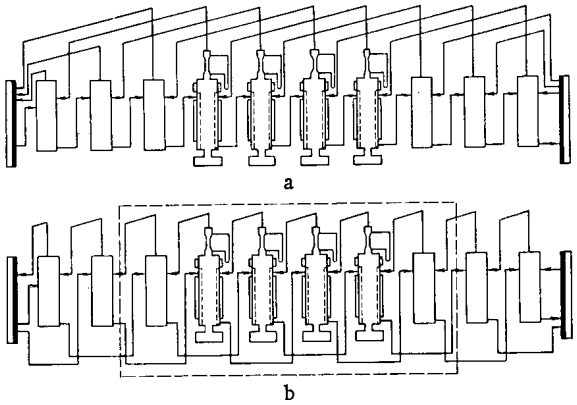

Fig. 1. Schematic diagram of mass-diffusion elements in an asymmetric cascade with a) $\theta = 1/4$; b) $\theta = 2/3$.

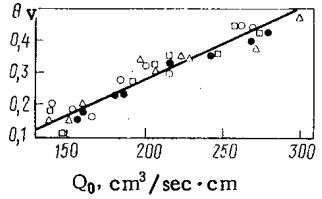

Fig. 2. Experimental dependence of coefficient of vapor distribution on Q_0 for asymmetric cascades with θ = 1/4 (○), 1/3 (●), 1/2 (Δ), 2/3 (□).

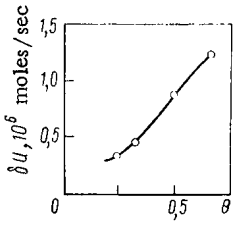

Fig. 3. Experimental dependence of separative power on coefficient of gas stream.

Declassified and Approved For Release 2013/02/14 : CIA-RDP10-02196R000800040001-2

determined according to [2] by taking account of the total vapor flow rate Q_0 by the formula (here and later the notation of [1, 2] is used):

$$\ln q = (1-\theta_V)\frac{l_e}{\Pi H_g n D_{10}} Q_0. \quad (1)$$

The flow rate of the light fraction L' was calculated from the pressure drop across the capillary, and the separative power δU from the expression

$$\delta U = L'\varepsilon^2 (1-\theta)/2. \quad (2)$$

Figure 1 shows a schematic diagram of the connection of elements in an asymmetric cascade with a coefficient of separation of the gas stream equal to 1/4 (k = 3, p − 1 = 1) and 2/3 (k = 1, p − 1 = 2) for reflux operation of the elements. The dashed lines indicate the part of the cascade whose elements operate with the same coefficient of separation of the gas stream. All measurements were performed in this part of the cascade. The variants $\theta < 1/4$ and $\theta > 2/3$ were not considered because of the substantial complication of the cascade circuit.

The results of the experiments for $Q_0 = 1.1 \cdot 10^{-2}$ moles/sec are shown in Table 2. The increase in the enrichment factor ε with increasing θ is adequately described by the theoretical expression

$$\varepsilon = \frac{\Delta D}{D}\frac{q\ln q}{q-1}\frac{1}{\theta}\ln\frac{1}{1-\theta}. \quad (3)$$

At the same time, the increase in L' with increasing θ was unexpected, and is not accounted for within the framework of the existing theory. It was observed to the same extent in both reflux and direct flow of gas through the barriers.

Specially performed experiments to determine the vapor distribution in asymmetrically connected elements showed that θ_V did not vary with a change in θ (Fig. 2), and consequently this effect is not related to the influence of vapor distribution. The change in resistance of the external pipelines resulting from their extension in the asymmetric cascade occurs for $\theta < 1/2$ and $\theta > 1/2$, and also does not explain the increase in flow rate of the light fraction with increasing θ.

Apparently, the observed effect of the increase in L' is a consequence of the effect of longitudinal flow of the vapor−gas mixture in the external gap on diffusive transfer of gas through the barrier. The variation of θ leads to a change in the relation between the longitudinal ($\sim L$) and transverse ($\sim Q_H$) velocities of the vapor−gas mixture in the external gap. This change clearly will affect the concentration of the gas in the gap (γ_a) and together with it the transverse concentration gradient across the barrier, which determines a relation between L' and θ. Further theoretical study is needed to explain this relation.

Nevertheless, the increase in L' is so considerable that it leads to a significant increase in the separative power of the element for an increase in θ (Fig. 3) in comparison with its separative power in a symmetric arrangement, and is of great practical importance. It should be noted, however, that this fact is the result of a specific property of mass-diffusion cascades in which the external flow rates are not determined by transfer compressors, but are established at a balanced level determined by the internal operating conditions of the elements themselves.

Table 3 lists the results of the calculation of rectangluar mass-diffusion cascades with θ = 1/3, 1/2, and 2/3, based on the use of experimental data. For a small increase in the number of stages necessary to preserve optimum conditions of the cascade, the gain in output in changing from a symmetric to an asymmetric arrangement with θ = 2/3 is ~74%, and the energy expenditure per unit of product, characterized by the ratio S/P, is decreased by more than 40%. The results presented show the advisability of using asymmetric mass-diffusion cascades with $\theta > 1/2$.

LITERATURE CITED

1. V. A. Chuzhinov et al., At. Energ., 44, 254 (1978).
2. B. Sh. Dzhandzhgava et al., At. Energ., 45, 129 (1978).

SHIELDING ACTIVATION DETECTORS WITH GADOLINIUM

V. I. Kulikov, S. S. Lomakin, and V. P. Taratulov

UDC 621.039.512

At the present time the activation method is being used extensively to measure the parameters of the neutron field in nuclear reactors. In particular, information can be obtained about the neutron spectrum if use is made of detectors containing ^{176}Lu, ^{151}Eu, ^{164}Dy, and ^{54}Mn as well as resonance detectors.

However, for a very important energy range, i.e., the intermediate range (the range where the thermal spectrum goes over into the epithermal spectrum), in practice, there are no activation detectors which would ensure the necessary accuracy of measurements. It must be pointed out that the value of the intermediate energy range is extremely large for fuel containing plutonium since ^{239}Pu resonance falls within it.

Information about the neutron spectrum in the intermediate energy range can be obtained by using a number of activation detectors placed in appropriate shielding (neutron-absorbing) filters. To data a number of studies have been carried out to determine the parameters characterizing the filters and shielded detectors [1-3]. Available data [4], however, are limited to several neutron-sensitive elements and a neutron temperature range of up to 200°C, which hinders the application of shielded detectors in nuclear power plant reactors.

Using one filter material or other, it is possible to change the behavior of the detector activation cross section in the thermal region, thus amplifying the contribution of epithermal neutrons or neutrons of the intermediate energy range. In this sense it is especially advantageous to employ the technique of "gray" gadolinium filters ($\Sigma_{act}t_f = 1$, where t_f is the filter thickness). If ^{176}Lu, ^{151}Eu, ^{103}Rh, and ^{115}In are used in combination with such filters, then the neutron sensitivity of the detectors turns out to be increased precisely in the intermediate energy range. For practical implementation of the method it is necessary to have the effective cross sections of the filter-shielded detectors.

The effective cross sections were calculated with allowance for the finite dimensions of the detectors which were in the form of flat disks in capsule-filters and of the filters by the technique presented in [5]. The effective thickness of the gaolinium filter was 8.26 μm and the thickness and diameter of the detectors were 0.1 and 7.8 mm, respectively.

On the basis of the effective cross sections found in this way, we calculated the parameters g(T) and s(T) (Table 1), determining the effective cross section in the Westcott model [6]. The calculations were carried out up to a temperature of 920°C.

The use of gadolinium filters causes, in all detectors studied, an increase in the sensitivity to a change in the neutron temperature. Figure 1 shows the dependence of the normalized reaction rate for detectors with filters on the neutron temperature in spectra with various hardnesses:

$$R = \frac{g(T) + rs(T)}{g(T_0) + rs(T_0)},$$

where $T_0 = 20$°C and r is the fraction of epithermal neutrons.

The choice of detectors with filters for measurements in spectra with various hardnesses is made conveniently if one is guided by the value of the relative sensitivity of the spectral index ε to the neutron temperature:

$$\varepsilon = \frac{I^N_{Cu}(T) - I^N_{Cu}(20°)}{I^N_{Cu}(20°)},$$

Translated from Atomnaya Énergiya, Vol. 49, No. 1, pp. 61-63, July, 1980. Original article submitted October 4, 1979.

0038-531X/80/4901-0499$07.50

TABLE 1. Parameters g(T) and s(T) for Detectors with Gadolinium Filters

Neutron temp., °C	^{164}Dy		^{176}Lu		^{103}Rh		^{151}Eu	
	g	s	g	s	g	s	g	s
20	1,569	2,980	1,151	16,465	1,766	63;194	1,217	9,981
120	2,071	2,282	9,553	4,015	2,469	72,032	1,462	11,811
220	2,508	1,641	13,695	—4,669	3,146	80,208	1,748	12,963
320	2,875	1,097	17,033	—9,494	3,785	88,459	2,122	13,326
420	3,181	0,646	19,488	—12,079	4,387	97,226	2,614	12,910
520	3,434	0,271	21,086	—13,277	4,960	106,564	3,228	11,735
620	3,644	—0,036	22,089	—13,683	5,515	116,137	3,943	9,908
720	3,817	—0,291	22,617	—13,548	6,066	125,430	4,732	7,655
820	3,960	—0,500	22,796	—13,065	6,632	134,004	5,563	5,246
920	4,079	—0,673	22,726	—12,365	7,233	141,618	6,409	3,006

TABLE 2. Values of Relative Sensitivity of Spectral Index ε

Irradiation conditions	$r = 0,1$				$r = 0,15$				$r = 0,2$			
	^{164}Dy	^{176}Lu	^{103}Rh	^{151}Eu	^{164}Dy	^{176}Lu	^{103}Rh	^{151}Eu	^{164}Dy	^{176}Lu	^{103}Rh	^{151}Eu
With gadolinium filter	0,22	0,38	0,18	0,18	0,17	0,23	0,16	0,17	0,15	0,12	0,14	0,16
Without filter	—0,02	0,24	0,07	—0,06	—0,03	0,17	0,08	—0,05	—0,04	0,10	0,08	—0,04

TABLE 3. Dependence of ε on T for r = 0.1

T, °C	With filter				Without filter			
	^{176}Lu	^{103}Rh	^{151}Eu	^{164}Dy	^{176}Lu	^{103}Rh	^{151}Eu	^{164}Dy
200	0,80	0,31	0,31	0,38	0,45	0,13	—0,10	—0,05
400	1,55	0,63	0,68	0,69	0,78	0,29	—0,12	—0,10
600	1,90	0,95	1,02	0,85	0,91	0,40	—0,13	—0,14
800	1,98	1,37	1,50	0,96	0,90	0,45	—	—0,17

TABLE 4. Values of Relative Sensitivity of Spectral Index ε Under change in r from 0.1 to 0.2

Irradiation conditions	$T = 320°$ C				$T = 720°$ C			
	^{164}Dy	^{176}Lu	^{103}Rh	^{151}Eu	^{164}Dy	^{176}Lu	^{103}Rh	^{151}Eu
With gadolium filter	0,19	0,60	0,10	0,10	0,35	0,84	0,22	0,54
Without filter	0,04	0,32	—0,03	—0,05	0,08	0,40	—0,07	—

Declassified and Approved For Release 2013/02/14 : CIA-RDP10-02196R000800040001-2

TABLE 5. Dependence of ε on r at 320°C

r	With filter		Without filter	
	^{176}Lu	^{103}Rh	^{176}Lu	^{103}Rh
0,05	1,60	0,60	0,89	0,14
0,10	1,24	0,49	0,70	0,20
0,15	0,91	0,42	0,51	0,22
0,20	0,70	0,35	0,35	0,23

TABLE 6. Dependence of ε on r at 720°C

r	With filter		Without filter	
	^{176}Lu	^{103}Rh	^{176}Lu	^{103}Rh
0,05	—	1,37	1,13	0,40
0,10	1,90	1,16	0,92	0,50
0,15	1,46	1,10	0,70	0,53
0,20	1,08	0,91	0,46	0,55

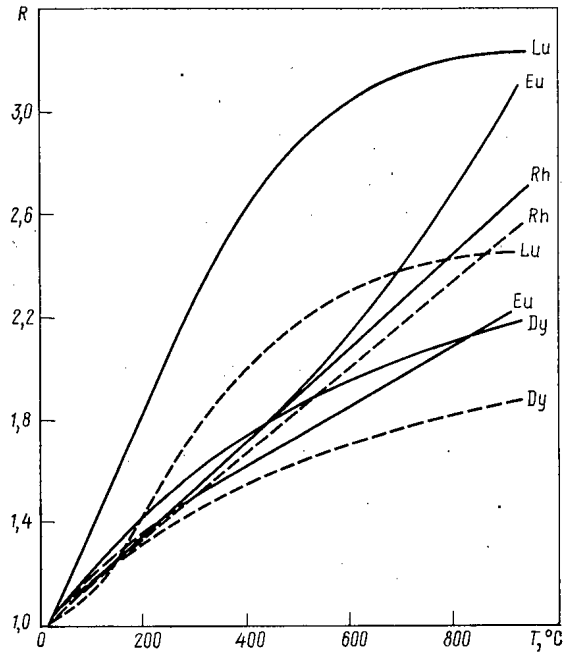

Fig. 1. Dependence of normalized reaction rate R on neutron temperature for detectors with filters at r = 0.1 and r = 0.2.

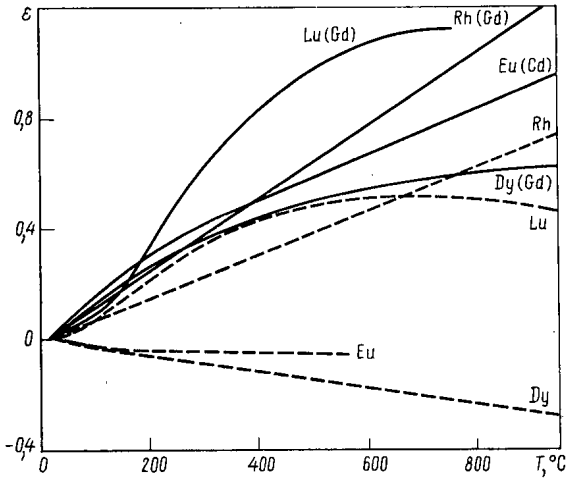

Fig. 2. Dependence of ε on T for ^{176}Lu, ^{103}Rh, ^{164}Dy, and ^{151}Eu detectors with and without filters at r = 0.2.

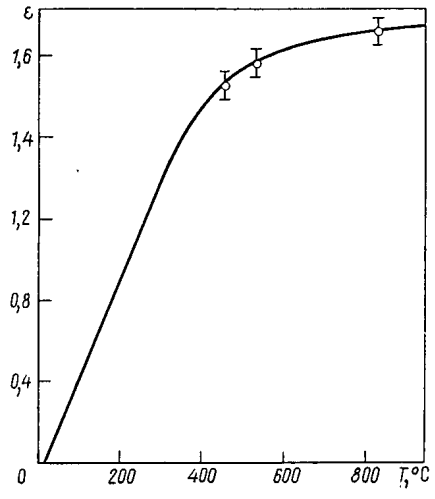

Fig. 3. Dependence of ε on T for ^{176}Lu detector in gadolinium filter.

where

$$I_{Cu}^{N}(T)=\frac{g^{N}(T)+rs^{N}(T)}{g^{Cu}(T)+rs^{Cu}(T)}.$$

Here N is the symbol of the neutron-sensitive element (^{176}Lu, ^{103}Rh, ^{164}Dy, and ^{151}Eu) which is used with or without the filter and Cu pertains to a copper detector used as a 1/v detector.

Table 2 gives the calculated values of ε for a temperature difference of 100°C for various detectors, some of them being copper detectors (without filter). Table 3 gives the values of ε for the same elements at a different temperature. The temperature dependence of ε for $r = 0.2$ is plotted in Fig. 2.

With a view to verifying the calculated values, we measured ε for ^{176}Lu in a gadolinium filter. Detectors with and without filters were irradiated simultaneously. The dimensions of the filters and the detectors corresponded to the values given above. As seen from Fig. 3, there is good agreement with the results of calculations.

Shielding detectors with gadolinium filters also substantially enchances the sensitivity of the detectors to a variation in the parameter r. Table 4 shows the change in ε, calculated for a fixed neutron temperature, while Tables 5 and 6 give the values of ε calculated for various r.

Analysis of the results shows that the use of gadolinium-shielded detectors makes it possible over a wide range to measure the neutron temperature as well as the epithermal parameter r with an error which is only half that in the case when detectors without filters are used. This follows from the fact that account is taken of the contribution of the error of measurement of the spectral index to the total error of measurement of T or r.

The relations presented here make it possible to choose the necessary detectors for concrete measurements in atomic power plant reactors.

LITERATURE CITED

1. G. Hickman and W. Leng, Nucl. Sci. Eng., No. 12, 523 (1962).
2. R. Stoughton and I. Halperin, Nucl. Sci. Eng., No. 15, 314 (1963).
3. H. Brown and T. Connolly, Nucl. Sci. Eng., No. 24, 6 (1966).
4. D. Albert and P. Schumann, Determination of Thermal Neutron Spectrum by Means of Activation Foils and Comparison with Theory. ZfK-RN156 (1968).
5. P. Schumann, Integrale Neutronenspectrometrie mit simulierten Nicht – 1/v-Aktivierungsindikatoren. ZfK-196 (1969).
6. C. Westcott et al., in: Proc. Int. Conf. on the Peaceful Uses of Atomic Energy, New York, United Nations, A/Conf. 15/P202 (1958).

REDUCTION OF ANGULAR DIVERGENCE OF INTERNAL ELECTRON BEAM OF SYNCHROTRON

Z. N. Esina and B. N. Kalinin

UDC 621.384.612.12

Considerable attention has recently been attracted by effects accompanying the passage of high-energy charged particles through single crystals, i.e., channeling of charged particles and coherent bremsstrahlung radiation. In order to study and make practical use of these effects it is necessary that the internal electron beam have a small angular divergence, not exceeding 10^4-10^5 rad. In the present paper, using the Tomsk synchrotron as an example, we analyze the possibilities of reducing the initial angular divergence of the electron beam at the target and the multiplicity of the passage of electrons through a thin crystalline target. In order to perform experiments with the internal electron beam in the synchrotron particles are discharged onto a target. The horizontal angular divergence of the beam at the target depends on the velocity of the radial displacement of the particles, which is proportional to the energy loss for synchrotron radiation. To reduce the angular divergence of the beam at the target it is proposed to use particle bunching according to phase during passage through nonlinear resonances of betatron oscillations. At the frequency $\nu \to \nu_{res} = p/q$, where p and q are integers, q is the order of the resonance of the betatron oscillation phase, $\Phi \to \pi/2q$ (it is assumed that there is no nonlinearity of the magnetic field – cubic or higher order, displaying a stabilizing effect on the amplitude of betatron oscillations [1]). As a result of the phase bunching of particles, the oscillation maximum falls at one and the same azimuth, while the horizontal angular divergence of the beam tends to zero. The particles are bunched according to phase most efficiently during slow passage through resonance, i.e., in a time $t \gg T_\Phi$, where T_Φ is the period of synchrotron oscillations. The time of passage through the resonance can be increased by extending the resonance radial near the target [2]. Technically this is done by means of windings to correct the magnetic field of the cyclic accelerator. The radius of the orbit to which this correction can be practically carried out determines the radius R_t at which the target is placed.

When thin crystal targets with a thickness of 10^{-4}-10^{-3} radiation length are used in cyclic accelerators there is repeated passage through the target and this results in an increased angular divergence of the electron beam owing to multiple scattering. The multiplicity of passage through the target was calculated as the sum of the probabilities of particles impinging on the target per revolution:

$$M = 1 + \sum_{i=1}^{N} S_i,$$

where i is the number of the revolution described by the particle after the first time it impinged on the target. As a result of bunching according to the betatron oscillation phase, a particle which passes through the target will subsequently reach the target for the next time after q revolutions. The probability of missing the target increases since after q revolutions the particle has an appreciable increase in radial coordinate because of the displacement pitch and the growth of the amplitude of radial betatron oscillations, which makes it possible to decrease the multiplicity of passage through the target.

Let us consider the possibility of using the resonance method to reduce the angular divergence of the internal beam in the Tomsk synchrotron with weak focusing at a maximum particle energy of 1.5 GeV and an equilibrium orbit radius of $R_0 = 423$ cm. To reduce the horizontal angular divergence of the beam and the multiplicity of passage use is made of third-order nonlinear resonance $\nu_r = 2/3$. Figure 1 shows the dependence of the maximum horizontal angular divergence of the beam on the energy. Curve 1 illustrates the case of the beam passing through resonance. Since the condition $\nu_r = \nu_{res} = \text{const}$ is not satisfied as the beam moves to the target, the resonance method does not yield a decrease of angular divergence. Curve 2 is obtained with observance of the requirement indicated: at $R = 420$ cm the frequency reaches resonance method makes it possible to reduce the angular divergence of the beam to ≈ 0.15 mrad. Curve 3 corresponds to the nonresonance case, $R_t = 417$ cm.

Translated from Atomnaya Énergiya, Vol. 49, No. 1, pp. 63-64, July, 1980. Original article submitted December 24, 1979.

0038-531X/80/4901-0503$07.50

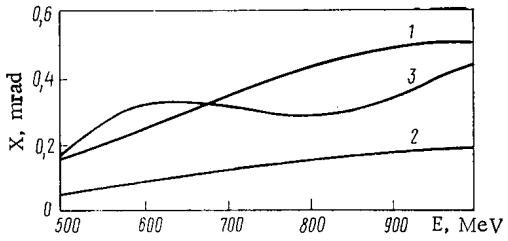

Fig. 1. Dependence of horizontal angular divergence of the beam at the target on the particle energy.

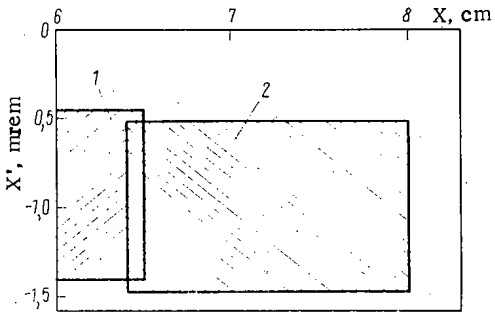

Fig. 2. Beam in phase plane.

Our numerical modeling of the process of multiple passage of electrons through a target took account of the ionization losses of energy and the change in the exit angle of the electrons. As a result of the calculation for a diamond target (thickness 0.35 mm, radial width 5 mm) we found that the multiplicity of passage practically does not depend on the radial position of the target in the interval $\Delta R = R_0 - R_t = 3$-5 cm and the electron energy in the range E = 500-1000 MeV and amounts to $M \approx 3$, which results in a substantial increase in the horizontal and vertical angular divergence of the beam. Figure 2 shows a beam in the phase plane at the moment of impingement on the target (1) and during three revolutions after passage through the target (2) with excitation of resonance of the radial betatron oscillations $\nu_r = 2/3$, E = 1000 MeV, $R_t = 417$ cm. The probability of particles impinging on the target in three revolutions is proportional to the area of the region of intersection of figures in the phase plane, related to the area of Fig. 1. Further reduction of the multiplicity of passage can be reached by reducing the radial width of the target.

In conclusion, we can draw the following conclusions. The use of the method of phase bunching of particles during passage through the resonance of radial betatron oscillations makes it possible to significantly reduce the initial horizontal angular divergence of the internal beam at the target.

The excitation of radial betatron oscillations during passage through resonance makes it possible to reduce the multiplicity of passage to 1. This results in a reduction of the horizontal and vertical angular divergence of the beam owing to multiple passages through the target.

LITERATURE CITED

1. M. Konte, JINR Preprint, E 9-4925, Dubna (1970).
2. V. A. Vizir', Z. N. Rakhmatulina, and I. P. Chuchalin, Izv. Vyssh. Uchebn. Zaved., Fiz., No. 6, 81 (1972).

NEW RUSSIAN JOURNALS

IN ENGLISH TRANSLATION

BIOLOGY BULLETIN
Izvestiya Akademii Nauk SSSR, Seriya Biologicheskaya

The biological proceedings of the Academy of Sciences of the USSR, this prestigious new bimonthly presents the work of the leading academicians on every aspect of the life sciences—from micro- and molecular biology to zoology, physiology, and space medicine.
Volume 7, 1980 (6 issues) $195.00

SOVIET JOURNAL OF MARINE BIOLOGY
Biologiya Morya

Devoted solely to research on marine organisms and their activity, practical considerations for their preservation, and reproduction of the biological resources of the seas and oceans.
Volume 6, 1980 (6 issues) $115.00

WATER RESOURCES
Vodnye Resursy

Evaluates the water resources of specific geographical areas throughout the world and reviews regularities of water resources formation as well as scientific principles of their optimal use.
Volume 7, 1980 (6 issues) $215.00

HUMAN PHYSIOLOGY
Fiziologiya Cheloveka

A new, innovative journal concerned *exclusively* with theoretical and applied aspects of the expanding field of human physiology.
Volume 6, 1980 (6 issues) $195.00

SOVIET JOURNAL OF BIOORGANIC CHEMISTRY
Bioorganicheskaya Khimiya

Features articles on isolation and purification of naturally occurring, biologically active compounds; the establishment of their structure, methods of synthesis, and determination of the relation between structure and biological function.
Volume 6, 1980 (12 issues) $245.00

SOVIET JOURNAL OF COORDINATION CHEMISTRY
Koordinatsionnaya Khimiya

Describes the achievements of modern theoretical and applied coordination chemistry. Topics include the synthesis and properties of new coordination compounds; reactions involving intraspheral substitution and transformation of ligands; complexes with polyfunctional and macromolecular ligands; complexing in solutions; and kinetics and mechanisms of reactions involving the participation of coordination compounds.
Volume 6, 1980 (12 issues) $255.00

THE SOVIET JOURNAL OF GLASS PHYSICS AND CHEMISTRY
Fizika i Khimiya Stekla

Devoted to current theoretical and applied research on three interlinked problems in glass technology; the nature of the chemical bonds in a vitrifying melt and in glass; the structure-statistical principle; and the macroscopic properties of glass.
Volume 6, 1980 (6 issues) $145.00

LITHUANIAN MATHEMATICAL JOURNAL
Litovskii Matematicheskii Sbornik

An international medium for the rapid publication of the latest developments in mathematics, this quarterly keeps western scientists abreast of both practical and theoretical configurations. Among the many areas reported on in depth are the generalized Green's function, the Monte Carlo method, the "innovation theorem," and the Martingale problem.
Volume 20, 1980 (4 issues) $175.00

PROGRAMMING AND COMPUTER SOFTWARE
Programmirovanie

Reports on current progress in programming and the use of computers. Topics covered include logical problems of programming; applied theory of algorithms; control of computational processes; program organization; programming methods connected with the idiosyncracies of input languages, hardware, and problem classes; parallel programming; operating systems; programming systems; programmer aids; software systems; data-control systems; IO systems; and subroutine libraries.
Volume 6, 1980 (6 issues) $115.00

SOVIET MICROELECTRONICS
Mikroelektronika

Reports on the latest advances in solutions of fundamental problems of microelectronics. Discusses new physical principles, materials, and methods for creating components, especially in large systems.
Volume 9, 1980 (6 issues) $160.00

Send for Your Free Examination Copy

PLENUM PUBLISHING CORPORATION, 227 West 17th Street, New York, N.Y. 10011
In United Kingdom: 88/90 Middlesex Street, London E1 7EZ England
Prices slightly higher outside the U.S. Prices subject to change without notice.